Calculation of entropy-dependent thermodynamic properties of fluids at high pressure with computer simulation

Inaugural-Dissertation
zur Erlangung des Doktorgrades
der Mathematisch-Naturwissenschaftlichen Fakultät
der Universität zu Köln

Simin Yazdi Nezhad
aus Mashhad, Iran

Köln 2016

For my parents and for my brothers

Berichterstatter:

Prof. Dr. U. K. Deiters
Insitut für Physikalische Chemie
Universität zu Köln

Priv. Doz. Dr. T. Kraska
Insitute für Physikalische Chemie
Universität zu Köln

Tag der mündlichen Prüfung: 20.01.2016

Acknowledgments

First of all, I would like to express my deep gratitude to my advisor Prof. Dr. Ulrich K. Deiters, for his enduring guidance and tremendous help in my research and the writing of this thesis.

I would like to express my gratitude to Dr. Tomas Kraska for his support of this project.

I am also grateful to all my friends and colleagues with whom I had a enjoyable time during my PhD study.

I am indebted to my parents for raising me and supporting me in all my life.

Notation

A	rotation matrix
E	energy
E_{kin}	kinetic energy
E_{pot}	potential energy
F	Helmholtz free energy
f	force
G	Gibbs free energy
$g(r)$	radial distribution function
h	Planck's constant
k_{B}	Boltzmann's constant
L	length of simulation box
m	mass
N	number of particles
N_{A}	Avogadro's constant
P	probability
p	pressure
$\mathbf{p}$	momentum
Q	partition function
r	distance
$\mathbf{r}$	location vector
r_{c}	cut-off radius of the pair potential
r_{hc}	hard-core radius
R	universal gas constant
S	entropy
S_{r}	residual entropy
T	temperature
$u(r)$	pair potential function
U	internal energy
ΔU	difference of internal energy
V	volume
V^{f}	molar free volume
$V_{\mathrm{id}}^{\mathrm{f}}$	free volume in an ideal gas
W	work
x	Monte Carlo shift parameter
Z	compressibility factor
$\mathbf{Z}$	configuration integral

ε_0	permittivity of vacuum
ε	depth of Lennard-Jones potential
ρ	number density
σ	diameter of a molecule
σ_{hs}	hard-sphere diameter
ξ	random number in range (0,1)
λ	thermal wavelength
μ	chemical potential
ϕ	Euler angle
θ	Euler angle
ψ	Euler angle
ω	molecular orientation
$*$	denotes reduced variables
$\langle \cdots \rangle$	ensemble average

Subscripts

c	cut-off
hs	hard sphere
kin	kinetic
m	molar
pot	potential
p	derivative at constant pressure
r	residual
T	derivative at constant temperature
V	derivative at constant volume

Acronyms

CPU	Central Processing Unit
CSJS-LJ	Carnahan–Starling + Jacobsen-Stewart Lennard-Jones equation of state
LJ	Lennard-Jones
KN-LJ	Kolafa–Nezbeda Lennard-Jones equation of state
mBWR1-LJ	modified Benedict–Webb–Rubin Lennard-Jones equation of state
mBWR2-nLJ	modified Benedict–Webb–Rubin Lennard-Jones chain equation of state
MC	Monte Carlo
MD	Molecular Dynamics
vdw	van der Waals

Zusammenfassung

Es ist lange bekannt, dass es Zusammenhänge zwischen der Entropie und dem freien Volumen eines Fluids gibt. Neuerdings wurde vor allem bei Simulationen flüssiger Metalle über Korrelationen zwischen der Entropie und der Diffusionskonstante berichtet.

Bei manchen Fluiden gibt es zudem einen Zusammenhang zwischen der residuellen Entropie und dem Verschiebungsparameter bei Monte-Carlo-Simulationen. Da dieser Parameter während einer Simulation ohnehin berechnet wird, eröffnet sich damit die Möglichkeit, entropieabhängige thermodynamische Größen ohne Mehraufwand zu bestimmen.

Es ist jedoch noch nicht klar, in welchen Klassen von intermolekularen Potentialen diese Beziehung angewandt werden könnte und welche Dichte oder Temperatur gewählt werden muss. Ein formaler statistisch-thermodynamische Beweis ist auch noch nicht erbracht worden.

In dieser Arbeit wurde eine neue, effiziente Methode zur Berechnung der residuellen Entropie entwickelt. Zum Vergleich wurde die Einfügungsmethode von Widom verwendet.

Die potentielle Energie des Systems wurde als Summe aller Zweikörper-Wechselwirkungspotentiale berechnet. Es wurden periodische Randbedingungen verwendet, um Oberflächeneffekte zu minimieren.

Die Simulation wurde für Ein- und Zweizentren-Moleküle durchgeführt, wobei zwischen den Zentren Mie-6 Potentiale, insbesondere Lennard-Jones-Potentiale, und Harte-Kugel-Potentiale angenommen wurden.

Im Rahmen dieser Arbeit wurde die Verbindung zwischen der residuellen Entropie und dem Monte-Carlo-Verschiebungsparameter in Flüssigkeiten mit hoher Dichte als Polynom zweiten Grades bestätigt. Das Anwendungsgebiet ist zu niedrigen Dichten durch einen Perkolationsübergang begrenzt.

Zum Vergleich wurden Entropien mit der Theorie von Scheraga, mit der radialen Verteilungsfunktion nach der Theorie von Baranyai und schließlich mit Hilfe von Zustandgleichungen für Harte-Kugel-Fluide bzw. Lennard-Jones-Fluide ermittelt.

.

Abstract

It has been long known that there is a connection between the entropy and the free volume of fluids. More recently, it has been shown that there is a correlation between the entropy and the diffusion constant in liquid metals by simulation.

In some fluids, a relevancy between the residual entropy and Monte Carlo shift parameter was discovered. Because this parameter is calculated during simulation in any case, it is possible to calculate the other thermodynamic properties that are connected to the entropy without additional cost.

However, it is not yet clear in which classes of intermolecular potentials this relationship could be applied and which density or temperature must be chosen. A formal statistical-thermodynamic proof is also still missing.

In this work, a new efficient method was developed to calculate the residual entropy. For comparison, the Widom test particle insertion method was used to calculate chemical potentials.

The potential energy of a system was calculated as a sum of the two-body interaction potentials. Moreover, periodic boundary conditions were used to minimize surface effects.

Simulations were performed for single- and two-center molecules. For the site-site interactions, Mie potentials, especially Lennard-Jones potentials and hard-sphere potentials were adopted.

In this work, the connection between the residual entropy and the Monte Carlo shift parameter in fluids at high densities was obtained as a second-order polynomial equation. The application range of this equation is limited at low densities by percolation.

For comparison, the entropy was determined by the theory of Scheraga, from the radial distribution function by the theory of Baranyai and finally with help of equations of state for Lennard-Jones and hard-sphere fluids.

Contents

List of Figures

List of Tables

Chapter 1

Introduction

Introduction

One of the main goals of research in the field of applied thermodynamics is the prediction of thermodynamic and transport properties of fluids and their mixtures. Among the various thermodynamic properties, knowledge of the phase behaviour of fluids is particularly important for many applications. The required thermodynamic properties can be calculated in two different ways:

1. Empirical methods, which were generated from a large set of experimental data. These methods are particularly suitable for application to systems for which there are many measured data.

2. Theoretical methods, which are based on statistical thermodynamic theories.

For almost half a century, computer simulation methods have been used in the research on liquids, particularly in scientific, engineering and industrial research. Over the previous decades, the speed of computers has rapidly increased. For this reason, computer simulation has become a very important tool for calculating the thermodynamic properties of fluids.

The first molecular simulations of liquids were performed by Metropolis on the MANIAC computer at Los Alamos [1, 2].

The main motivation of molecular simulation is the calculation of accurate properties of statistical mechanical systems. Molecular simulations can be described as computational statistical mechanics. Molecular simulations determine macroscopic properties with the use of computer programs. This allows the precise evaluation [1] of theoretical models of molecular behavior, whereas "classical" statistical thermodynamics are frequently restricted to the use of simplistic models.

Molecular simulation can be done in two different ways: molecular dynamics simulation (MD) and Monte Carlo simulation (MC).

Molecular dynamics simulation (MD): as the name indicates, molecular dynamics makes it possible to obtain the dynamic properties of the system. MD uses the following steps to calculate macroscopic thermochemical properties:

▶ Setting up the system in an initial configuration

▶ Solving Newton's equations of motion for the system of molecules:

$$\frac{\mathrm{d}^2 \overrightarrow{r_i}}{\mathrm{d}t^2} = \frac{\overrightarrow{F_i}}{m_i} \qquad\qquad i = 1, 2, 3, \ldots$$

---

[1] with errors depending on the computer speed and size.

where F_i, m_i, and r_i are the force on particle i, mass, and position of particle i, respectively. The momenta and the molecular coordinations change according to the intermolecular forces experienced by the individual molecules [77].

▶ Calculating average properties (energy, pressure, pair correlation functions) after the system has reached equilibrium.

Monte Carlo simulation (MC): the details of the Monte Carlo simulation is presented in section 2.1.3 on page 28.

The molecular dynamics and Monte Carlo simulation methods are different in a several of ways:

▶ Molecular dynamics simulation (MD) provides information about the time dependence of the properties of the system, whereas there is no temporal relationship between successive Monte Carlo configurations.

▶ In a Monte Carlo simulation (MC) the outcome of each trial move depends only on its immediate predecessor, whereas in molecular dynamics it is possible to predict the configuration of the system at any time in the future or indeed at any time in the past.

▶ Molecular dynamics has a kinetic energy contribution to the total energy, whereas in the Monte Carlo simulation the total energy is determined directly from the potential energy function.

▶ Monte Carlo simulation calculates the changes in intermolecular energy, whereas molecular dynamics uses intermolecular forces to evolve the system.

Until 1970, computer simulation was only feasible for studies of structural and simple thermodynamic properties, such as pressure, enthalpy, energy and pair correlation functions. Some properties such as entropy, Helmholtz energy and chemical potential are difficult to calculate because they are not representable as ensemble averages of mechanical properties. Today, different methods are available for the calculation of chemical potential and free energies, etc.:

▶ **The Widom test particle insertion method:**
The most widely used methods for the calculation of chemical potentials, free energies and etc. are based directly or indirectly on the insertion method of Widom [3]. The Widom test particle method has been used to obtain phase diagrams for pure [6, 7] and binary mixtures [8, 9].
In this method, a new particle is added at a random location and the change in average energy is calculated. The details of this method will be discussed in section

2.9.3 on page 56.

▶ **The two-ensemble method: (know as Gibbs ensemble method)**

The two-ensemble method for the calculation of phase equilibria with Monte Carlo simulation was developed by Panagiotopoulos [10, 11].

A distinguishing feature of the two-ensemble method is that it entails two simulation boxes ("subsystems") that are coupled to each other. The coupling between them is done in such a way as to achieve coexistence between two phases. This methode uses insertion steps to bring both ensembles to equilibrium with each other [31].

▶ **The grand canonical ensemble simulation:**

In simulations using the grand canonical ensemble (μ, V, T), the calculation of chemical potentials is not needed. The particle numbers are allowed to fluctuate by insertions and deletions steps.

Insertion steps which add a new particle to a random location in a fluid are only possible if enough place for a new particle is available. Simulation methods based on insertion steps tend to become inefficient if the systems have very high densities (compressed fluid, solid, etc). Moreover, they become inefficient or very complicated if the particles do not have spherical shapes.

To avoid these problems, **deletion methods** have been suggested (for example by Boulougouris et al. [12]). But they cause statistical problems [20–22] and fall down if they are used for molecules with long-range interactions [23, 24].

▶ **Estimation of the entropy from radial distribution function (RDF)** [64] and **Scheraga theory**: [52, 53]

These are two other methods to calculate residual entropy, which are explained later in detail.

There are other methods to determine chemical potentials and free energies, for example **umbrella sampling** [15], the method of **Hoheisel and Deiters** (This method is universally applicable [16], but needs a lot of time for the calculations and cannot be automatized easily) and the method of **Kofke** [13, 14] (that can be used along phase boundary curves), but they are used infrequently. An overview of available methods is presented in the book of Frenkel and Smit [30].

It has long been known that the entropy and the free volume of a fluid are connected [17]; this had been published in **1981** by Speedy [18]. More recently, correlations between the entropy and the diffusion have been reported in the simulation of liquid metals [19].

In the present work, the Monte Carlo method, combined with the Widom test particle method, is used to calculate chemical potentials and residual entropies of the nobel gas argon, hard-sphere argon, a dimer CH_3-CH_3. Furthermore, a new method for computing the entropy of fluids is introduced and tested, which avoids some of the shortcomings of the Widom method.

The Chapter 2 gives a short introduction the statistical thermodynamic and the principles of Monte Carlo simulation. Chapter 3 gives a description of the simulation program and its details, and at last, Chapter 4 and Chapter 5 present the results and the conclusion of this project, respectively.

Chapter 2

Statistical Thermodynamics

2.1 Principles of Monte Carlo simulation

2.1.1 Concept of ensembles

The relationship between the microscopic description of individual molecules and the macroscopic properties of a collection of molecules is a central concept in statistical mechanics [30].

The state of a macroscopic system can be specified by a few properties. For example, a pure liquid can be described completely by its mass, pressure and temperature. However, for each macroscopic state, there exists a large number of microscopics states corresponding to it. For classical systems, the positions and momenta of all theirs constituent molecules characterize each microscopics state.

Table 2.1: Some microscopic and macroscopic properties

properties of individual molecules (microscopic properties)	properties of bulk fluid (macroscopic properties)
intermolecular force	the equation of state
molecular geometry	internal energy
velocities	heat capacity
position	pressure

An ensemble of systems is a collection of various microscopics states of the system, which correspond to the single macroscopic state of the system whose properties are investigated.

As there are several ways to specify the macroscopic state of the system, various ensembles types can be defined. The commonly used ensembles are given in Table 2.2.

The ensembles in Table 2.2 can be divided into two categories. The grand canonical ensemble represents open systems in which the number of particles can be changed; the isothermal-isobaric, canonical and microcanonical ensembles are for closed systems, in which the number of particles is constant [77].

Because of the equivalence of the ensembles in the thermodynamic limit, it is possible to transform between different ensembles [42]. The choice of the ensemble for a simulation is entirely a matter of convenience. If a system has a fixed number of molecules and is kept at either constant volume and temperature or constant pressure and temperature, the best choices are isothermal-isobaric and canonical ensembles, respectively.

The most important ensembles, which are used besides the classical canonical ensembles in computer simulation are the grand canonical ensemble (μ, V, T) and the isobaric-isothermal ensemble (N, p, T).

Table 2.2: Summary of common statistical ensemble. Table taken from [77].

type of ensemble	constant variables	Z	P_i	description
microcanonical	N, V, E	$\sum_i \delta(E_i - E)$	$\frac{\delta(E_i - E)}{Q_{NVE}}$	isolated system
canonical	N, V, T	$\sum_i e^{-\beta E_i(N,V)}$	$\frac{e^{-\beta E_i(N,V)}}{Q_{NVT}}$	closed isothermal system
grand canonical	μ, V, T	$\sum_i e^{\beta N_i \mu} Q_{NVT}$	$\frac{e^{-\beta(E_i - \mu N_i)}}{Q_{\mu VT}}$	open isothermal system
isothermal-isobaric	N, p, T	$\sum_i e^{\beta p V_i} Q_{NVT}$	$\frac{e^{-\beta(E_i + p V_i)}}{Q_{NpT}}$	closed isothermal-isobaric system

In Table 2.2, Z and P_i stand for the partition function and the probability of observing the i-the state, respectively.

2.1.2 Boltzmann factors and ensemble averages

The microscopic states of a canonical ensemble with N particles are not all equally probable [26]. The probability $P(i)$ of a microscopic state i with the energy E_i is proportional to the Boltzmann factor $\exp(-E_i/(k_\mathrm{B}T))$, where k_B is the Boltzmann constant: [27]

$$P(i) \propto \exp\left(\frac{-E_i}{k_\mathrm{B}T}\right) \tag{2.1}$$

The points in phase space are distributed according to a probability. Moreover, the total energy of a state is sum of the potential and the kinetic energy. Therefore Equation (2.1) can be rewritten as

$$P(i) = \frac{e^{-\beta E_i(N,V)}}{Q_{NVT}} \tag{2.2}$$

$$E = \langle E_{\mathrm{kin}} \rangle + \langle E_{\mathrm{pot}} \rangle \tag{2.3}$$

$$Q_{NVT} = \sum_i e^{-\beta E_i(N,V)} \tag{2.4}$$

where Q_{NVT} is the canonical partition function and acts as a normalizing factor.

From the probability distribution, the ensemble average of a property A can be calculated in the following way:

$$\langle A \rangle_{\text{ens}} = \sum_i A_i \, P_i \tag{2.5}$$

where $\langle A \rangle_{\text{ens}}$ is the ensemble average of the system.

2.1.3   Monte Carlo simulation (MC)

The word Monte Carlo was coined by Metropolis because of the use of random numbers, and used for first time in 1943 by three scientists at the Los Alamos National Laboratory in New Mexico—Nicolas Metropolis, John von Neumann, and Stanislaw Ulam—to study the diffusion of neutrons in fissionable materials [25].

The MC method can be used in different fields from economics or nuclear physics to the regulation of traffic flow. It is a stochastic technique for studying many-body systems and for obtaining thermodynamic properties that can be expressed as an ensemble averages. The pressure and internal energy are examples of such properties. Basic characteristics and some advantages of Monte Carlo method are :

• Different types of probability distributions can be assigned to the inputs of the model. When the distribution is known, the one that represents the best fit can be chosen.

• The use of random numbers characterizes Monte Carlo simulation as a stochastic method. The random numbers have to be independent; no correlation should exist between them.

• Simulations provide detailed information on the model systems.

The steps in Monte Carlo simulation corresponding to the uncertainty propagation are relatively simple: [77]

1. Generating a trial configuration randomly.

2. Evaluating an acceptance criterion by calculation of the change in energy, and other properties in the trial configuration.

3. Comparing the acceptance criterion to a random number and either accepting or rejecting the trial configuration.

2.1.4   Hit-or-miss Monte Carlo: calculation of π

The naive MC technique (this method is called naive Monte Carlo because it works with random sampling) can be used as a method of integration, for example for the

evaluation of π. This calculation can be done by finding the area of a circle of radius R. Figure 2.1 shows the circle, centred at the origin and inscribed in a square [42].
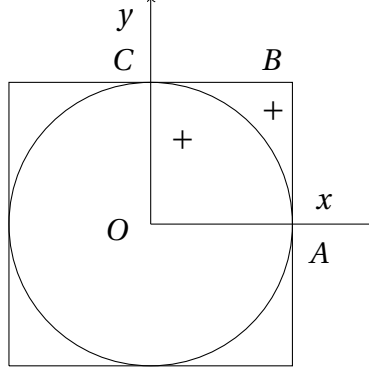
Figure 2.1: Monte Carlo calculation of π.

Now points are chosen randomly inside the square. Points with $x^2 + y^2 < 1$ lie inside the circle. The area of the circle can then be approximately obtained from:

$$4 \times \frac{\text{area of circle}}{\text{area of enclosing square}} \simeq 4 \times \frac{\text{number of points inside the circle}}{\text{total number of points}} \qquad (2.6)$$

Then π can be computed from:

$$\pi = \frac{4\pi R^2}{(2R)^2} = 4 \times \frac{\text{area of circle}}{\text{area of enclosing square}} \qquad (2.7)$$

2.1.5   The Metropolis method

Metropolis (1953) described a new approach where instead of choosing configuration randomly from an equidistribution (naive Monte Carlo method), the configuration is chosen with the probability $\exp(-E/k_B T)$ (Boltzmann factor)[28]. For a system in which the potential energy depends on position, Metropolis' idea can be expressed by the following equation:

$$\langle A \rangle = \frac{1}{X} \sum_{i=1} A(q_i) \qquad (2.8)$$

In Equation (2.8), X is the number of Monte Carlo steps, A is a property, and q_i are configurations sampled according to the Metropolis prescription (it means that the points are chosen with a Boltzmann weights).

According to Metropolis Monte Carlo algorithm, the reasonable approach is to start with configuration q_1. The first element that to be computed in Equation (2.8) is in value of property A. After that, q_1 is randomly perturbed to obtain a new configuration

q_2. At constant temperature, constant volume and constant particle number (ensemble NVT), the probability of accepting point q_2 is :

$$P_{\text{accept}} = \min\left[1, \frac{\exp(-E_{q_2}/k_{\text{B}}T)}{\exp(-E_{q_1}/k_{\text{B}}T)}\right] \qquad (2.9)$$

If the energy of point q_1 is higher than the energy of point q_2 ($E_{q_2 q_1} = E_{q_2} - E_{q_1} < 0$) the point is accepted (such a prospective change in the conformation is called a move) and if the energy of point q_1 is less than the energy of point q_2 ($E_{q_2 q_1} = E_{q_2} - E_{q_1} > 0$), P_{accept} is compared with a random number ξ between 0 and 1 and the move is accepted if $P_{\text{accept}}(q_1 \rightarrow q_2) \geq \xi$.
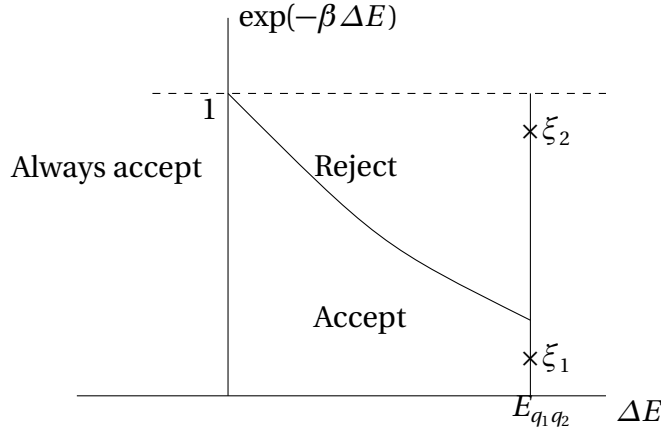
Figure 2.2: Accepting or refusal of the moves in the MC simulation.
Diagram taken from [42].

The meaning of accepting is that the value of A is calculated for each Monte Carlo step and this value is added to the sum in Equation (2.8), and after that this process repeats again. If the second Monte Carlo step is not acceptable, the first step is repeated and the value of first step is added to the sum in Equation (2.8) and for the second time a new random perturbation is tried. Such a sequence of phase points, where each new point depends only on the immediately preceding point, is called a Markov chain [29].

In equilibrium, the average number of accepted moves from a state q_1 to any other state q_2 is exactly cancelled by the number of reverse moves from q_2 to q_1.

$$P(q_2)\pi(q_2 \rightarrow q_1) = P(q_1)\pi(q_1 \rightarrow q_2) \qquad (2.10)$$
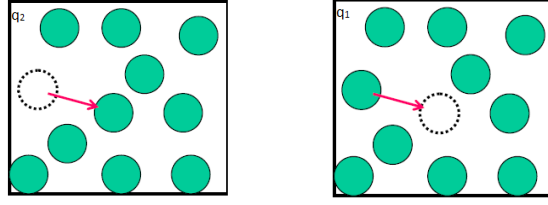
Figure 2.3: Displacement in Monte Carlo simulation.

where $\pi(q_1 \rightarrow q_2)$ is the transition probability to go from configuration q_1 to q_2, and $P(q_2)$ denotes the number of points in any configuration q_2. Furthermore, $P(q_2)$ is proportional to the Boltzmann distribution :

$$P(i) \propto \exp\left(\frac{-E_i}{k_\mathrm{B}T}\right) \tag{2.11}$$

It is useful to split up the determination of $\pi(q_1 \rightarrow q_2)$ into two steps:

1. Choose a new random configuration q_1 with transition matrix probability $\alpha(q_2 \rightarrow q_1)$

2. Accept or reject this new configuration probability with an acceptance probability $\mathrm{acc}(q_2 \rightarrow q_1)$
In other words, the transition probability is rewritten as [30]:

$$\pi(q_2 \rightarrow q_1) = \alpha(q_2 \rightarrow q_1) \times \mathrm{acc}(q_2 \rightarrow q_1) \tag{2.12}$$

Many MC methods take α to be symmetric :

$$\alpha(q_2 \rightarrow q_1) = \alpha(q_1 \rightarrow q_2) \tag{2.13}$$

The detailed balance condition (Equation (2.10)) therefore implies that:

$$\frac{\pi(q_2 \rightarrow q_1)}{\pi(q_1 \rightarrow q_2)} = \frac{\mathrm{acc}(q_2 \rightarrow q_1)}{\mathrm{acc}(q_1 \rightarrow q_2)} = \frac{P(q_1)}{P(q_2)} = \frac{\exp(-(E_{q_1} - E_{q_2}))}{k_\mathrm{B}T} \tag{2.14}$$

The choice of Metropolis (Equation (2.9)) is:

$$\mathrm{acc}(q_2 \rightarrow q_1) = \begin{cases} P(q_1)/P(q_2) & \text{if} \quad P(q_1) < P(q_2) \\ 1 & \text{if} \quad P(q_1) \geq P(q_2) \end{cases} \tag{2.15}$$

In summary, in the Metropolis scheme, the translation probability for going from state q_2 to state q_1 is given by:

$$\pi(q_2 \rightarrow q_1) = \begin{cases} \alpha(q_2 \rightarrow q_1) & \text{if} \quad P(q_1) \geq P(q_2) \\ \alpha(q_2 \rightarrow q_1)[\pi(q_1/q_2)] & \text{if} \quad P(q_1) < P(q_2) \end{cases} \qquad (2.16)$$

$$\pi(q_2 \rightarrow q_2) = 1 - \sum_{q_1 \neq 0} \pi(q_2 \rightarrow q_1) \qquad (2.17)$$

Suppose that the trial move is from state 0 to state n with $u(n) > u(0)$. According to Equation (2.14), this trial move should be accepted with a probability:

$$\text{acc}(q_2 \rightarrow q_1) = \exp\left(-\beta \left[U(q_1) - U(q_2)\right]\right) < 1 \qquad (2.18)$$

2.2   Trial moves

2.2.1   Translational moves

A perfectly acceptable method for creating a trial displacement is to add random number between $+\Delta r_{\text{max}}$ and $-\Delta r_{\text{max}}$ to the x, y and z coordinations of the molecular center of mass:

$$x'_i = x_i + (2\xi - 1)\Delta r_{\text{max}} \qquad (2.19)$$

$$y'_i = y_i + (2\xi - 1)\Delta r_{\text{max}} \qquad (2.20)$$

$$z'_i = z_i + (2\xi - 1)\Delta r_{\text{max}} \qquad (2.21)$$

where ξ is an equidistributed random number between 0 and 1, Δr_{max} is the maximal displacement and x_i, y_i, z_i and x'_i, y'_i, z'_i are the old and new coordinations of atoms relative to the center of gravity, respectively.

If Δr_{max} is very large, there will probably a collision, and the resulting configuration will have a high energy and the trial move will probably be rejected. If Δr_{max} is very small, the change in potential energy is probably small, and most moves will be accepted [30, 42].

2.2.2 The maximum displacement

The Monte Carlo simulation is efficient if the mean squared displacement per move is as large as possible. Because of this, Δr_{max} is optimized after each cycle.

The mean squared displacement is calculated according to Equation (2.22):

$$\langle \Delta r \rangle = \sqrt{\frac{1}{N} \sum_{i=1}^{N} (\Delta r_i)^2} \qquad (2.22)$$

where N is the number of particles in simulation box and Δr_i is the displacement of particle i.

At the start of Simulation, first of all, the maximum displacement is set to the half of the length simulation box length. During the simulation, the division of the number of accepted movements per total number of movement tries are calculated (called as a). The following steps are done to calculate the maximum displacement of particles in simulation box:

1- Calculation of correction factor F according to Equation (2.23):

$$F = \exp(\max(-0.4, \min(0.4, a - a_0))) \qquad (2.23)$$

where a_0 is the desired average acceptance ratio, which is fixed at the start of program. In most cases, the best results are achieved by $a_0{=}0.5$, which is therefore used as a default value in our simulation program. For hard body system, a value in the range 0.3–0.4 is better.

2- If $\Delta r\,\mathrm{e}^{F} < 0.5L$ then:

$$\Delta r \rightarrow \Delta r\,\mathrm{e}^{F} \qquad (2.24)$$

In the other case

$$\Delta r = 0.5L \qquad (2.25)$$

where L is the length of simulation box.

2.2.3 Orientational move of rigid molecules

The rotation of rigid molecule is often described in terms of the Eulerian angles (ϕ, θ, ψ). A change in orientation can be achieved by taking small displacements in each of Euler angles of molecule i [42].

$$\phi_i = (2\xi - 1)\Delta\phi_{\max} \tag{2.26}$$

$$\theta_i = (2\xi - 1)\Delta\theta_{\max} \tag{2.27}$$

$$\psi_i = (2\xi - 1)\Delta\psi_{\max} \tag{2.28}$$

where $\Delta\phi_{\max}$, $\Delta\theta_{\max}$ and $\Delta\psi_{\max}$ are the maximum rotations in the Euler angles. Alternatively a new configuration is generated using:

$$e_{i,x}^n = \mathbf{A}_x e_i^m \tag{2.29}$$

$$e_{i,y}^n = \mathbf{A}_y e_i^m \tag{2.30}$$

$$e_{i,z}^n = \mathbf{A}_z e_i^m \tag{2.31}$$

where e_i^n and e_i^m represent the old and new coordinates (after rotation) of atom i in a molecule relative to the center of gravity, respectively. $\mathbf{A}_x$, $\mathbf{A}_y$ and $\mathbf{A}_z$ are rotation matrices about the x, y and z axes

$$\mathbf{A}_x = \begin{pmatrix} 1 & 0 & 0 \\ 0 & \cos\phi & \sin\phi \\ 0 & -\sin\phi & \cos\phi \end{pmatrix} \tag{2.32}$$

$$\mathbf{A}_y = \begin{pmatrix} \cos\theta & 0 & -\sin\theta \\ 0 & 1 & 0 \\ \sin\theta & 0 & \cos\theta \end{pmatrix} \tag{2.33}$$

$$\mathbf{A}_z = \begin{pmatrix} \cos\psi & \sin\psi & 0 \\ -\sin\psi & \cos\psi & 0 \\ 0 & 0 & 1 \end{pmatrix} \tag{2.34}$$

where ϕ, θ and ψ are random angles and can be calculated according to Equations (2.26) to (2.28). According to Equations (2.19) to (2.34), the rotation of atom i about x, y and z axis can be obtained according to Equations (2.35) to (2.40):

rotate about x axis

$$y' = y\cos\phi + z\sin\phi \tag{2.35}$$

$$z' = -y\sin\phi + z\cos\phi \tag{2.36}$$

rotate about y axis

$$x' = x\cos\theta - z'\sin\theta \tag{2.37}$$

$$z'' = x\sin\theta + z'\cos\theta \tag{2.38}$$

rotate about z axis

$$x'' = x'\cos\psi + y'\sin\psi \tag{2.39}$$

$$y'' = -x'\sin\psi + y'\cos\psi \tag{2.40}$$

where x, y, z, x', y', z' and x'', y'', z'' are the old and new coordinates of atom relative to the center of gravity.

2.2.4 Calculation of maximum rotation angle

The maximum rotation angle in simulation program is calculated according to the following steps:

1- If gyration radius is equal to 0, then $\phi_{\max}=0$

2-If $\phi_{\max}\neq 0$ then:

$$\phi_{\max} = \min(\pi, f_{\text{rot}} \times \Delta r_{\max}/r_{\text{gyr}}) \tag{2.41}$$

where r_{gyr} is the gyration radius. f_{rot} is the ratio traslation to rotation (called as maximum displacement to maximum rotation conversion) that is fixed at the start of program. If no value is specified for f_{rot}, then the program is started with $f_{\text{rot}}=1$.

2.2.5 Volume change in NpT ensemble

In addition to particle moves, simulations using the NpT ensemble, require random volume changes. Acceptance of the new volume rejection is done according to following steps:

1. If the new energy of system is lower than the old one, then the new volume is accepted.
2. If the new system energy is larger than the old one, then a random number is chosen and compared with $\exp(-a)$. a is calculated according to Equation (2.42) [30, 31, 35, 42],

$$a = \exp\left[-\beta\left(\Delta U + p\,\Delta V\right) + N \ln\left(\frac{V_{\text{new}}}{V_{\text{old}}}\right)\right] \qquad (2.42)$$

where Δ here indicates the change of the quantity from the old to the new configuration and a is the acceptance probability in isothermal-isobaric simulation.

If the random number is smaller than $\exp(-a)$, then the new volume is accepted, else the new volume is rejected.

Eppenga and Frenkel [34] showed that it may be more convenient to make the random changes in $\ln V$ rather than V itself. A random number $\Delta(\ln V)$ is chosen uniformly in some range $(-\Delta(\ln V_{\text{max}}), \Delta(\ln V_{\text{max}}))$, the volume multiplied by $\exp(\Delta(\ln V))$, and the molecular positions scaled accordingly. The only change to the acceptance/rejection procedure is that the factor N in Equation (2.42) is replaced by $N+1$ [42].

2.2.6 Calculation of the maximum expansion factor

In NpT simulation, the volume is changed after each Monte Carlo cycle. The following steps are done for the calculation of the maximum expansion factor:

1-Calculation of accepted expansion per total numbers of expansions attempts.

2-Calculation of correction factors F according to Equation (2.23).

3-Calculation of the maximum box length expansion factor $(\Delta \ln V_{\text{max}})$:

$$\Delta \ln V_{\text{max}} \rightarrow \Delta \ln V_{\text{max}} e^{F} \qquad (2.43)$$

The volume changes are optimized to bring the average acceptance ratio to 0.50 .

2.3 Periodic boundary conditions (PBC)

Computer simulations using atomic potentials are typically performed on small systems, usually of the order of a few hundred to a few thousand molecules. Assuming

a simple cubic lattice of 1000 molecules, 488 (about 49%) lie on the surface [30]. These molecules would experience different forces than the other molecules. In order to avoid surface effects and make the system resemble an infinite one [41], it is common to use periodic boundary conditions.
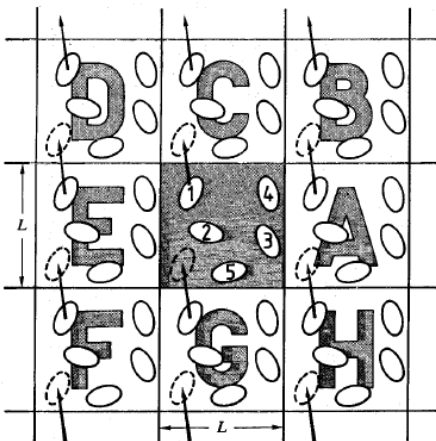
Figure 2.4: Two dimensional periodic system.
Figure taken from
[42].

In Figure 2.4, the central box represents the simulated system, the surrounding boxes are lattice exact copies, and this is continued in all directions. The choice of the position of the original box (computational cell) has no effect on the forces or the behavior of the system.

Each particle in the simulation box has a copy in each of the other cells, and it is interacting not only with other particles in the computational box, but also with their images in the adjacent boxes.

In the course of the simulation, the molecules in each of the boxes move in the same way. Hence, if a molecule leaves the simulation box at one side, an identical molecule enters the box at the other side. Because of this reason, the number of particles in the simulation box is constant, the system has no limits and disturbing surface effect should disappear.

Molecules can enter and leave each box across each of the four edges. In a three-dimensional example, molecules would be free to cross any of six cube faces [42].

If the origin of the coordinate system is taken as the centre of the simulation box of the length L, all the coordinates are within of $-L/2$ and $+L/2$. Consequently, when a molecule leaves the box, its mirror images are obtained by either adding or subtracting L to its coordinations [77].

The most commonly shaped simulation cell are cubic or cuboid. It is also possible to use cells of other shapes, such as:

• hexagonal prism

• rhombic dodecahedro

• truncated octahedron

• parallelpiped

    All of these alternative geometries structure can regularly cover total space. They can serve to create an the infinite number of periodic images. However, the meaning of minimum image distance is different for each structure.
    The choice of one of these geometries can be motivated by:

• The particular symmetry: for example, a simulation box with a hexagonal form can better accommodate a fluid or crystal with hexagonal ordering.

• Decrease the number of particles that are used in a simulation. For example the octahedron resembles a cube with its corners cut-off and fewer atoms can be located in it. For systems in which a macromolecule is solved, the octahedron reduces the number of solvent molecules required.

2.4   Minimum image convention
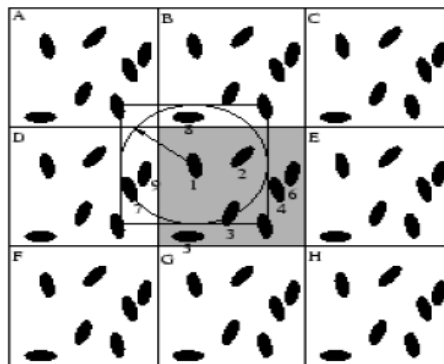
Figure 2.5: The minimum image convention in two-dimensional system.
Figure taken from
[42].

    The size of computational cells in periodic system must be at least equal to $2r_c$, where r_c is the cut-off distance of the interaction potential. Therefore we consider only

interactions between the molecules and the closest images of its neighbours (short–ranged forces); and it does not interact with its own image. This is named **minimum image convention**.

2.5 Intermolecular Interactions

Intermolecular interactions are represented by a potential function. This potential is a function of the positions of the nuclei and describes the potential energy of two- three- ... etc. body interactions. It should be noted that the molecules are considered as n–center objects with spherical centers.

$$u(\mathbf{r^N}) = \sum_i u_1(\mathbf{r^N}) + \sum_i \sum_{j>i} u_2(\mathbf{r^N}) + \sum_i \sum_{j>i} \sum_{k>j} u_3(\mathbf{r^N}) + \ldots \tag{2.44}$$

where $\mathbf{r^N} = (\mathbf{r_1}, \mathbf{r_2}, \cdots, \mathbf{r_N})$ stands for the complete set of $3N$ particle coordinates and $u(\mathbf{r^N})$ is the interaction potentials of these particles in a system.

The first term in Equation (2.44) represents the potential of an external field (for example from the container walls) and the second and third term are the potentials of pair and triplet interactions, respectively.

In simulation, the comparison between second, third and higher terms shows that the second term has a much higher value than the third and higher terms. The first term is irrelevant, if no chemical reactions occur and there is no external force field. Moreover, three-or more-body interactions impose a very large increase in computing time compared with two-body calculations [77]. Therefore the potential energy of systems is calculated with sum of the second term:

$$u(\mathbf{r^N}) = \sum_i \sum_{j>i} u_2(\mathbf{r^N}) \tag{2.45}$$

where $\mathbf{r_{ij}} = |\mathbf{r_i} - \mathbf{r_i}|$ denotes the distance vector from particle i to j.

2.6 Calculation of thermodynamic properties from ensemble averages

2.6.1 The effect of kinetic energy in Monte Carlo simulation

The calculation of ensemble averages was presented in section 2.1.2 on page 27. This section explains *why the Monte Carlo simulation delivers only "configurational energy" and not kinetic energy*. According to Equations 2.2, 2.3 and 2.4, the ensemble averages of a property can be calculated by the following equations:

$$\langle A \rangle = \frac{\int \exp\left[-\beta\left(E_{\text{kin}}(\mathbf{p}) + E_{\text{pot}}(\mathbf{r})\right)\right] A \, d\mathbf{p} d\mathbf{r}}{\int \exp\left[-\beta\left(E_{\text{kin}}(\mathbf{p}) + E_{\text{pot}}(\mathbf{r})\right)\right] d\mathbf{p} d\mathbf{r}} \tag{2.46}$$

$$\langle A \rangle = \frac{\overbrace{\int e^{-\beta E_{\text{kin}}(\mathbf{p})} d\mathbf{p}}^{\text{constant}} \int e^{-\beta E_{\text{pot}}(\mathbf{r})} A \, d\mathbf{r}}{\underbrace{\int e^{-\beta E_{\text{kin}}(\mathbf{p})} d\mathbf{p}}_{\text{constant}} \int e^{-\beta E_{\text{pot}}(\mathbf{r})} d\mathbf{r}} \tag{2.47}$$

The integral over the momentum cancels out in the averaging and it remains:

$$\langle A \rangle = \frac{\int e^{-\beta E_{\text{pot}}(\mathbf{r})} A \, d\mathbf{r}}{\int e^{-\beta E_{\text{pot}}(\mathbf{r})} d\mathbf{r}} \tag{2.48}$$

where $\mathbf{p}$ is momentum of particle and $\mathbf{r}$ is the cartesian coordinate of particle.

Equation 2.48 shows, that the Monte Carlo simulation uses only potential energy to calculate the averages of thermodyanamic properties and kinetic energy has no effect on those averages.

2.6.2   Residual thermodynamic properties

A residual property is defined as the difference between real gas property and an ideal gas property at the same density, composition and temperature. For example, if M is the actual value of thermodynamic property (like the Gibbs free energy) for a nonideal gas and M_{ideal} is the value the property will have if the gas was ideal. The residual property M_{r} is defined as:[77]

$$M_{\text{r}} = M - M_{\text{ideal}} \tag{2.49}$$

2.6.3   Calculation of residual internal energy

The residual internal energy of monoatomic species is calculated with the following equation:

$$U_r = \sum_{i=1}^{N} \sum_{i<j} u(r_{ij}) + N u_{\text{tail}} \tag{2.50}$$

where $u(r)$ is the Lennard-Jones potential, u_{tail} is the tail correction of the Lennard-Jones potential and N is the number of particles in simulation.

The residual internal energy in 2-center moleculs is calculated with Equation (2.51):

$$U_r = \sum_{i}^{N}\sum_{i<j}\sum_{k}^{M_i}\sum_{l}^{M_j} u(r_{ij}) + u_{tail} \tag{2.51}$$

where M_i and M_j are the number of sites in molecules i and j, respectively.

The quadraple sum in Equation (2.51) designates the molecular pair interactions and the atoms interctions in each moleculs. For more detail about the Lennard-Jones tail correction, please see section 2.7.2 on the page 45.

2.6.4   Calculation of residual pair virial

The residual pair virial is calculated with the following equation: (2.52):

$$w_r = \sum_{i}^{N} w(r) + w_{tail}(r) \tag{2.52}$$

where w_r is residual pair virial, $w(r)$ is the intermolecular pair virial and $w_{tail}(r)$ is the pair virial tail correction. For more detail about virial tail correction, please see section 2.7.7 on the page 47.

2.6.5   Calculation of virial pressure in NVT ensemble

There are several different (but equivalent) ways to measure the pressure of a classical N–body system. The most common among these are based on the virial equation for the pressure [36]:

$$p_{virial} = \rho\, k_B T + \frac{1}{3V}\left\langle \sum_{i=1}^{N} \overrightarrow{f}(r_{ij}) \cdot \overrightarrow{r_{ij}} \right\rangle \tag{2.53}$$

where ρ is the density of particles and $f(r_{ij})$ is the pair force exerted on particle i by particle j, derived from a pair potential and sum is over all pairs of particles in the system. $\langle \ldots \rangle$ denotes the canonical averages.

The virial pressure in molecules is calculated by Equation (2.54): [37]

$$p_{virial} = \rho\, k_B T + \frac{1}{3V}\left\langle \sum_{i=1}^{N}\sum_{i<j}\sum_{k=1}^{M_i}\sum_{l=1}^{M_j} (r_{ss}\partial\, u(r_{ss})\partial\, r)\cos(\overrightarrow{r_{ss}},\overrightarrow{r_{cc}})r_{cc}/r_{ss} \right\rangle \tag{2.54}$$

where r_{cc} is the distance between the mass centers of molecules and r_{ss} is the distance between molecules sites.

2.6.6   Calculation of the virial pressure in NpT ensemble

As a proof that the NpT simulation was correct, it is always useful to compute the virial pressure during a constant pressure simulation. On average, the virial pressure should always be equal to the applied pressure.This is easy to prove as follows:
First of all, note that the viral pressure p_{virial} of an N-particle system at volume V is equal to: [30]

$$p_{\text{virial}}(V) = \left(\frac{\partial F}{\partial V} \right)_{NT} \tag{2.55}$$

where F is Helmholtz free energy of system. In an isothermal-isobaric ensemble, the probability of finding the system with volume V is equal to:

$$P(V) = \frac{\exp[-\beta(F(V) + pV)]}{Q(N, p, T)} \tag{2.56}$$

where

$$Q(N, p, T) \equiv \beta p \int \exp[-\beta(F(V) + pV)] \mathrm{d}V \tag{2.57}$$

According to Equation 2.5 in section 2.1.2, the average value of the virial pressure can be calculated by the following equation:

$$\langle p_{\text{virial}} \rangle = \frac{\beta p \int p \exp[-\beta(F(V) + pV)]}{Q(N, p, T)} \mathrm{d}V \tag{2.58}$$

$$\langle p_{\text{virial}} \rangle = p \tag{2.59}$$

2.6.7 Calculation of packing density

The packing density or packing fraction is calculated according to Equation (2.60):

$$\eta = \frac{\pi N \sigma_{\mathrm{hs}}^3}{6V} \tag{2.60}$$

where η is the packing fraction. The Equation (2.60) shows that the packing fraction of system is connected with the volume of system. It should be noted that in NVT ensembles the system volume stays constant after each Monte Carlo cycle. In other words, packing fraction stays constant during NVT simulation. But in NpT simulations, the volume of system is changed after each cycle.

The simulation program is able to calculate the packing fraction in the system after each cycle, and the average of packing fractions is printed at the end of the simulation program. For more details about the simulation program, the reader is referred to chapter 3.

2.6.8 Long-range corrections

Periodic boundary conditions decrease the number of interactions and thus the time of calculation. Moreover, another problem of the calculation of the potential energy is that the Lennard-Jones potential has an infinite range. However, it is impossible for two particles to get far from each other because of periodic boundary conditions.

The attractive force gets infinitely weak at large distance, which it is not a physical problem, but it is a problem from computational point of view. This will limit the speed of the computation in large systems and is time-consuming.

To tackle the problem, it is necessary to pay attention to cut-off at the finite distance and choose it less than $L/2$ (L is length of the periodic box). In this case, only the interaction of a given particle with the nearest periodic image of any other particle is considered.

For more detail about the correction of the viral pressure, please see section 2.6.5 on page 41

2.7 Site–site potentials

2.7.1 The Lennard-Jones potential (LJ potential)

The Lennard-Jones potential has been widely used by both theoretical and computer simulation methods [39, 46]. This potential is an important model to explain the behavior of simple fluids, and has been used to study vapour–liquid and liquid–liquid equilibria, melting, behavior of fluids confined within small pores, small atomic clusters, a variety of surface and transport properties [40].

The LJ potential approximates the interaction between two particles (like and unlike). Repulsive force (Pauli repulsion force) and attraction force (van der Waals force and dipole–dipole) dominate at short and large distances, respectively [43].
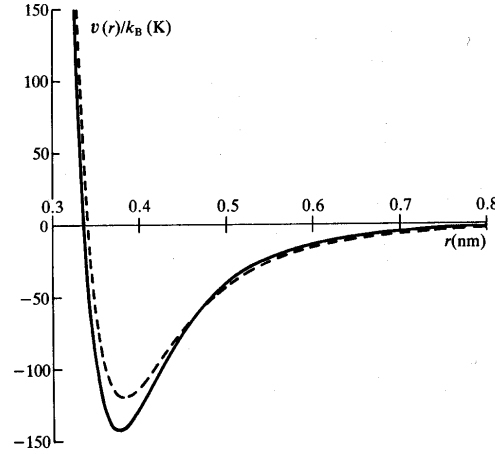
Figure 2.6: Argon pair potential, BBMS pair potential for argon (solid line) and Lennard-Jones (12/6) (dashed line).
Figure taken from
[42].

The Lennard-Jones potential for a system of spherical particles is as follows:

$$u(r_{ij}) = 4\varepsilon \left[\left(\frac{\sigma}{r_{ij}} \right)^{12} - \left(\frac{\sigma}{r_{ij}} \right)^{6} \right] \tag{2.61}$$

where r_{ij} is the distance between the mass centres of the particles, ε is the depth of the potential and σ is the distance at which energy interaction becomes zero.

According to the Equation (2.61), the LJ potential is zero if the two molecules are at infinite distance from one another.

At $r_{min} = 2^{\frac{1}{6}}\sigma$, the potential function has the value $-\varepsilon$. When $r > r_{min}$, the attractive force exceeds the repulsive force, which corresponds to the term $(\sigma/r_{ij})^6$. The attraction is caused by the van der Waals forces (induced dipole–dipole interaction).

When the distance between the mass centers of particles is smaller than r_{min}, the repulsive forces exceed the attractive forces, which corresponds to term $(\sigma/r_{ij})^{12}$ of the formula.

However the power-law representation of the potential is better suited for computer calculations. Hence, the Lennard-Jones potential is widely used in numerical simulations of the behaviour of matter.

2.7.2 Correction of the Lennard-Jones potential

It is known that the Lennard-Jones potential is not really zero at the cut-off distance. Fortunately, the potential energy can be corrected for this effect in mean field manner by adding so called tail-corrections [30],

$$u_{\text{tail}} = \frac{N\rho}{2} \int_{r_c}^{\infty} 4\pi r^2 u(r) \mathrm{d}r \tag{2.62}$$

where ρ is the numerical density, N is number of particles, r is distance, $u(r)$ is the Lennard-Jones potential and u_{tail} and r_c are the long-range correction for potential energy and cut-off distance, respectively.

If this formula is applied to the Lennard-Jones potential (Equation(2.61)), Equation (2.63) is obtained:

$$u_{\text{tail}} = \frac{8\pi\rho N\varepsilon\sigma^3}{9} \left[\left(\frac{\sigma}{r_c}\right)^9 - 3\left(\frac{\sigma}{r_c}\right)^3 \right] \tag{2.63}$$

With increasing intermolecular separation, most short-range potentials weaken rapidly. So, for distances greater than 5σ, the Lennard-Jones potential is practically zero. Therefore $2.5\sigma \leq r_c \leq 5\sigma$ is an appropriate choice for the Lennard-Jones potential.

2.7.3 The Lorentz-Berthlot mixing rules

The Lorentz-Berthlot (LB) mixing rules estimate the intermolecular pair potential parameters in mixtures. According to these rules the potential parameters ε_{ij} and σ_{ij} of mixtures can be calculated by the following equations: [68, 69]

$$\varepsilon_{ij} = \sqrt{\varepsilon_{ii}\varepsilon_{jj}} \tag{2.64}$$

$$\sigma_{ij} = \frac{\sigma_{ii} + \sigma_{jj}}{2} \tag{2.65}$$

2.7.4 The Mie potential

London showed from the theory of dispersion forces in quantum mechanics that the exponent of the second term in the Lennard-Jones potential is equal to 6, but 12 as exponent in first term does not have any scientific basis and came from experiment data. It should be noted that the use of 12 as power in first term of Lennard-Jones potential has a great advantage in computer simulations because 12 is two times more than the exponent of the second term, and this gives higher computational speed.

Equation (2.66) is called Mie potential; it was proposed by Mie in 1903. Evidently, the Lennard-Jones potential is a special form of the Mie potential,

$$u(r) = \alpha\varepsilon\left[\left(\frac{\sigma}{r}\right)^n - \left(\frac{\sigma}{r}\right)^m\right] \qquad\qquad n \neq m \qquad\qquad (2.66)$$

where

$$\alpha = \left(\frac{n}{n-m}\right)\left(\frac{n}{m}\right)^{\frac{m}{(n-m)}} \qquad\qquad\qquad (2.67)$$

and ε is the intermolecular energy parameter for which $u_{\min}(r) = \epsilon$ and σ is the inter-molecular length parameter for which $u(r) = 0$ is the intermolecular distance.

2.7.5   Correction of the Mie-potential

Substitution of Equation (2.66) into Equation (2.62) yields the Mie-potential tail corrections (Equation (2.68)),

$$u_{\text{tail}}(r) = 2N\pi\rho\varepsilon\alpha\left[\frac{1}{n-3}\left(\frac{\sigma^n}{r_{\text{c}}^{n-3}}\right) - \frac{1}{m-3}\left(\frac{\sigma^m}{r_{\text{c}}^{m-3}}\right)\right] \qquad\qquad (2.68)$$

where $u_{\text{tail}}(r)$ is the long-range correction of the potential and r_{c} is the cut-off distance.

2.7.6   Calculation of Mie force

The connection between potential and force is explained by Equation (2.69) [76]:

$$f(r) = \frac{-\partial u(r)}{\partial r} \qquad\qquad\qquad (2.69)$$

After inserting Equation (2.66) in Equation (2.69), the Mie force can be calculated for various exponents in the repulsive term,

$$f(r) = \alpha\varepsilon\left[\left(\frac{n\sigma^n}{r^{n+1}}\right) - \left(\frac{m\sigma^m}{r^{m+1}}\right)\right] \qquad\qquad (2.70)$$

where σ and r are diameter of a molecule and distance between particles, respectively.

2.7.7   Correction of Mie potential pair virial

The tail correction of the intermolecular pair virial is computed with the Equation (2.71).

$$w_{\text{tail}}(r) = 2\pi\rho N \int_{r_{\text{c}}}^{\infty} \frac{-\partial u(r)}{\partial r} r^3 \mathrm{d}r \tag{2.71}$$

When the Mie-potential (Equation (2.67)) is substituted into Equation (2.71), the tail correction of the intermolecular pair virial is obtained as Equation (2.72),

$$w_{\text{tail}}(r) = 2N\pi\rho\varepsilon\alpha \left(\frac{n\sigma^n}{(n-3)r_{\text{c}}^{n-3}} - \frac{m\sigma^m}{(m-3)r_{\text{c}}^{m-3}} \right) \tag{2.72}$$

where N is number of particles.

2.7.8   Calculation of virial compression factor

The Virial compression factor (Z_{virial}) is calculated from the virial pressure. The Virial pressure was explained before in section 2.6.5 on page 41 [30].

$$Z_{\text{virial}} = 1 + \frac{1}{3N k_{\text{B}} T} \left\langle \sum_{i=1}^{N} \sum_{i<j} w(r) + w_{\text{tail}}(r) \right\rangle \tag{2.73}$$

2.7.9   The hard-sphere Potential

If the molecules are rigid spheres, they are not deformed by collision, and no attractive force acts between the molecules. The pair potential is given by the following equation,

$$u(r) = \begin{cases} \infty & r \leq \sigma_{\text{hs}} \\ 0 & r > \sigma_{\text{hs}} \end{cases} \tag{2.74}$$

where σ_{hs} is the hard-sphere diameter.

The Equation (2.74) shows that, if the distance between two particles is less than the sum of their radiuses, then the potential of particles is ∞ and if the distance between two particles is greater than the sum of their radiuses, then the potential energy of them is equal to 0.

2.7.10 Calculation of Carnahan-Starling compressibility factor

The Carnahan-Starling equation of state is an approximate equation for the fluid phase to calculation of compressibility factor. This equation is given by [68],

$$Z_{CS} = 1 + \frac{\eta(4 - 2\eta)}{(1 - \eta)^3} \tag{2.75}$$

where Z is compressibility factor and η is the packing fraction that is already mentioned in section 2.6.7 on the page 43.

2.8 Radial distribution function
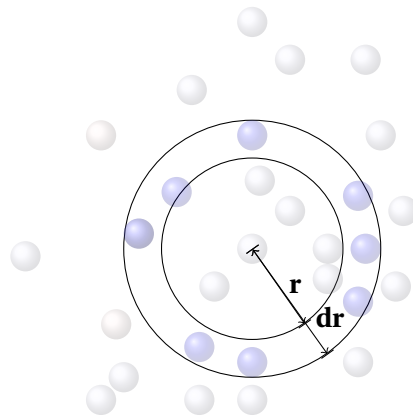
Figure 2.7: Space distribution for the evaluation of the radial distribution function.

The radial distribution function $g(r)$ describes how the particles in a system (such as liquids and gases) are packed around each other. In the real fluid like liquids, where continuous movement of the particles must be considered, it is extremely useful to be able to deal with the average structure. It should be noted, that the radial distribution function in molecules and mixture most be calculate considering the site-site radial distribution function. For instance, in mixture Neon and Krypton, we distinguish only two atomic sites, neon and krypton, thus three site-site RDF, namely $g_{Ne-Ne}(r)$, $g_{Ne-Kr}(r)$ and $g_{Kr-Kr}(r)$ should be calculated.

2.8.1 Radial distribution function in Lennard-Jones fluids

The following steps explain, how is calculated the radial distribution function in Lennard-Jones fluids:

- First of all a test particle i with position r_i is chosen.

- The space around the test particle i is divided into shells by a series of small concentric spheres with increasing radius Δr.

- A particle j in a shell has a distance $r_{ij} = |r_i - r_j|$ from particle i where $r - \Delta r < r_{ij} < r$. $n_i(r, \Delta r)$ determine the number of particles in the shell.

- The number of particles in the shell is divided by the volume of the shell and after that the average should be divided by the reference particles.

$$g(r) \simeq \frac{1}{N} \sum_i^N \frac{n_i(r, \Delta r)}{4\pi r^2 \Delta r} \qquad (2.76)$$

- In last step, the radial distribution function is normalized by the particle density:

$$g(r) = \frac{V}{4\pi r^2 \Delta r N^2} \sum_i^N n_i(r, \Delta r) \qquad (2.77)$$

In a very short r the radial distribution function must be zero, because two particles can not occupy the same space and they can not approach more closely. Outside the van der Waals diameter there is a peak because the remaining N-1 particles try to diffuse into the region occupied by the first one at the origin.

The peaks are particulary sharp in crystalline materials, where atoms are confined in their positions. At very long ranges every RDF tends to a value of 1, which happens because the RDF describes the average density at this range. The algorithm to caculation of radial distribution function is presented in chapter 6 on the page 119.

2.8.2 Radial distribution function in hard-sphere fluids

In 1957, Percus and Yevick (PY) presented an equation for the calculation of the radial distribution function $g(r)$ of hard-sphere fluids [44]. In their theory, the total correlation function $h(r)$ is defined by

$$h(r_{12}) = g(r_{12}) - 1 \qquad (2.78)$$

For $r \to \infty$, the total correlation function goes to zero because there exists no correlation between the two molecules 1 and 2. The direct correlation function $c(r)$ is defined by

$$h(r_{12}) = c(r_{12}) + \rho \int h(r_{23}) c(r_{13}) \mathbf{dr}_3 \qquad (2.79)$$

where ρ is the particle number density. Equation (2.79) is called the Ornstein-Zernicke relation [45]. It expresses the fact that the total correlation between two molecules 1 and 2 can be split in two contributions. There is a direct effect described by $c(r_{12})$, which is of short range, i.e. approximately of the range of the pair potential. In addition to this direct effect there is an indirect effect, in which molecule 1 influences molecule 3, which in turn acts on molecule 2 [50].

A density expansion can be made, in which higher order terms reflect the indirect effects of molecules 4, 5,$\cdots$ on the correlation between the molecules 1 and 2. The important advantage of $c(\mathbf{r})$ over $g(\mathbf{r})$ lies in its short range, which essentially agrees with that of the pair potential [50].

The direct correlation function $c(r)$ represents the direct correlation between two particles in system containing N-2 other particles. According to Percus and Yevick (PY), it can be represented by

$$c^{\mathrm{PY}}(r) = g^{\mathrm{PY}}(r)(1 - e^{U/k_{\mathrm{B}}T}) \tag{2.80}$$

Substitution of Equations (2.78) and (2.80) into Equation (2.79) relation yields

$$g^{\mathrm{PY}}(r_{12})e^{U(r_{12})/k_{\mathrm{B}}T} = 1 + \rho \int \left[g^{\mathrm{PY}}(r_{23}) - 1\right] g^{\mathrm{PY}}(r_{13})(1 - e^{U(r_{13})/k_{\mathrm{B}}T})d\mathbf{r}_3 \tag{2.81}$$

For hard-sphere molecules

$$g_{\mathrm{hs}}(r) = 0 \qquad\qquad r \leqq \sigma_{\mathrm{hs}} \tag{2.82}$$

and the pair correlation function has a discontinuity at $r = \sigma_{\mathrm{hs}}$. However, the background correlation function $y_{\mathrm{hs}}(r)$ has the property of being finite for $r < \sigma_{\mathrm{hs}}$ and $r > \sigma_{\mathrm{hs}}$ and is continuous at $r = \sigma_{\pm\mathrm{hs}}$.

$$y_{\mathrm{d}}(r) = e^{U_{\mathrm{hs}}(r)/k_{\mathrm{B}}T} g_{\mathrm{hs}}(r) \tag{2.83}$$

According to Equations (2.80) and (2.83), the direct pair correlation function for hard-sphere is:

$$c_{\mathrm{hs}}^{\mathrm{PY}}(r) = -y_{\mathrm{hs}}^{\mathrm{PY}}(r) \qquad\qquad \text{for} \quad r \leqq d_- \tag{2.84}$$

$$c_{\mathrm{hs}}^{\mathrm{PY}}(r) = 0 \qquad\qquad \text{for} \quad r \geqq d_+ \tag{2.85}$$

where d is the sphere diameter. Substituting Equations (2.83) and (2.84) into (2.81) gives the Percus-Yevick equation for hard-spheres:

$$y_{\mathrm{hs}}^{\mathrm{PY}}(r_{12}) = 1 + n \int_{r_{13}<\sigma} y_{\mathrm{hs}}^{\mathrm{PY}}(r_{13}) \mathrm{d}r_3 - \rho \int_{\substack{r_{13}<\sigma_{\mathrm{hs}} \\ r_{23}>\sigma_{\mathrm{hs}}}} y_{\mathrm{hs}}^{\mathrm{PY}}(r_{13}) y_{\mathrm{hs}}^{\mathrm{PY}}(r_{23}) \mathrm{d}\mathbf{r}_3 \qquad (2.86)$$

The Equation (2.86) can be solved analytically with the Laplace transform method giving [51, 54, 55],

$$c_{\mathrm{hs}}^{\mathrm{PY}}(r^*) = -\lambda_1 - 6\eta\lambda_2 r^* - 0.5\eta\lambda_1 r^{*3} \qquad r^* = r/\sigma_{\mathrm{hs}} \leqq 1_- \qquad (2.87)$$

$$c_{\mathrm{hs}}^{\mathrm{PY}}(r^*) = 0 \qquad\qquad\qquad r^* \geqq 1_+ \qquad (2.88)$$

where

$$\lambda_1 = \frac{(1+2\eta)^2}{(1-\eta)^4} \qquad (2.89)$$

and

$$\lambda_2 = \frac{-(1+0.5\eta)^2}{(1-\eta)^4} \qquad (2.90)$$

In Equations (2.87),(2.89) and (2.90), η denotes the packing fraction which was presented before in section 2.6.5.

At suitable spacing δ, which we wish to tabulate $h(r)$, we have $n+1$ points 0, δ, 2δ, ..., nδ=1. In $0<r \leq 1$,

$$q_k = q(k\delta) \qquad k = 0,1,2,3,\dots,n \qquad (2.91)$$

Perram's numerical method to calculate the pair correlation function of a hard-sphere system with PY-approximation is described by the following formulas:[50, 70]

$$[r^* h_d(r^*)]_{n+k} = \frac{12\eta\Delta r^*}{1-6\eta\Delta r^* q_0} \sum_{j=1}^{n-1} q_j [r^* h_d(r^*)]_{n+k-j} \qquad (2.92)$$

with

$$r^* = \frac{r}{d} \tag{2.93}$$

$$h_d(r^*) = g_d(r^*) - 1 \tag{2.94}$$

$$q_j = q(i\Delta r^*) = \frac{1 + 2\eta((i\Delta r^*)^2 - 1)}{2(1-\eta)^2} - \frac{1.5\eta(i\Delta r^* - 1)}{(1-\eta)^2} \tag{2.95}$$

and

$$[r^* h_d(r^*)]_n = \frac{(-1 + 4.5\eta - 2\eta^2)}{2(1-\eta)^2} \tag{2.96}$$

2.9 Calculation of entropy-related properties

The simulation program (see chapter 3) is able to calculate some important thermodynamic properties, such as chemical potential, internal energy, compression factor, Monte Carlo shift parameter etc. (see section 3.1 in chapter 3).

As stated before, the aim of this project is to explain the connection between residual entropy and Monte Carlo shift parameter in fluids. But with the simulation program, it is not possible to calculate residual entropy directly. The following sections (2.9.1 to 2.9.2) explain how to calculate the residual entropy from NVT and NpT simulations.

2.9.1 The chemical potential

Chemistry usually involves solutions, reacting systems and mixtures in which the amounts of substance, n_i of each present can be variable. When this happens, the extensive properties, $Z = V, S, U, H, A$ or G become functions of the composition variables. This can be mathematically expressed as [32]:

$$Z = f(X, Y, n_1, n_2, \ldots) \tag{2.97}$$

where X and Y represent the state variables, and each n_i gives the amount of substance for the ith component. The total differential dZ is given by

$$dZ = \left(\frac{\partial Z}{\partial X}\right)_{Y,n} dX + \left(\frac{\partial Z}{\partial Y}\right)_{X,n} dY + \sum_i \left(\frac{\partial Z}{\partial n_i}\right)_{X,Y,n_{j\neq i}} dn_i + \cdots \tag{2.98}$$

where the subscripts of the partial derivations $(\partial Z/\partial n_i)_{X,Y,n_{j\neq i}}$ mean that variables X, Y, and all amounts of substance except that for the ith species, stay constant.

Substitution of the Gibbs free energy into Equation (2.98) gives

$$dG = \left(\frac{\partial G}{\partial T}\right)_{p,n} dT + \left(\frac{\partial G}{\partial p}\right)_{T,n} dp + \sum_i \left(\frac{\partial G}{\partial n_i}\right)_{T,p,n_{j\neq i}} dn_i \tag{2.99}$$

where the derivatives inside the summation are taken at constant T and P and the first two partial derivatives are taken at constant composition.

The quantity $(\partial G/\partial n_i)_{T,p,n_{j\neq i}} dT$ is called the chemical potential of the ith component and given the symbol μ_i so that

$$\mu = \left(\frac{\partial G}{\partial n_i}\right)_{T,p,n_{j\neq i}} \tag{2.100}$$

We know that

$$-S = \left(\frac{\partial G}{\partial T}\right)_{p,n} \tag{2.101}$$

and

$$V = \left(\frac{\partial G}{\partial p}\right)_{T,n} \tag{2.102}$$

Substitution of Equations (2.100), (2.101) and (2.102) into Equation (2.99) gives

$$dG = -SdT + Vdp + \sum_i \mu_i dn_i \tag{2.103}$$

Under the conditions of constant temperature(T) and pressure(p), Equation (2.103) becomes Equation (2.104)

$$dG = \sum_i \mu_i dn_i \tag{2.104}$$

It is possible to define μ_i, starting with

$$U = f(S, V, n_1, n_2) \tag{2.105}$$

The total differential in internal energy can be given as Equation (2.106)

$$dU = \left(\frac{\partial U}{\partial S}\right)_{V,n} dS + \left(\frac{\partial U}{\partial V}\right)_{S,n} dV + \sum_i \left(\frac{\partial U}{\partial n_i}\right)_{S,V,n_{j\neq i}} dn_i \tag{2.106}$$

With constant n's, Equation (2.107) is obtained from Equation (2.106)

$$dU = \left(\frac{\partial U}{\partial S}\right)_{V,n} dS + \left(\frac{\partial U}{\partial V}\right)_{S,n} dV \tag{2.107}$$

where

$$T = \left(\frac{\partial U}{\partial S}\right)_{V,n} \tag{2.108}$$

$$-p = \left(\frac{\partial U}{\partial V}\right)_{S,n} \tag{2.109}$$

Substituting Equations (2.108) and (2.109) in Equation (2.106) gives

$$dU = TdS - pdV + \sum_i \left(\frac{\partial U}{\partial n_i}\right)_{S,V,n_{j\neq i}} dn_i \tag{2.110}$$

According to the fourth Gibbs Equation, we know that

$$dG = dU + d(pV - TS) \tag{2.111}$$

If $d(pV - TS)$ is added to both sides of Equation (2.110), we obtain

$$dG = TdS - pdV + \sum_i \left(\frac{\partial U}{\partial n_i}\right)_{S,V,n_{j\neq i}} dn_i + pdV + Vdp - TdS - SdT \tag{2.112}$$

Cancellation of terms gives

$$dG = -SdT + Vdp + \sum_i \left(\frac{\partial U}{\partial n_i}\right)_{S,V,n_{j\neq i}} dn_i \tag{2.113}$$

Comparing the terms in Equations (2.103) and (2.113) leads to

$$\mu_i = \sum_i \left(\frac{\partial U}{\partial n_i} \right)_{S,V,n_{j\neq i}} dn_i \tag{2.114}$$

Substitution the Equations (2.108), (2.109) and (2.114) in Equation (2.106) finally gives

$$dU = T dS - p dV + \sum_i \mu_i dn_i \tag{2.115}$$

2.9.2 Homogeneous functions and entropy

According to Euler equation, the fact that energy of any system can be expressed as a homogeneous 1st order function of the extensive variable S, V and n_i implies that the function U scales with the size of the system. In other word, if S, V and n_i are all multiplied by some factor λ, then U will be changed by the same factor: [33, 65]

$$U(\lambda S, \lambda V, \lambda n_1, \cdots, \lambda n_m) = \lambda U(S, V, n_1, \cdots, n_m) \tag{2.116}$$

With respect to λ, Equation (2.106) can be rewritten as

$$dU(S,V,n) = \left[\left(\frac{\partial U}{\partial(\lambda S)} \right)_{V,n} \frac{d(\lambda S)}{d\lambda} + \left(\frac{\partial U}{\partial(\lambda V)} \right)_{S,n} \frac{d(\lambda V)}{d\lambda} + \left(\frac{\partial U}{\partial(\lambda n)} \right)_{S,V} \frac{d(\lambda n)}{d\lambda} \right] d\lambda \tag{2.117}$$

which simplifies to

$$dU(S,V,n) = \left[\left(\frac{\partial U}{\partial(\lambda S)} \right)_{V,n} S + \left(\frac{\partial U}{\partial(\lambda V)} \right)_{S,n} V + \left(\frac{\partial U}{\partial(\lambda n)} \right)_{S,V} n \right] d\lambda \tag{2.118}$$

Setting $\lambda = 1$ in Equation (2.118), we obtain:

$$dU = \left[\left(\frac{\partial U}{\partial S} \right)_{V,n} S + \left(\frac{\partial U}{\partial V} \right)_{S,n} V + \left(\frac{\partial U}{\partial n} \right)_{S,V} n \right] d\lambda \tag{2.119}$$

The partial derivatives in Equation (2.119) are now just the definitions of the extensive variables T, p, and n. Equation (2.119) can be integrated over λ, giving

$$U = TS - pV + \sum_i \mu_i n_i \tag{2.120}$$

2.9.3   Widom insertion method (PI method)

The Monte Carlo method (MC) is an efficient method for the determination of thermodynamic properties. But the calculation of free energy by MC simulation method is not directly possible because entropy can not be obtained as an ensemble average [39].

Because of this problem, several methods have been proposed to calculate the configurational free energy for fluids and solids [49, 52].

The Widom insertion method (or Widom sampling) is a general simulation technique to obtain the residual chemical potential (species in a pure fluid or in a mixture), which was proposed by Benjamin Widom in 1963 [3–5].

This approach is most widely applied in molecular computer simulation [47, 48], but has also been applied in the development of analytical statistical models.

As a rule, first of all, a Monte Carlo simulation should be done to obtain an equilibrium; after that, a new particle is inserted in a random coordination in simulation box.

This new position is chosen randomly, so that all of the positions in simulation box have the same probability to be selected. The new particle is only added for the calculation of the internal energy difference, and after that removed.

$$\mu^r = \mu - \mu_{\text{ideal}} = -k_B T \ln \left\langle \exp \frac{-\Delta U}{k_B T} \right\rangle_N \tag{2.121}$$

where k_B is the Boltzmann constant, T is the absolute temperature, ΔU is the difference in internal energy before and after the insertion of the test particle and $\langle \dots \rangle$ denotes canonical ensemble averaging over all configuration of the N positions in the volume V.

The internal energy difference (ΔU) can be obtained by calculating the internal energy before and after the insertion of a new particle. The test particle insertion method has proved very useful for obtaining chemical potential at low density systems. This method, however, is difficult to apply at high densities due to the extremely low acceptance ratios of the particle insertions. Furthermore, this method is inefficient, if the newly added particle does not have a spherical shape.

2.9.4   Alternatives routes to the entropy

There are several other methods to calculate the residual entropy in fluids. Two of them are **Scheraga's theory** and **the estimation of entropy from the radial distribution function**. To measure the accuracy of results (chapter 4), the results of simulation program are compared with the results of these methods (see section 4.7 in chapter 4). These two methods are explained briefly in sections 2.9.5 and 2.9.6, respectively.

2.9.5 Scheraga's theory

Scheraga's theory is a method to calculate entropy and free energy of solids and fluids from the radial free space distribution function (RFSDF) [53].

The RFSDF is defined as the following ratio in the Metropolis Monte Carlo procedure [52],

$$y(r) = \frac{\text{total number of acceptances of displacement} \, r}{\text{total number of attempts of displacement} \, r}, \tag{2.122}$$

where the function $y(r)$ starts with $y=1$ at $r=0$ and decreases to zero at high densities (large r). But $y(r)$ has limiting values other than zero at low and moderately high density, when r exceeds some distance larger than the cell radius [52].

The cell radius is about twice the average of nearest neighbor distances. $y_\infty < 1$ means that a particle can escape from the cell constructed to new positions outside the cell with a probability of y_∞.

At low density, the value of y_∞ departs from zero because there, a particle can escape easily from its position. In other words, the particles in this system behave like an ideal gas, and in an ideal gas $y_\infty = 1$.

The molar free volume is defined as:

$$V^{\mathrm{f}} = y_\infty V_{\mathrm{id}}^{\mathrm{f}} + (1 - y_\infty)(4\pi N) \int_0^\infty C[y(r) - y_\infty] r^2 \mathrm{d}r \tag{2.123}$$

Here is V^{f}, the molar free volume, $V_{\mathrm{id}}^{\mathrm{f}}$ is the free volume in an ideal gas with same density, N is the number of particles in the system and C is a normalization factor that is equal to $(1 - y_\infty)^{-1}$.

Equation (2.123) can be rewritten as:

$$\frac{V^{\mathrm{f}}}{V_{\mathrm{id}}^{\mathrm{f}}} = y_\infty + (4\pi\rho\sigma^3) \int_0^\infty [y(r') - y_\infty] r'^2 \mathrm{d}r' \tag{2.124}$$

Here are $\rho = N/V$, $r' = r/\sigma$ and σ, the hard-sphere diameter or the parameter σ in the Lennard-Jones potential. It should be noted, that $y(r') - y_\infty$ in Equation (2.124) decreases to zero at the cell radius.

According to free-volume theory [43], the partition function of system Q_{N} with N molecules at temperature T can be approximated in terms of single molecule partition function Q,

$$Q_{\mathrm{N}} \simeq Q^{\mathrm{N}} \simeq \left[\lambda^{-3} \sigma V^{\mathrm{f}} \exp\left(\frac{-\psi_0}{2k_{\mathrm{B}}T} \right) \right]^N \tag{2.125}$$

where λ is the thermal wavelength $(\lambda = h/(\sqrt{2\pi m k_{\mathrm{B}}T}))$, k_{B} and ψ_0 being the Boltzmann's constant and the average potential energy in a cell, respectively.

The entropy is given by: [26]

$$\frac{S_r}{R} = T\left(\frac{\partial \ln Q_N}{\partial T}\right)_V + \ln Q_N \tag{2.126}$$

Here is R, the universal gas constant and T is absolute temperature. For interactive systems other than the hard-sphere system, it was assumed that at fixed volume V, the first term in Equation (2.126) is small compared to the second term. Therefore, Equation (2.127) can be obtained from Equations (2.125) and (2.126):

$$\frac{S_r}{R} = \ln\left(\frac{V^f}{V_{id}^f}\right) \tag{2.127}$$

2.9.6   The estimation of entropy from radial distribution function

The thermodynamic entropy of a system can be written as

$$S = S_1 + S_2 + S_3 + \ldots = S_{id} + S_r, \tag{2.128}$$

where S_n is the entropy contribution due to the n-particles spatial correlation [56].

The entropy of an ideal gas S_{id} can be calculated as the following equation

$$S_{id} = N k_B\left[\ln\left(\frac{V}{N}\left(\frac{4\pi m U}{3N h^2}\right)^{3/2}\right) + \frac{5}{2}\right], \tag{2.129}$$

where U and h are the internal energy and plank's constant, respectively. The S_r can be estimated from the two-body contribution to the residual entropy $S_r^{(2)}$ in an expansion of S_r with respect to the radial distribution function $g(r)$ [63, 64].

$$S_r^{(2)} = (-2N\pi\rho\, k_B)\int \{[g(r)\ln g(r)] - [g(r) - 1]\} r^2 \mathrm{d}r, \tag{2.130}$$

where $g(r)$ is radial distribution function of pure species (that was discussed before in sections 2.8.1 and 2.8.2), r is distance and k_B and ρ are the Boltzmann constant and numerical density, respectively.

The quantity $S_r^{(2)}$ formally emerges as the leading order term in the N-body distribution function expansion of the excess entropy of an isotropic liquid [60]. The definition (2.130) was originally introduced by Nettleton and Green [61] and later developed by Raveché [56], using an alternative approach as an expression for the two-body contribution to the excess entropy appropriate for use only in the grand canonical ensemble

[62]. This restriction was later lifted by Baranyai and Evans, who showed that the expression is actually ensemble–invariant [63].

If the value of $g(r)$ is close to 1, Equation (2.130) can be rewritten:

$$\ln[g(r)] \approx \ln[1 + g(r) - 1] \approx g(r) - 1 \qquad (2.131)$$

$$S_{\mathrm{r}}^{(2)} \approx (-2N\pi\rho\, k_B)\int [g(r) - 1]^2 r^2 \mathrm{d}r \qquad (2.132)$$

2.10 Percolation theory

2.10.1 Introduction

The aim of this section and the next one is explain *what is percolation* and *how it affects the results of entropy determination by means of Monte Carlo simulation*. Before answering these questions, first of all it is useful to discuss the relevance of percolation theory for this work.

During the simulation runs in NVT ensemble (for more details please see chapter 3), the energy is calculated for series of systems with different gradually increasing volumes.

It is seen in the results that the acceptance ratios do not stay constant with increase of volume. At particular volume, the ratio even begins to increase.

In this work, only the effects of percolation because of free volume is treated.

2.10.2 The percolation problem

Percolation is a standard model for disordered systems [66, 67, 72], with-wide spread applications in nature, and was introduced by Broadbent and Hammersley in 1957 as a mathematical model for random particles [71, 73, 74]. Percolation theory is the test ground for studying more complicated critical phenomena and a great source of intuition.

Percolation processes are those in which, by the random addition of a number of objects, a contiguous path which spans the entire system in created. In general, particles may be distributed continuously in space and the overlap between particles determines the conected paths [31].

There are two different kinds of percolation:
site and **bond percolation**.

The difference between site percolation and bond percolation is that in site percolation, the sites of a lattice have been occupied randomly with fixed acceptance, whereas in bond percolation the points in fixed positions connect each other. The Figures 2.8
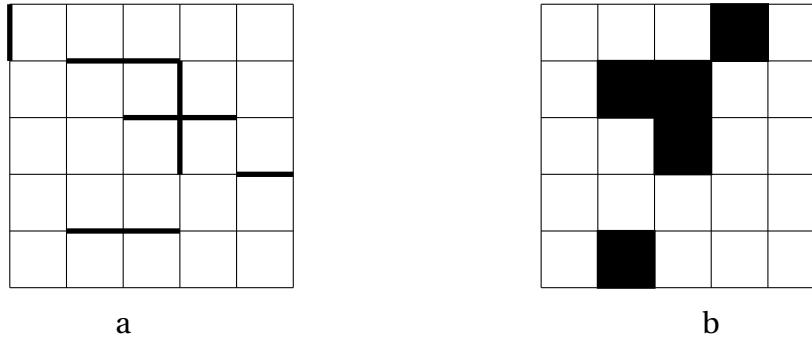
Figure 2.8: a.Bond and b.side percolation.

illustrate the both kind of percolation.

Percolation can be happen in one, two and three dimensions.

1-dimensional percolation:

Figure 2.9: Percolation in one dimension.

Figure 2.9 presents percolation on a 1-dimension lattice. Sites are occupied with probability P. In the part of the infinite 1-dimension lattice in Figure 2.9, there is one cluster with size 5, one cluster with size 2, and three clusters with size 1.

2-dimensional percolation: Figure 2.10 illustrates 2-dimension percolation. A lattice square that is randomly filled with black and white sites. A cluster is a connected group of white sites. Percolation occurs if it is possible to move from one site of this cluster to another side by repeatedly stepping to an adjacent white side without touching the black site.

The size of clusters plays very important roles in percolation. If there are only few white sites, the clusters are too small to connect to opposite sides of the square lattice.

If the number of white sites is large, it is possible to connect to the top and the bottom of the lattice. If almost all sites are white, there are many possible paths.

P_{path} is the probability of a path from top to bottom of square. It depends on the linear size of the lattice L and probability that a site is white (P).

If the probability of white side is P, the probability that a side is black should be 1-P. As L increases, P_{path} shows a very intriguing limiting behaviour. In two dimensions, below a critical value $P_c \approx 0.593$ is approximately zero. On the other hand, for all P larger than P_c , P_{path} is almost equal to 1. It means that for large lattices there

Figure 2.10: Percolation in two dimensions.
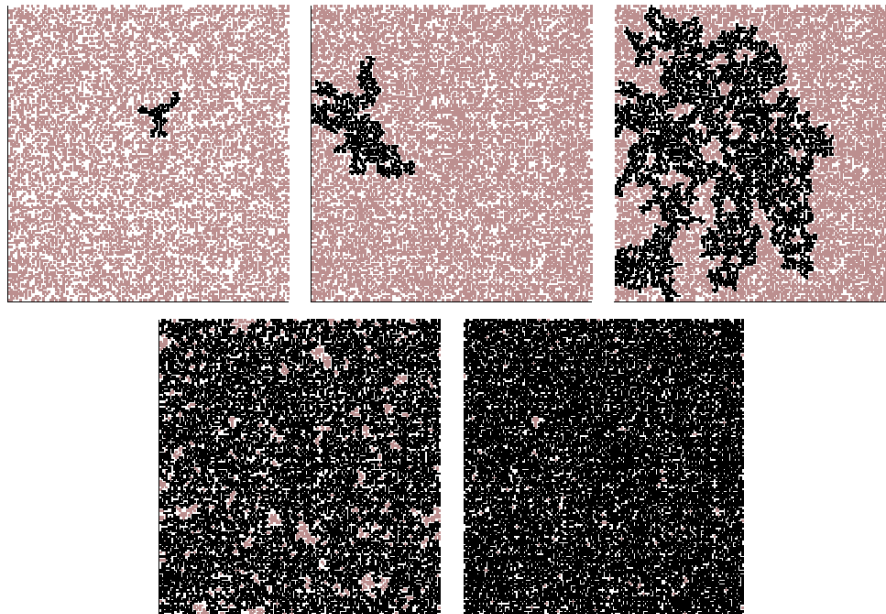
Figure 2.11: Percolation in 2 dimension square lattices with size $L = 150 \times 150$.
Occupation probability P=0.45, 0.55, 0.59, 0.65, and 0.75, respectively. Figure taken from
[75].

is a sudden change in the global connecting.

$$\lim_{L\to\infty} P_{\text{path}}(P,L) = \begin{cases} 0 & \text{for} \quad P < P_{\text{c}} \\ 1 & \text{for} \quad P \geq P_{\text{c}} \end{cases} \tag{2.133}$$

In the limit of infinite L, P_{path} becomes a step function, jumping from 0 to 1 at P_c .In finite lattices $L < \infty$, if the occupation probability P is small, there is only a very tiny probability of having a cluster percolation between two opposite boundaries. For P close to 1, certainly will have been a cluster percolating through the system. In Figure 2.11, sites in 2 dimension square lattices are occupied at random with increasing occupation probability P.

The occupied sites belonging to the largest cluster are shown in black while the occupied sites are shown in purple and unoccupied sites are white. Notice that for $P_c \approx 0.59$, a percolating cluster appears for the first time [75].

2.11   Reduced Units

In simulation, it is common to measure quantities (pressure, temperature, density, etc.) in reduced units. It means that a convenient unit of energy length and mass are chosen and the other quantities are measure in term of these basic units. The following parameters are chosen as the basic units in Lennard-Jones term:

- unit of energy (ε)

- unit of mass (m)

- unit of length (σ)

and all of the following units can be expressed from these basic units:

- the reduced pair potential: $u^* = \dfrac{u}{\varepsilon}$

- the reduced pressure: $P^* = \dfrac{P\sigma^3}{\varepsilon}$

- the reduced density: $\rho^* = \rho\sigma^3$

- the reduced temperature: $T^* = \dfrac{k_{\text{B}}T}{\varepsilon}$

- the reduced length: $r^* = \dfrac{r}{\sigma}$

- the reduced energy: $E^* = \dfrac{E}{\sigma}$

- the reduced force: $f^* = \dfrac{f\sigma}{\varepsilon}$

Another, practical reason for using reduced units is that when we work with real (SI) units, we find that the absolute numerical values of the quantities that we are

computing are either much less or much larger than 1 (double precession range is 10^{-308} to 10^{+308}).

If we multiply several such quantities using standard floating-point multiplication, we risk that, at some stage, we will obtain a results that creates an overflow or underflow. Conversely, in reduced units, almost all quantities of order 1 (say, between 10^{-3} to 10^{+3}). Hence, if we suddenly find a very large number in our simulation, then there is a good chance that we have made an error somewhere [30].

Chapter 3

Simulation Programs

3.1　Details of the computer simulation program mc++

mc++ is a Monte Carlo simulation program written in C++. It uses an object-oriented design and strictly separates molecular properties (the so-called models) from ensemble data and simulation control parameters: It is thus possible to use mc++ with various pair potentials. mc++ uses classes to handle data relevant for the simulation.

input and output:

The main class in the simulation program is class **mc**. The purpose of this class is to get the input data to start the calculation and to print the results after finishing of simulation program. The simulation program requires the following parameters:

- number of processors to be used.

- simulation type (NVT or NpT).

- number of components.

- the name of each components.

- number of sites.

- site data (x, y, z, type, molar mass (g/mol), $\sigma_{\mathrm{hs}}(\text{Å})$).

- number of molecules of this kind.

- parameters for site-site interactions (depends on pair potential, for example for Lennard-Jones potential $\varepsilon/k_{\mathrm{B}}$ (K) and $\sigma_{\mathrm{LJ}}(\text{Å})$).

- $V_{\mathrm{m}}(\text{cm}^3/\text{mol})$, $T(\text{K})$ or $p(\text{MPa})$, $T(\text{K})$.

- number of compression cycles (only in NVT simulation).

- number of equilibration cycles.

- number of production cycles.

During the run the program, after each 100 cycles, the simulation program reports the number of cycles, the maximum displacement, the size of box, reduced density, and internal energy. After finishing of calculation, the simulation program reports the following results:

- Z_{virial} (compression factor from virial theorem)

• Z (compression factor from p and V)

• Z_{CS} (from density and given pressure, only for NpT simulation)

• U_r (J/mol K)(residual internal energy)

• μ_r (J/mol)(residual chemical potential)

• V_m(cm^3/mol)

• p_{red}(reduced pressure)

• dx(Å) (displacement parameter of Monte Carlo simulation)

• dx^2(Å^2) (quadratic average displacement of Monte Carlo simulation)

• acc$_t$ (average acceptance ratio)

For mixtures, some orientation correlation data are printed too.

class Canonical:

This class contains descriptions of a simulation ensemble and vector of molecules. The following calculations are done in this class:

• **bf_insertion:** Calculation of Boltzmann factor of change energy (that be needed to calculation of chemical potential according to Widom test insertion method).

• **change_v:** Tentative volume change.

• **configure:** Set up all vectors and matrices with their proper sizes.

• **dx2:** Calculation of dx^2 (square distance from initial configuration).

• **expand:** Do a volume expansion.

• **init_gas:** Initialize an ensemble by placing molecules at random into a very large volume

• **move:** Random shift and rotation of a molecule .

• **usum1:** Calculation of interaction energies and rotation (one molecule against the others).

• **usum2:** Calculation of the total residual energy.

- **utail:** Calculation of energy tail correction summation.

- **virsum2:** Calculation of the total virial of the ensemble including the tail correction.

class MC_statistics:

The statistical averages of Monte Carlo simulation are calculated in this class. Moreover, the following operations are done in this class:

- **adjust_dx:** A new maximum length shift parameter is calculated so that the acceptance ratio is maintained.

- **adjust_qv:** optimize parameters for isobaric volume changes.

class Model1:

The class contains functions to read the molecular structure, the site data and check the molecules for overlapping. Moreover the following function is in this class:

- **normalize:** Shift the center of gravity to zero.

class Model1set:

This class contains merely one function:

- **sitecount:** determine the number of different site types.

class Model2:

This class contains the pair potentials and their parameters. The following parameters are calculated in this class:

- **u:** calculation of pair potential between two sites.

- **utail:** calculation of energy tail correction.

- **fr:** calculation of force-distance product.

- **frtail:** calculation of tail correction force-distance product.

class Molecule

This class contains the coordinates for each molecules. The only function in this class is:

- **displace:** random displacement of rigid molecules.

Figure 3.1: Schematic representation of the simulation program mc++.
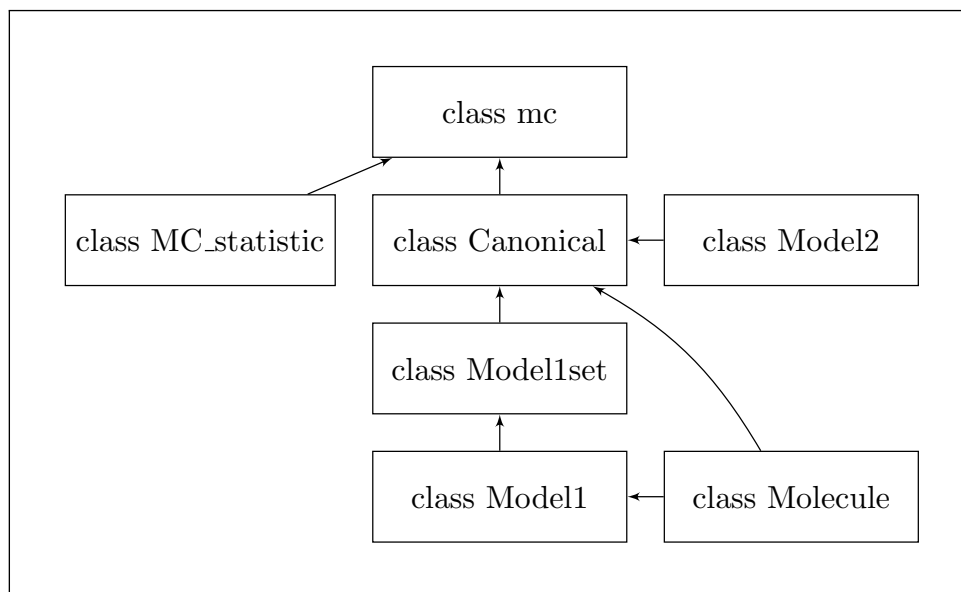
3.2   Random number generator

Monte Carlo simulations are heavily depends on the fast, efficient generation of streams of random numbers [31]. Some of the the random number's applications in Monte Carlo simulation are:

- Random distribution of particles in the system.

- Selection of the particle randomly and try to move it.
- Random choice of the translation and rotation of particles.
- Random change of the volume in NpT simulation.
- Random change of the volume in NVT simulation during the compression phase.

Many applications of randomness have to develop several different methods to generate random data. But in all of them, linear congruential random number generators multiply the last random integer by some big factors, add another integer to it and normalize this integer to the interval between zero and unity. In this project, the following method was used to produce the random number [78]:

$$X_{n+1} = \mathrm{MOD}(aX_n + c, m) \qquad (3.1)$$

where a= 150889, c=1366 and m=714025.

3.3   Equilibration and production phase

The Monte Carlo simulation comprises an equilibration phase followed by production phase. There is a period of time required in equilibration phase for the system to lose the memory of its initial configuration [79].

During equilibration, appropriate thermodynamic and structural quantities such as the total energy (and the partitioning of the energy among the various components), mean square displacement and order parameters (as appropriate) are monitored until they achieve stable values, whereupon the production phase can commence.

During an isothermal-isobaric simulation (and compression phase in canonical ensemble) the volume will change once per cycle and therefore should also be monitored to ensure that a stable system density is achieved [80]. Moreover the number of insertion attempts per cycle in canonical ensemble and isothermal-isobaric ensemble by simulation program equals one.

3.4   The inner hard core of Lennard-Jones sites

In the Monte Carlo simulation, the locations of particles are chosen totally randomly. This is why it is possible that the distance between two particles gets smaller than σ_{LJ}. As far as we are concerned, the Lennard-Jones potential tends to infinity with increasing the distance between particles. To avoid Lennard-Jones potential overflow, σ_{hs} is used to accept or reject the coordinates of particles i.e. if the distance between two particles is smaller than σ_{hs} then the distributions of particles is rejected and we try for new one and if the distance between two particles is bigger than σ_{hs}, we have to check the Metropolis criterion. It should be noted that in the simulation program, σ_{hs} is usually set to $0.8\sigma_{\mathrm{LJ}}$.

3.5 The computer systems

The following table shows the computer systems of work group, which were used for the computer simulations.

Table 3.1: The computer systems used for the simulations

Name: rhenium processor: Intel(R), core(TM), Duo(2) clock frequency: 2400 MHz architecture: 64 bit, 2 cores RAM: 2 GB Cache: 2048 kB os: Linux	Name: radon5 processor: AMD Opteron(tm) processor 6128 HE clock frequency: 2000 MHz architecture: 64 bit, 2×8 cores RAM: 8 GB Cache: 4096 kB os: Linux
Name: radon4 processor: AMD Opteron(tm) 2356 clock frequency: 2.2 GHz architecture: 64 bit, 2×4 cores RAM: 4 GB Cache: 512 kB os: Linux	Name: radon6 processor: Intel(R) Pentium(R) 2.66 GHz clock frequency: 3150 MHz architecture: 64 bit, 1 core RAM: 2 GB Cache: 1024 kB os: Linux
Name: radon7 processor : Intel(R) Xenon(R) E5-2650 clock frequency: 2 GHz architecture: 64 bit, 2×8 cores RAM: 8 GB Cache: 20480 kB os: Linux	

Chapter 4

Results and discussion

4.1   The test of the computer simulation program

To determine the accuracy of the simulation program, the simulation results for pure argon were compared with the results of three different equations of state of the LJ fluid (mBWR1-LJ, mBWR2-nLJ, CSJS-LJ, KN-LJ) that can be used with the ThermoC program under the same conditions [68, 84].

ThermoC is a modular program package for the calculation of thermodynamics data (phase equilibria, caloric data and pVT data) of pure fluids and fluid mixtures from equations of state and mixing rules. Some advantages of ThermoC are: [84]

• ThermoC can calculate a wide range of thermodynamic properties.

• ThermoC can easily be extended to new equations of state and/or mixing theories.

• ThermoC can handle a wide variety of mixing rule or mixing theories.

• ThermoC can handle most equations of state, cubic, non-cubic, semiempirical, or multi-parameter reference equations.

Some examples for equation of state that can be chosen in ThermoC are:

• **mBWR1-LJ (modified Benedict–Webb–Rubin Lennard-Jones (12/6))**

As shown in the name, the mBWR1-LJ equation of state describes the behaviour of Lennard-Jones (12/6) fluid. The first version of mBWR1-LJ was published in 1979 (also known as Nicolas equation of state) [81, 85].

• **mBWR2-nLJ (modified Benedict–Webb–Rubin Lennard-Jones (12/6) chain)**

mBWR2-nLJ non-cubic equation of state is similar to the older Nicolas equation of state [81], but based on a more extensive and accurate set of simulation data. This EOS describes the behaviour of the Lennard-Jones (12/6) fluid as well as flexible LJ tangent-sphere chains.

The chain term is based on the behaviour of the background correlation function (cavity correlation function) at contact and uses a superposition approach to relate this function for chain molecules to that of spherical particles [82, 83].

- **KN-LJ (Kolafa–Nezbeda Lennard-Jones (12/6))**

  This noncubic EOS describes the behaviour of the Lennard-Jones (12/6) fluid. It consists of a hard-sphere repulsion term with a temperature-dependent collision diameter and an empirical attraction term (2-dimensional polynomial) [86].

- **CSJS-LJ (Carnahan–Starling + Jacobsen-Stewart Lennard-Jones (12/6))**

  This noncubic EOS describes the behaviour of the Lennard-Jones (12/6) fluid. It consists of a hard-sphere repulsion term with a temperature-dependent collision diameter and an empirical attraction term of the Jacobsen-Stewart type [87, 88].

The results of these equations of state for the thermodynamic properties of argon at temperatures above the critical temperature are presented in Figures 4.1 to 4.8. There is a very good agreement between the results of ThermoC and the simulation program. This confirms the high accuracy of simulation results.

- - - KN-LJ, - - - mBWR1-LJ, - - - mBWR2-nLJ, - - - CSJS-LJ ,- ⨯ - Simulation
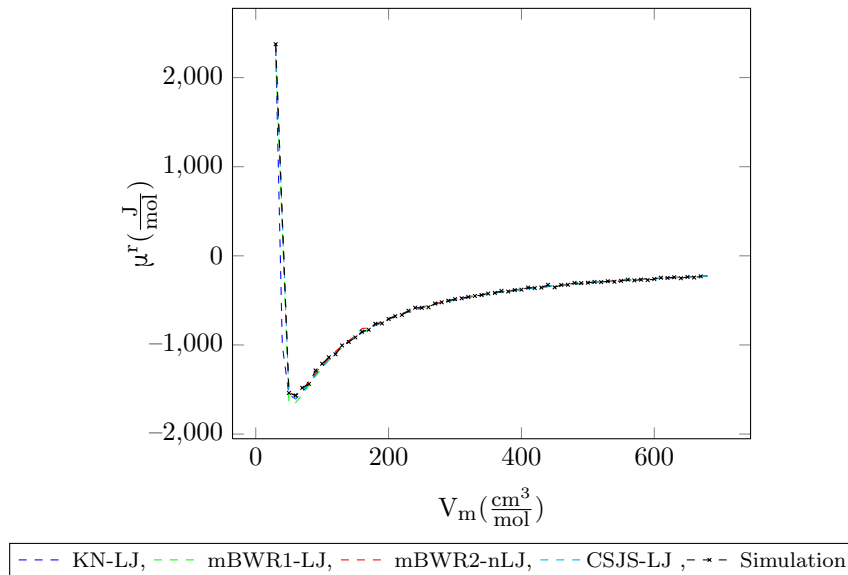
Figure 4.1: Residual chemical potential vs. molar volume for argon, T=200 K 500 particles, acceptance ratio=50%.
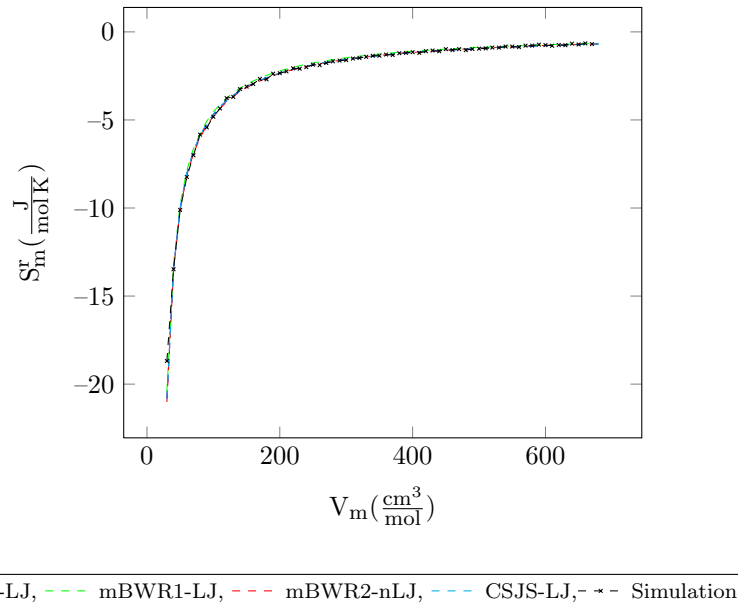
Figure 4.2: Molar residual entropy vs. molar volume for argon, T=200 K
500 particles, acceptance ratio=50%.
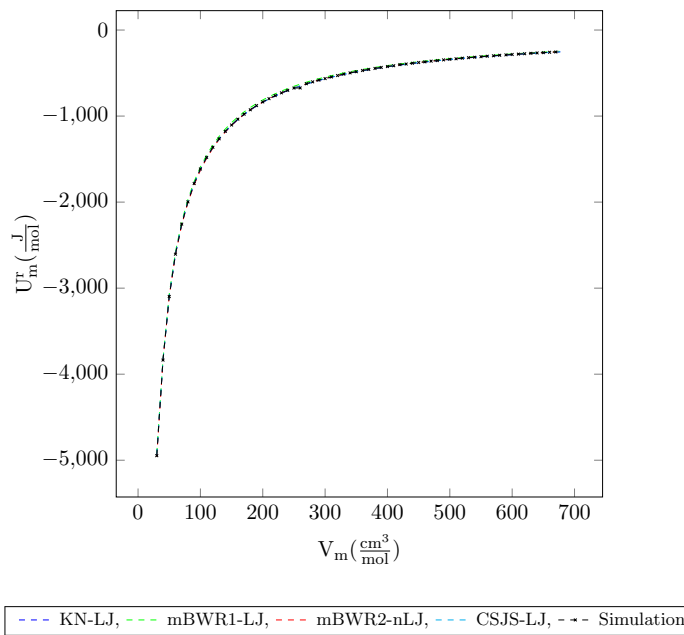
Figure 4.3: Molar internal energy vs. molar volume for argon, T=200 K
500 particles, acceptance ratio=50%.
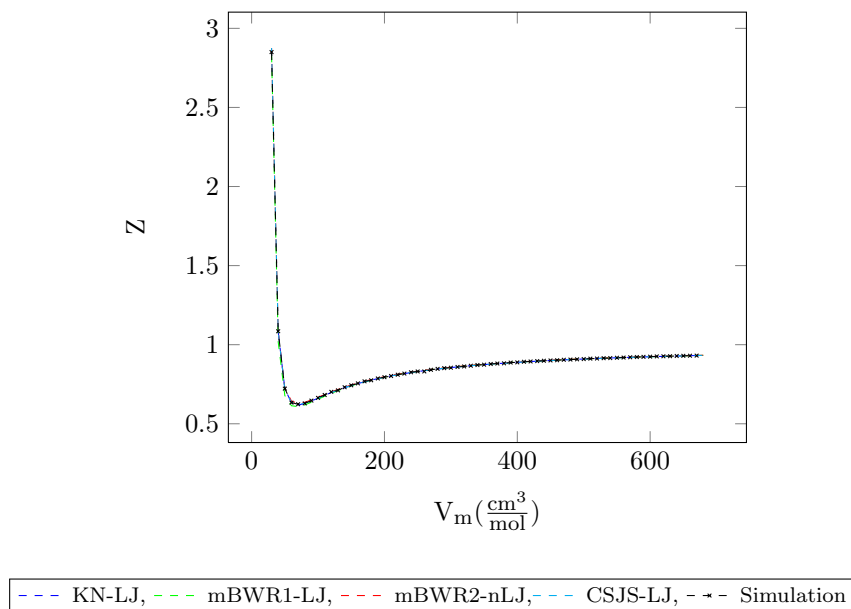
Figure 4.4: Compression factor vs. molar volume for argon, T=200 K
500 particles, acceptance ratio=50%.
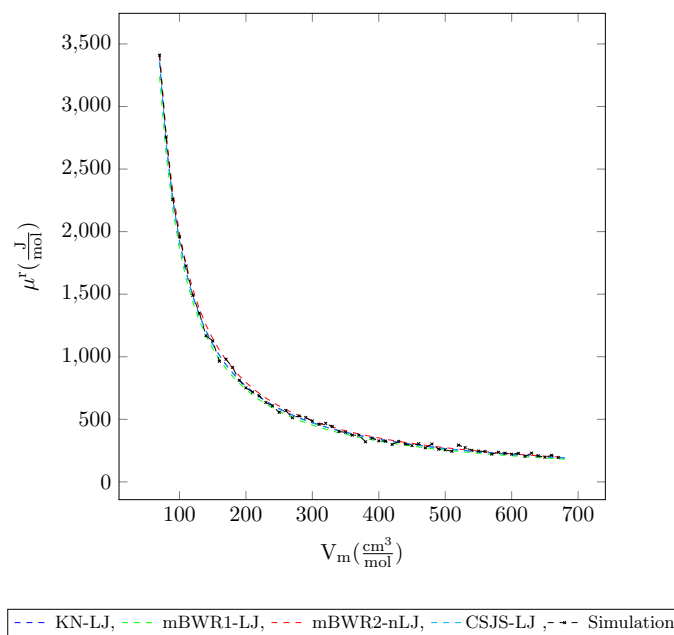
Figure 4.5: Residual chemical potential vs. molar volume for argon, T=600 K
500 particles, acceptance ratio=50%.
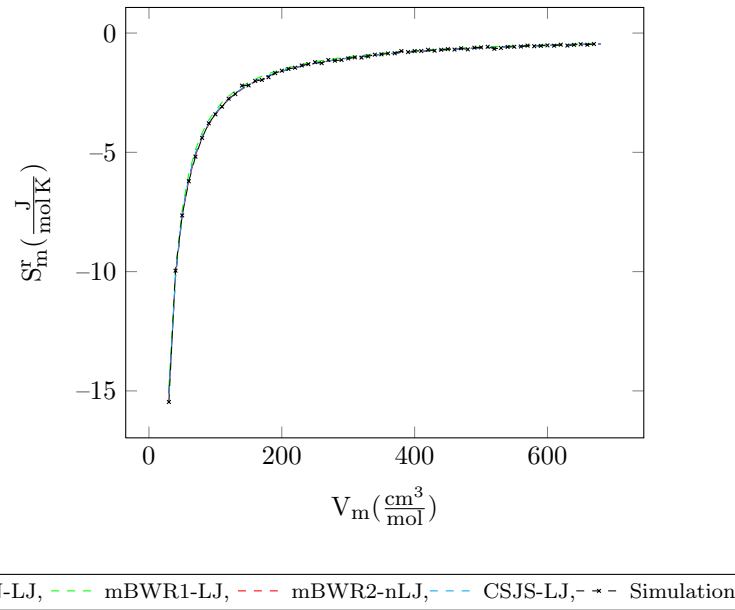
Figure 4.6: Residual molar entropy vs. molar volume for argon, T=600 K
500 particles, acceptance ratio=50%.
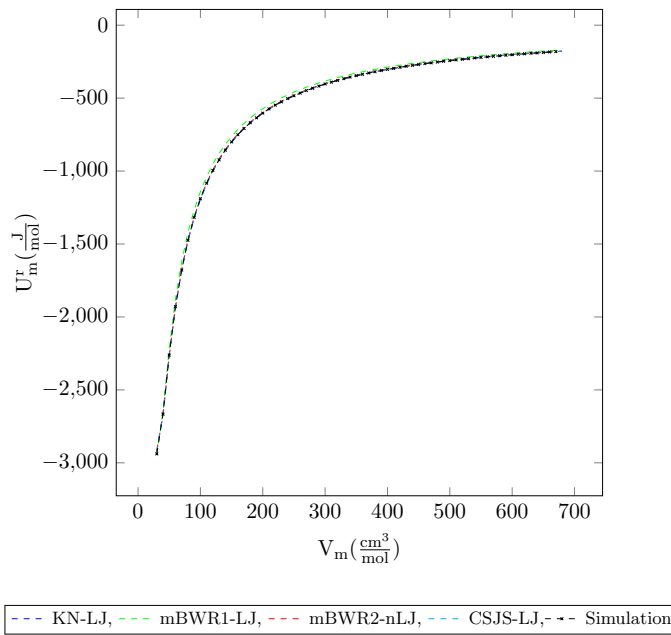
Figure 4.7: Molar internal energy vs. molar volume for argon, T=600 K
500 particles, acceptance ratio=50%.
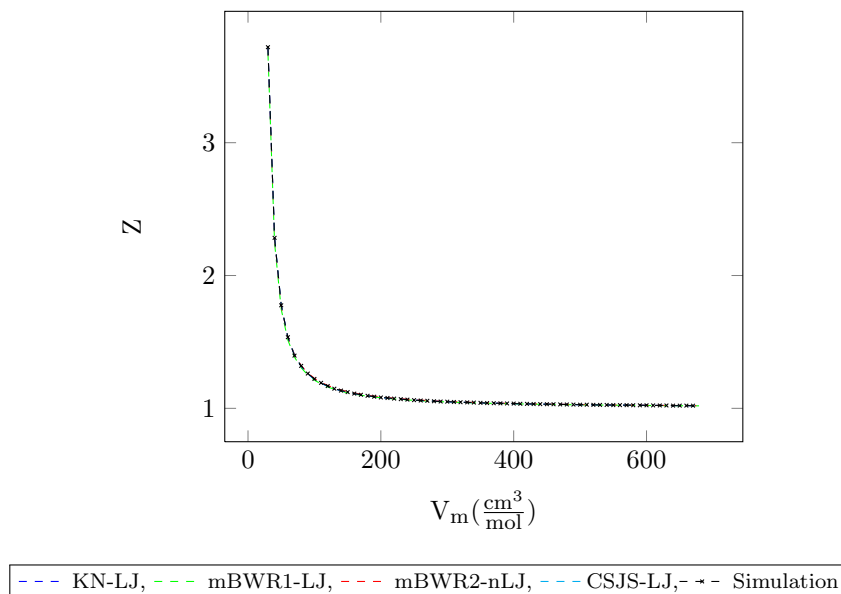
Figure 4.8: Compression factor vs. molar volume for argon, T=600 K
500 particles, acceptance ratio=50%.

4.2 Calculation of the residual entropy for LJ fluids

4.2.1 1-center Lennard-Jones argon

To describe the connection between the residual entropy (S_r) and the Monte Carlo shift parameter (dx), the simulation program was applied to 1-center Lennard-Jones fluid argon at constant temperatures, volume and particles number (NVT ensemble).

Figure 4.10 shows the results of these simulations for the densities 30 to 670 cm^3mol^{-1} with an acceptance ratio of 50%. The details of the simulations are presented in Table 4.1.

Table 4.1: Simulation details for 1-center Lennard-Jones argon.

site	acceptance ratio	σ_{LJ} (Å)	σ_{hs}(Å)	ε/k_B(K)	number of atoms	atom coordinates (Å)
1	50%	3.405	2.724	119.8	500	$(0.00, 0.00, 0.00)$
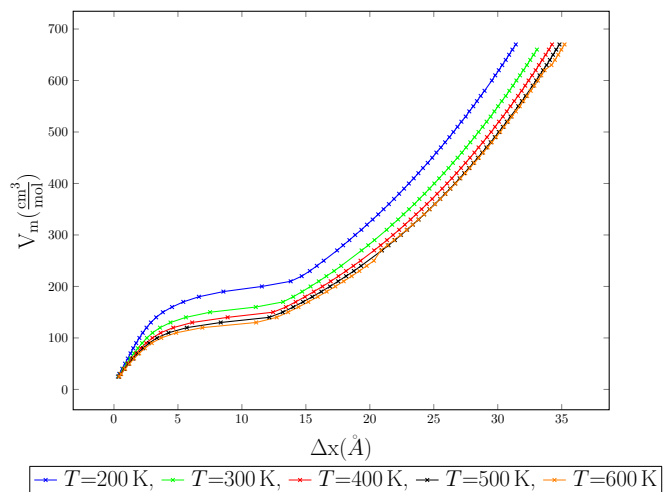
Figure 4.9: Molar volume vs. MC shift parameter for various temperatures for 1-center LJ fluid argon.
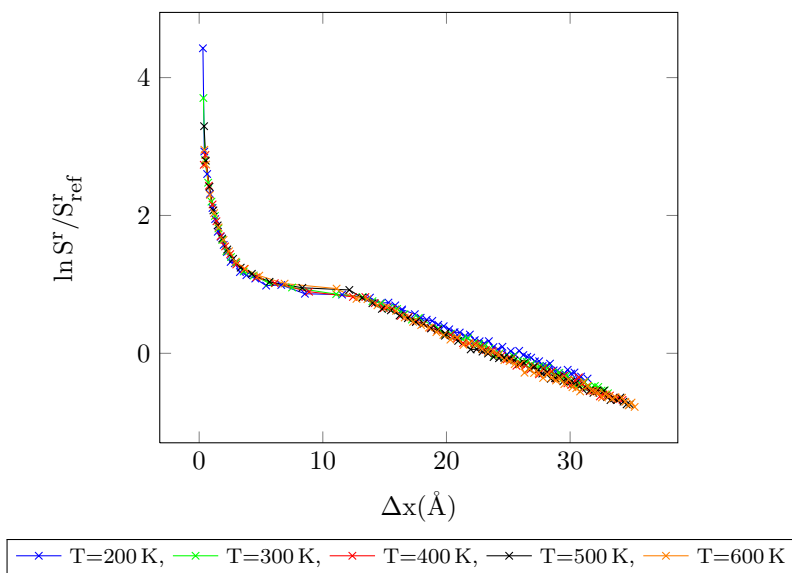
Figure 4.10: Entropy vs. MC shift parameter for various temperatures for 1-center LJ fluid argon, acceptance ratio 50%.

All diagrams consist of two parts. In the first part of diagrams (the curve part), the acceptance average stays stable during simulation run (acceptance ratio = 50%), but in second part (the linear part), the acceptance average increases with increasing in the volumes at constant temperature (50% < acceptance ratio) because of percolation.

The begin of percolation varies with temperature. The begin of percolation in 1-center Lennard-Jones argon at different temperatures is presented in the Table 4.2.

Table 4.2: Begin of percolation for 1-center Lennard-Jones argon at 50% acceptance ratio.

T (K)	V (cm^{3}mol^{-1})
200	200
300	160
400	150
500	140
600	130

4.2.2 Lennard-Jones argon dimers

The details and results of simulations in Lennard-Jones argon dimers are given in Table 4.3 and Figure 4.12, respectively. As can be seen, the diagram for Lennard-Jones argon dimers shows the same behaviour as that for 1-center Lennard-Jones argon.

It can be seen, the only difference between the results of simulation in 1-center Lennard-Jones argon and Lennard-Jones argon dimers appears at temperature 200 K after the begin of percolation. The onset points of percolation in Lennard-Jones argon dimers at the temperatures 200 K, 300 K, 400 K, 500 K and 600 K are presented in Table 4.4.
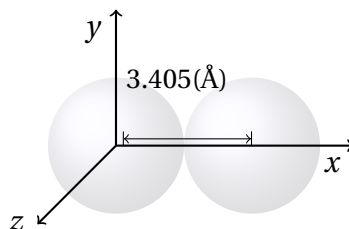
Figure 4.11: Atom coordination of Lennard-Jones argon dimers.

Table 4.3: Simulation details for Lennard-Jones argon dimers.

site	acceptance ratio	$\sigma_{\mathrm{LJ}}(\text{Å})$	$\sigma_{\mathrm{hs}}(\text{Å})$	$\varepsilon/k_{\mathrm{B}}(\text{K})$	number of atoms	atoms coordinates(Å)
2	50%	3.405	2.724	119.8	500	$(0.00, 0.00, 0.00)$
						$(3.405, 0.00, 0.00)$
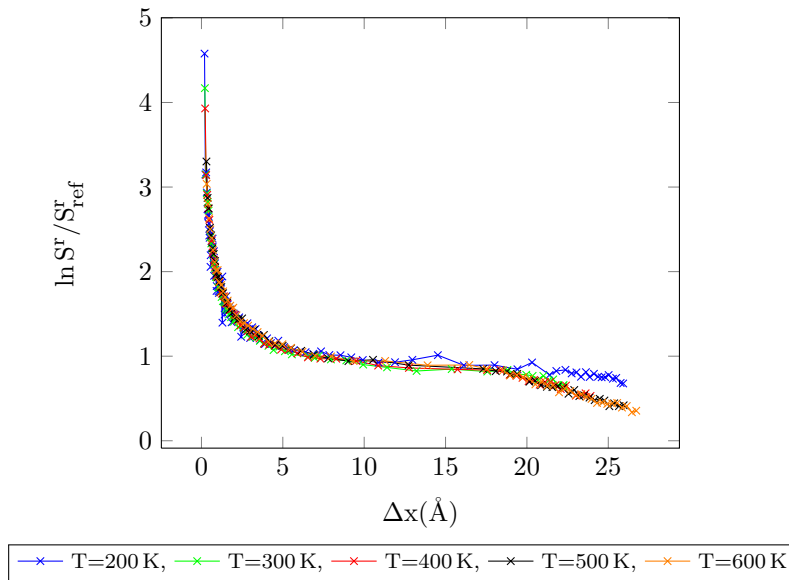
Figure 4.12: Entropy vs. MC shift parameter for various temperatures for Lennard-Jones argon dimers, acceptance ratio 50%.

Table 4.4: Begin of percolation for Lennard-Jones argon dimers, temperatures 200 K to 600 K, acceptance ratio 50%.

T (K)	V (cm^{3}mol^{-1})
200	780
300	540
400	460
500	420
600	400

4.2.3 Linear Lennard-Jones argon trimers

Figure 4.14 presents the results of simulations in linear Lennard-Jones argon trimers. The details of simulations and the beginning point of percolation at different temperatures are presented in Tables 4.5 and 4.6, respectively.

The comparison between percolation starting point in 1-center Lennard-Jones argon, Lennard-Jones argon dimers and linear Lennard-Jones argon trimers shows that under the same conditions (the volume, number of particles, temperatures etc.), percolation occurs in linear Lennard-Jones argon trimers at lower densities than 1-center Lennard-Jones argon and Lennard-Jones argon dimers.

It is obvious that the volume at the onset of percolation for linear Lennard-Jones argon trimers is about six times larger than for 1-center Lennard-Jones argon and about two times larger than for Lennard-Jones argon dimers at the same reduced density and temperatures.
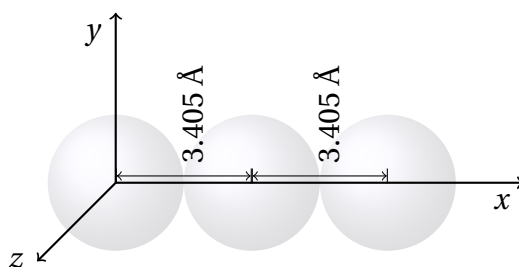
Figure 4.13: Atom coordinates of linear Lennard-Jones argon trimers.

Table 4.5: Simulation details for linear Lennard-Jones argon trimers.

site	acceptance ratio	σ_{LJ} (Å)	σ_{hs} (Å)	ε/k_B (K)	number of atoms	atoms coordinates (Å)
						$(0.00, 0.00, 0.00)$
3	50%	3.405	2.724	119.8	500	$(3.405, 0.00, 0.00)$
						$(6.81, 0.00, 0.00)$
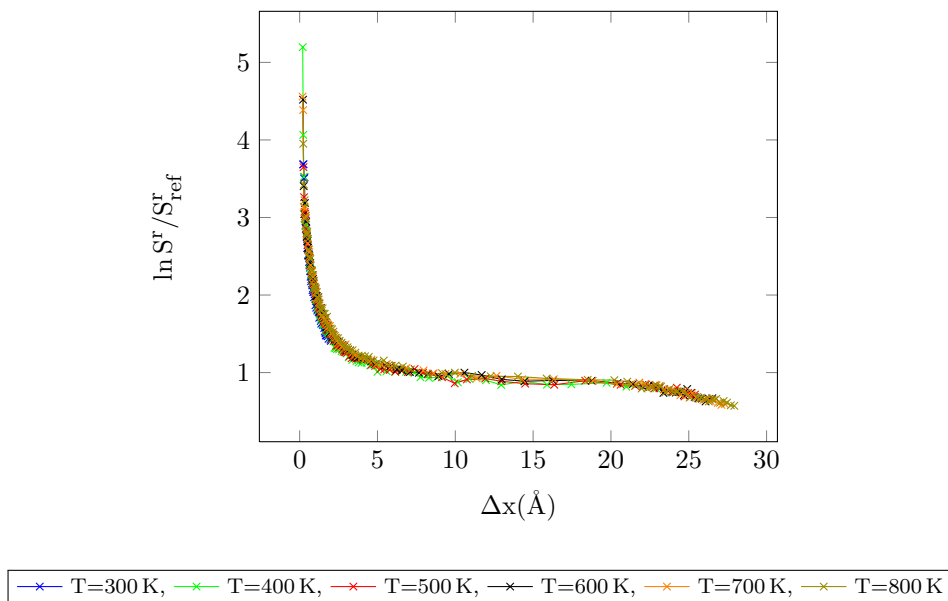
Figure 4.14: Entropy vs. MC shift parameter for various temperatures for linear Lennard-Jones argon trimers, acceptance ratio 50%.

Table 4.6: Begin of percolation for linear Lennard-Jones argon trimers at different temperatures.

T (K)	V (cm^{3}mol^{-1})
400	960
500	860
600	800
700	760
800	730

4.2.4   Non-linear Lennard-Jones argon trimers

The details of simulation in non-linear Lennard-Jones argon trimers are presented in Table 4.7. Obviously, the only difference between the simulation of linear Lennard-Jones argon trimers (Table 4.5) and non-linear Lennard-Jones argon trimers (Table 4.7) is the arrangement of atoms.

The results of simulation in non-linear Lennard-Jones argon trimers are presented in Figure (4.16). The beginning points of percolation for non-linear Lennard-Jones argon trimers (at different temperatures) are presented in Table 4.8. As can be seen, the percolation of non-linear Lennard-Jones trimers starts at a lower density than for monomers and dimers, but at a higher density than for linear Lennard-Jones argon trimers (under the same conditions).

Table 4.7: Simulation details for non-linear Lennard-Jones argon trimers.

site	acceptance ratio	σ_{LJ}(Å)	σ_{hs}(Å)	ε/k_B(K)	number of atoms	atoms coordinates (Å)
						$(0.00, 0.00, 0.00)$
3	50%	3.405	2.724	119.8	500	$(3.405, 0.00, 0.00)$
						$(0.00, 3.405, 0.00)$
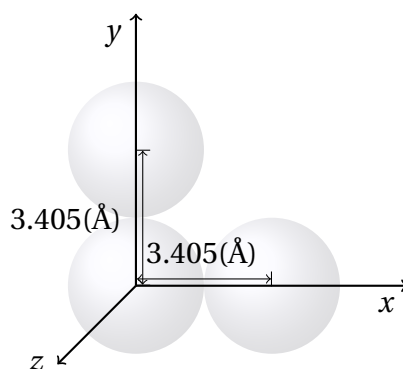
Figure 4.15: Atom coordinates of non-linear Lennard-Jones argon trimers.

Table 4.8: Begin of percolation for non-linear Lennard-Jones argon trimers at different temperatures.

T (K)	V (cm^{3}mol^{-1})
400	900
500	800
600	750
700	710
800	690
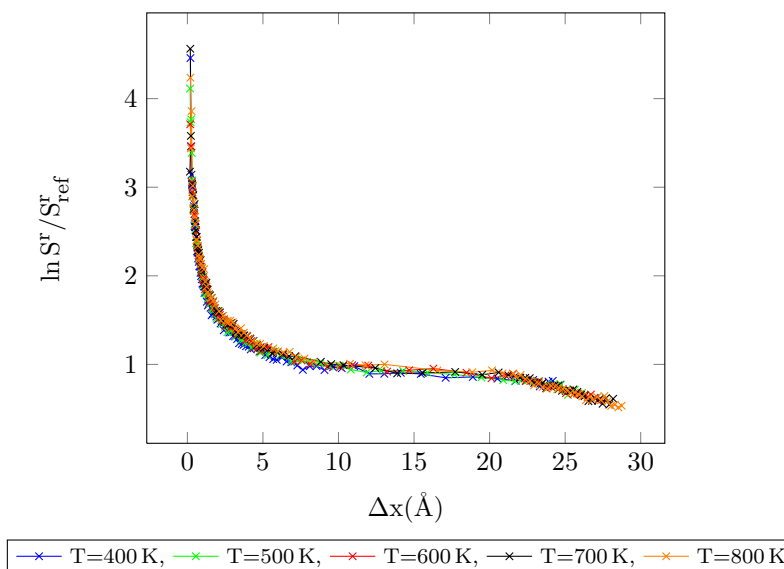
Figure 4.16: Entropy vs. MC shift parameter for various densities for non-linear Lennard-Jones argon trimers, acceptance ratio 50%.

4.2.5   1-center Mie-potential argon

One option of the simulation program is the calculation of thermodynamic properties with chosen acceptance ratio for different exponents in the repulsive term of the Mie-potential.

To obtain the connection between residual entropy and Monte Carlo shift parameter in fluids at high densities, simulations were performed for 1-center Mie-potential argon at temperatures above the critical point (200 K, 500 K and 800 K) and an acceptance ratio of 50%. The details of simulations have already been given in section 4.2.1.

Table 4.9: Begin of percolation for 1-center Mie-potential argon, T=200 K.

Mie-potential	acceptance ratio	$V\,(\mathrm{cm^3mol^{-1}})$
(8/6)	50%	100
(10/6)	50%	120
(12/6)	50%	200
(16/6)	50%	170
(10/6)	30%	70
(12/6)	30%	110
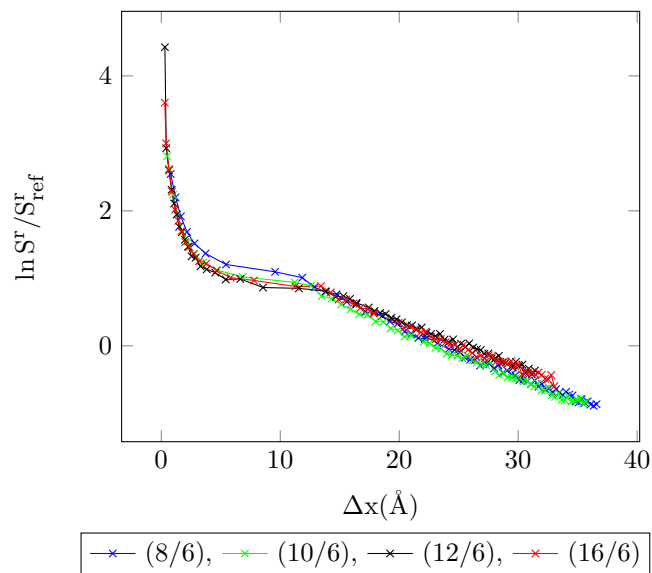
Figure 4.17: Entropy vs. MC shift parameter for 1-center Mie-potential argon, acceptance ratio 50%, T=200 K.
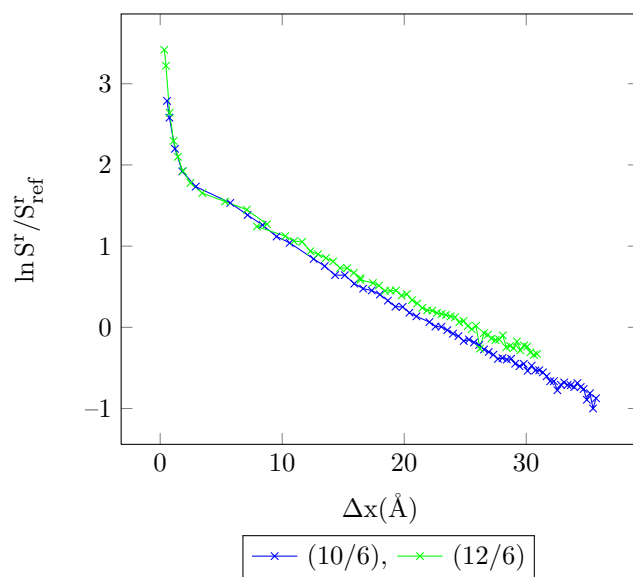
Figure 4.18: Entropy vs. MC shift parameter for 1-center Mie-potential argon, acceptance ratio 30%, T=200 K.
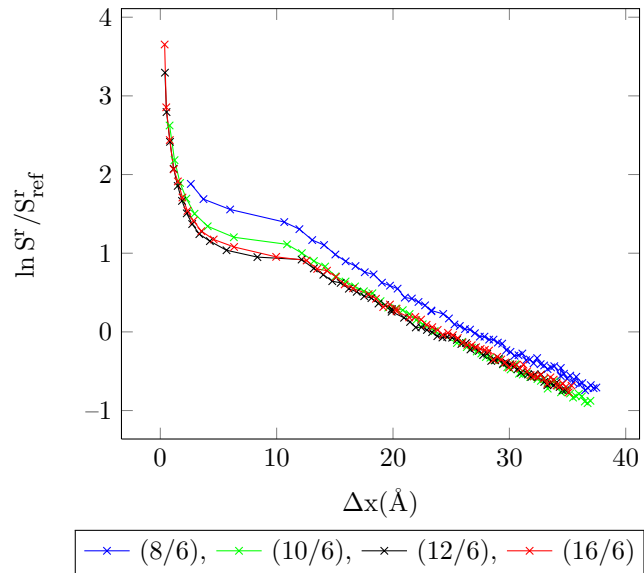
Figure 4.19: Entropy vs. MC shift parameter for 1-center Mie-potential argon, acceptance ratio 50%, T=500 K.
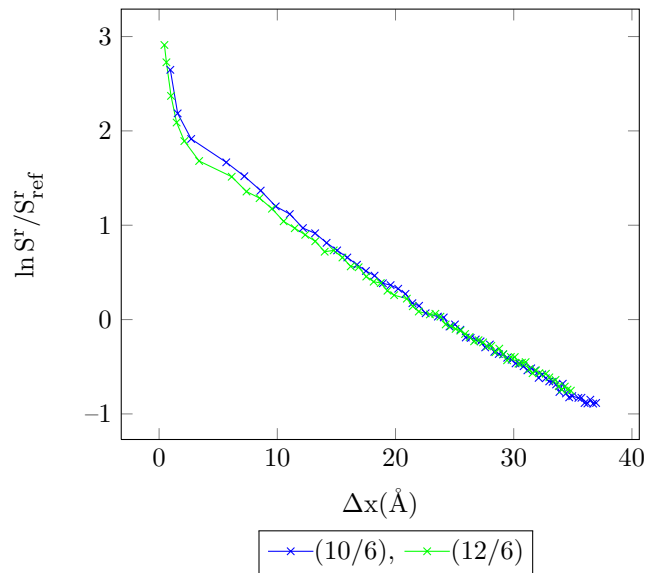
Figure 4.20: Entropy vs. MC shift parameter for 1-center Mie-potential argon, acceptance ratio 30%, T=500 K.

The onset points of percolation for the 1-center Mie-potential argon at 200 K are presented in Table 4.9. According to Table 4.9, the percolation occurs in 1-center Lennard-Jones argon (12/6) at a lower density than for another exponents of the repulsive term under the same conditions. On the other side, for the same temperature and same exponent in the repulsive term of Mie-Potential, percolation occurs at higher density with decreasing acceptance average.

The results of the simulation program for 1-center Mie-potential argon at 500 K are given in Figure 4.19. The conditions of simulation are as same as for 200 K. It can be seen that the changes of residual entropy vs. Monte Carlo shift parameter in (8/6) Mie-potential argon are not in good agreement with other simulation results under the same conditions.

Figure 4.19 shows that the change of residual entropy against Monte Carlo shift parameter in (10/6) Mie-potential argon (at the temperature 500 K) agrees with (12/6) and (16/6) Mie-potential argon for the region after the percolation, but there is a very small deviation before the percolation begins.

The results of the simulation for 1-center Mie-potential argon (10/6) and (12/6) at 500 K and an acceptance average of 30%[1] are illustrated in Figure (4.20). From this Figure, it can be seen that the results for (10/6) and (12/6) agree fairly after percolation. There it is a very small difference between their results before percolation.

Table 4.10: Begin of percolation for 1-center Mie-potential argon, T=500 K.

Mie-potential	acceptance ratio	$V(\text{cm}^3\text{mol}^{-1})$
(8/6)	50%	90
(10/6)	50%	100
(12/6)	50%	140
(16/6)	50%	140
(10/6)	30%	60
(12/6)	30%	80

According to Table 4.10, the begin of percolation shifts to low density with increasing repulsion exponent of the Mie-potential under the same conditions (number of particles, temperature, volume, etc.). With increasing of acceptance ratio, the percolation occurs at lower density.

Figures 4.21 and 4.22 represent the results of simulations for 1-center Mie-potential argon at 800 K with acceptance ratios 50% and 30%, respectively. The fitting parameters are given in Table 4.11.

---

[1]The aim to calculate the residual entropy with an acceptance of 30% has the propose to show the effect of change in acceptance ratio on the starting point of percolation and the change residual entropy, but the results with acceptance ratio 30% are not used in the finial equation.
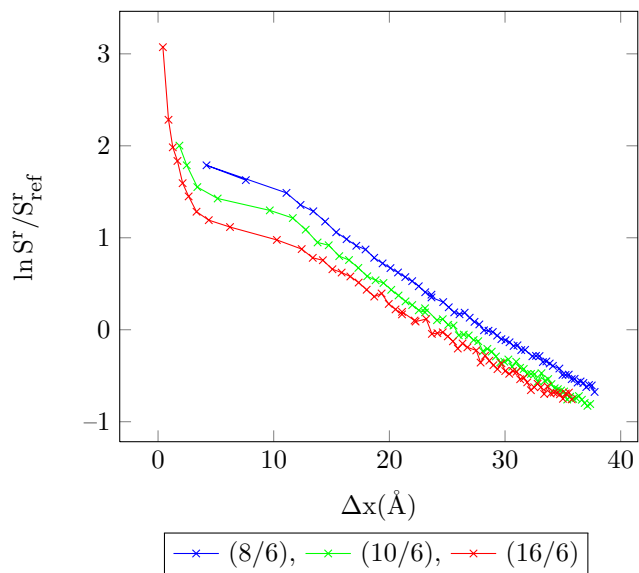
Figure 4.21: Entropy vs. MC shift parameter for 1-center Mie-potential argon, acceptance ratio 50%, T=800 K.
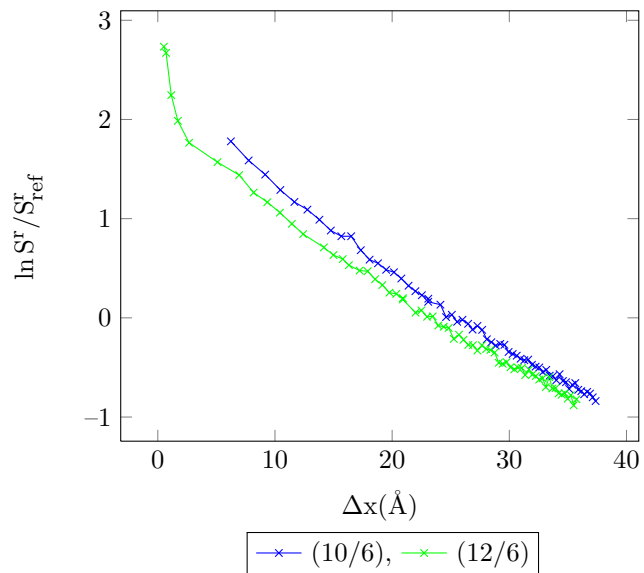
Figure 4.22: Entropy vs. MC shift parameter for 1-center Mie-potential argon, acceptance ratio 30%, T=800 K.
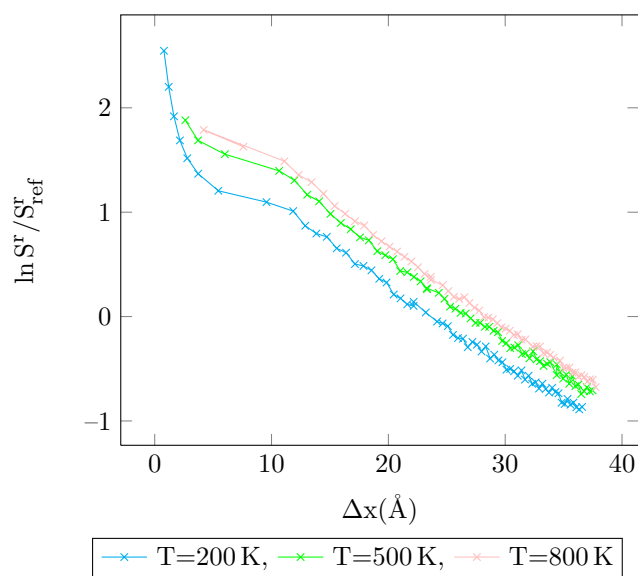
Figure 4.23: Entropy vs. MC shift parameter for 1-center Mie-potential argon (8/6) at different temperatures, acceptance ratio 50%.
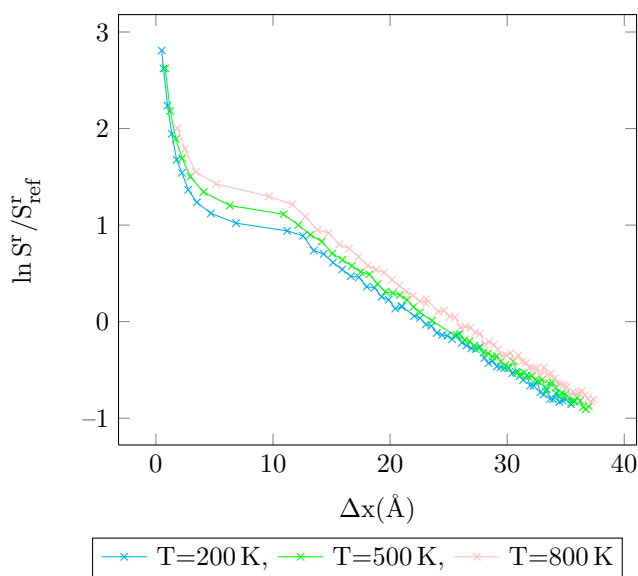
Figure 4.24: Entropy vs. MC shift parameter for 1-center Mie-potential argon (10/6) at different temperatures, acceptance ratio 50%.
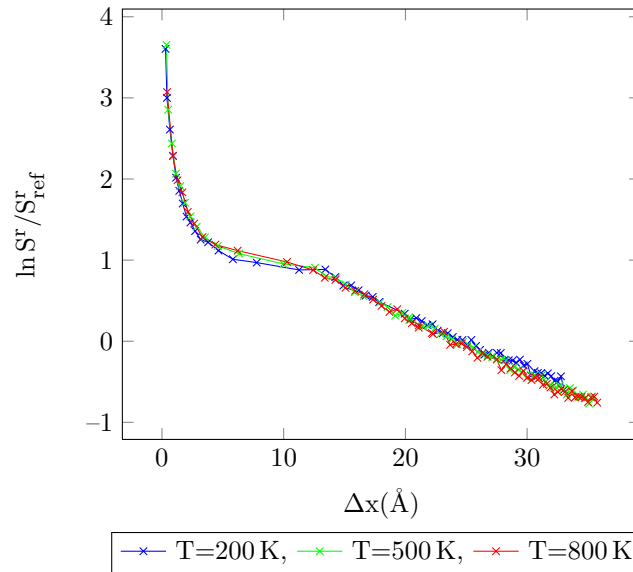
Figure 4.25: Entropy vs. MC shift parameter for 1-center Mie-potential argon (16/6) at different temperatures, acceptance ratio 50%.

Table 4.11: Begin of percolation for 1-center Mie-potential argon, T=800 K.

Mie-potential	acceptance ratio	$V\,(\mathrm{cm^3mol^{-1}})$
(8/6)	50%	90
(10/6)	50%	90
(12/6)	30%	70
(16/6)	50%	120

4.2.6   Mie-potential argon dimers

Calculations of the residual entropy for Mie-potential argon dimers were performed for different exponents in the repulsive term of Mie-potential (m/6). The details of simulation were presented in section 4.2.2. Figures 4.26 to 4.34 give the results of simulation in Mie-potential argon dimers at different temperatures and acceptance ratio.
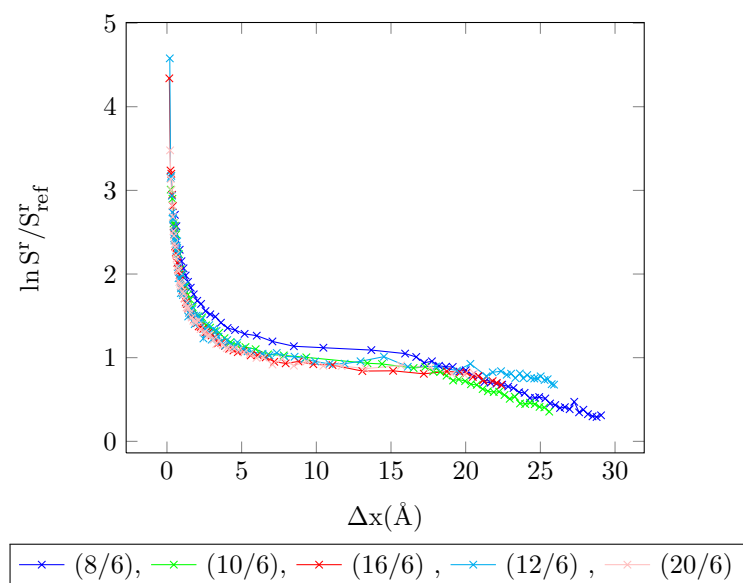
Figure 4.26: Entropy vs. MC shift parameter for Mie-potential argon dimers, acceptance ratio 50%, T=200 K.
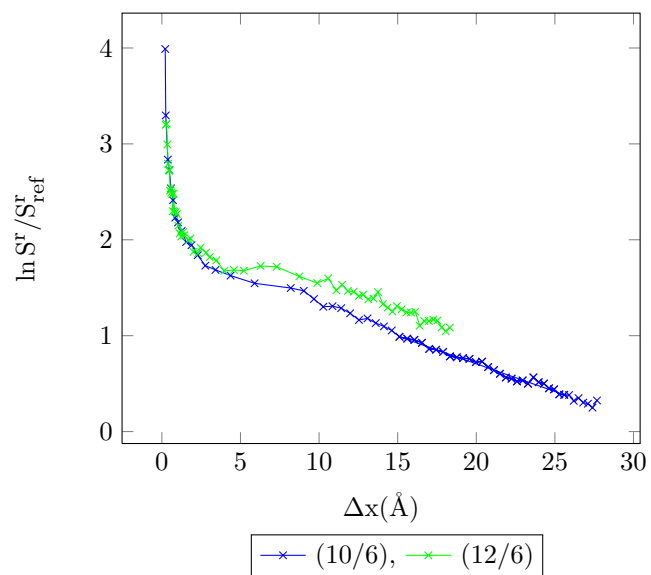
Figure 4.27: Entropy vs. MC shift parameter for Mie-potential argon dimers, acceptance ratio 30%, T=200 K.

Table 4.12: Begin of percolation for Mie-potential argon dimers, T=200 K.

Mie-potential	acceptance ratio	$V(\text{cm}^3\text{mol}^{-1})$
(8/6)	50%	310
(10/6)	50%	360
(12/6)	50%	780
(16/6)	50%	560
(20/6)	50%	620
(10/6)	30%	210
(12/6)	30%	250
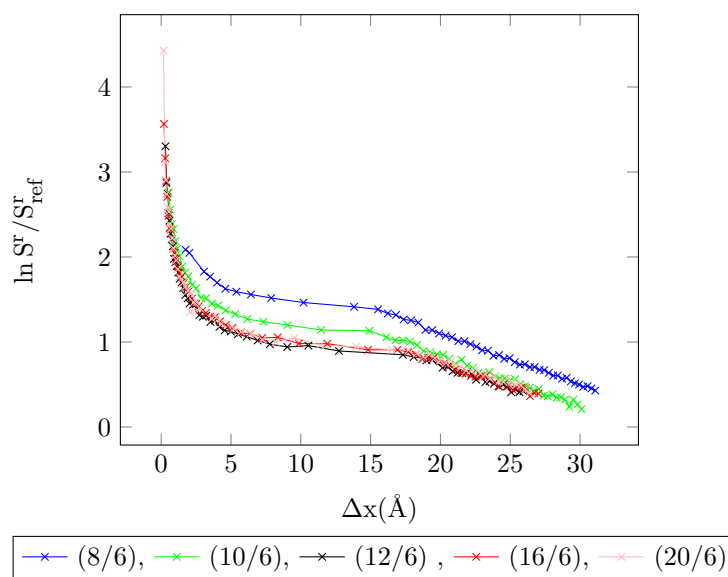
Figure 4.28: Entropy vs. MC shift parameter for Mie-potential argon dimers, acceptance ratio 50%, T=500 K.
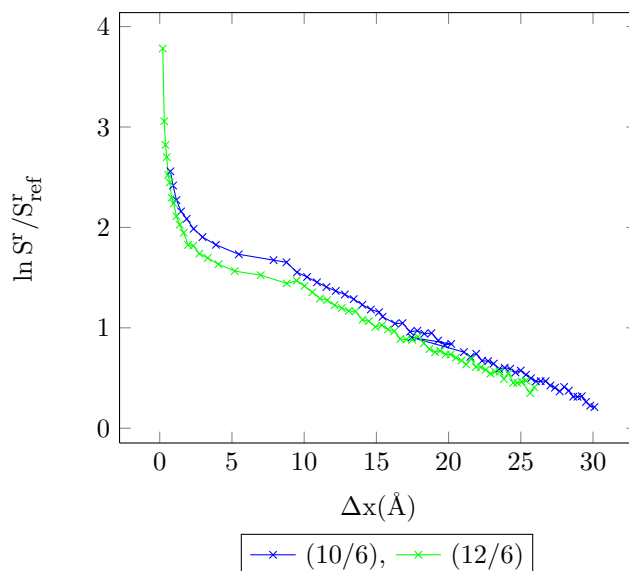
Figure 4.29: Entropy vs. MC shift parameter for Mie-potential argon dimers, acceptance ratio 30%, T=500 K.

Table 4.13: Begin of percolation for Mie-potential argon dimers, T=500 K.

Mie-potential	acceptance ratio	V (cm^{3}mol^{-1})
(8/6)	50%	270
(10/6)	50%	300
(12/6)	50%	420
(16/6)	50%	390
(20/6)	50%	420
(10/6)	30%	180
(12/6)	30%	240

Table 4.14: Begin of percolation for Mie-potential argon dimers, T=800 K.

Mie-potential	acceptance ratio	V (cm^{3}mol^{-1})
(8/6)	50%	260
(10/6)	50%	280
(16/6)	50%	360
(20/6)	50%	380
(10/6)	30%	170
(12/6)	30%	210
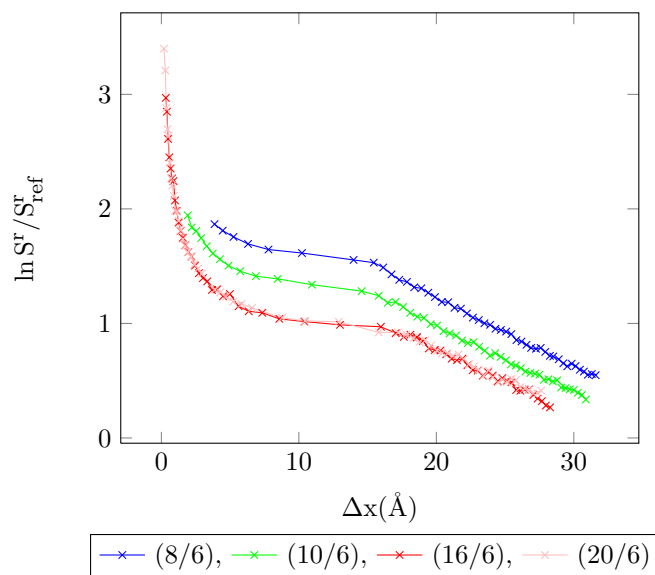
Figure 4.30: Entropy vs. MC shift parameter for Mie-potential argon dimers, acceptance ratio 50%, T=800 K.
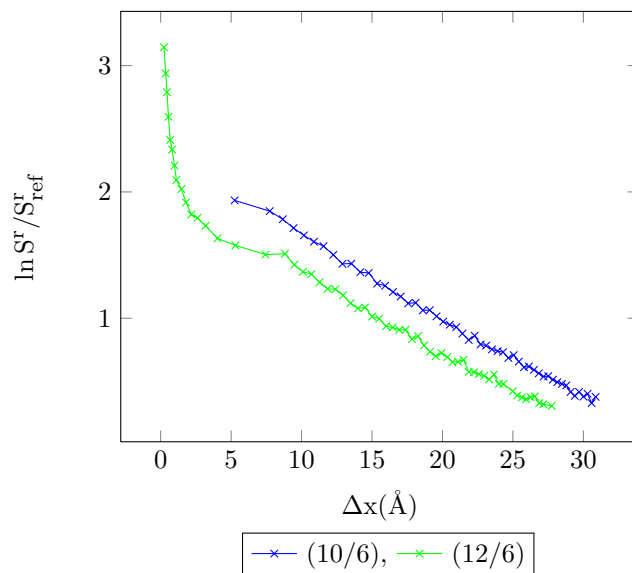
Figure 4.31: Entropy vs. MC shift parameter for Mie-potential argon dimers, acceptance ratio 30%, T=800 K.
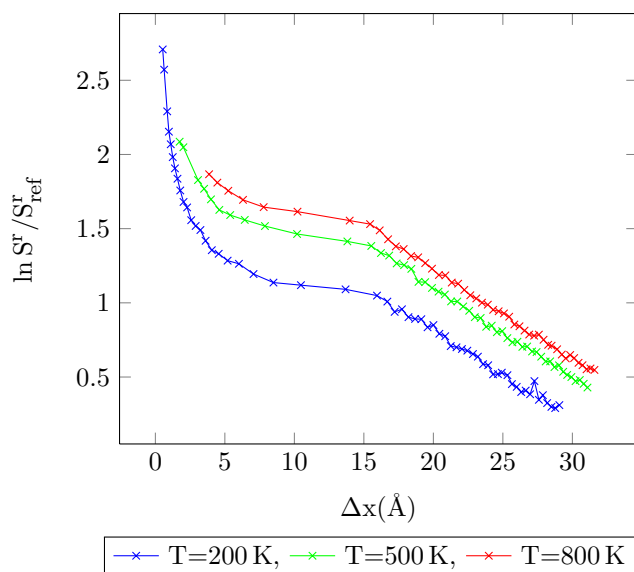
Figure 4.32: Entropy vs. MC shift parameter for Lennard-Jones argon dimers (8/6) at different temperatures, acceptance ratio 50%.
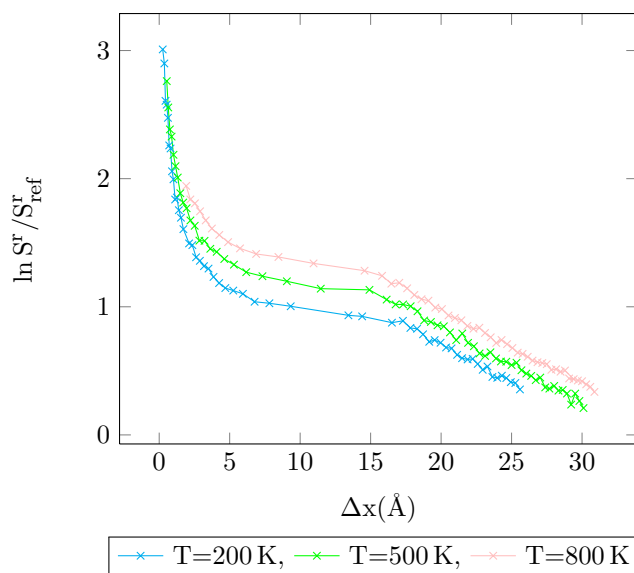
Figure 4.33: Entropy vs. MC shift parameter for Lennard-Jones argon dimers (10/6) at different temperatures, acceptance ratio 50%.
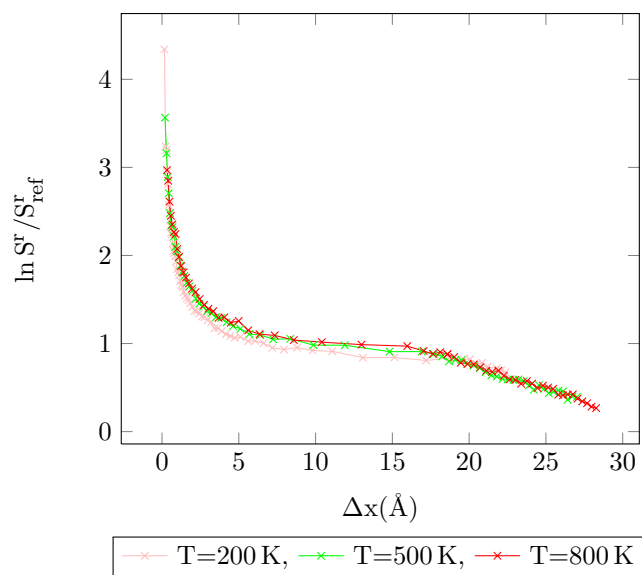
Figure 4.34: Entropy vs. MC shift parameter for Lennard-Jones argon dimers (16/6) at different temperatures, acceptance ratio 50%.
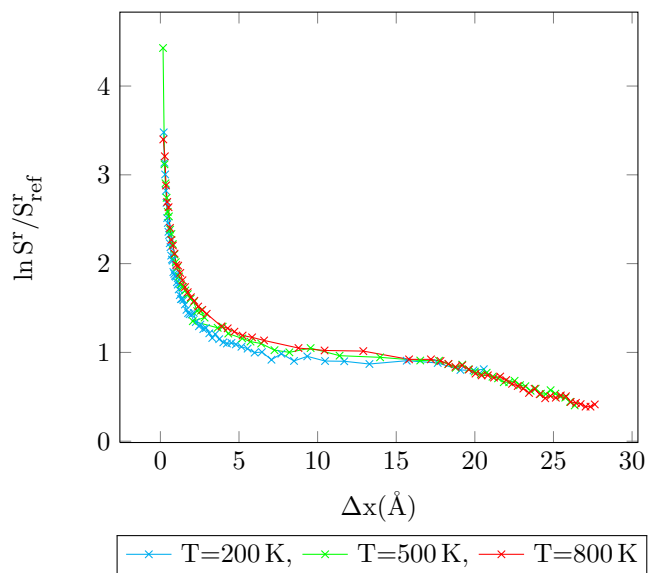
Figure 4.35: Entropy vs. MC shift parameter for Lennard-Jones argon dimers (20/6) at different temperatures, acceptance ratio 50%.

4.2.7 Linear Mie-potential argon trimers

Simulation details for linear Mie-potential argon trimers are given in Table 4.5 in section 4.2.3. The simulation results and the percolation beginning point are presented in Figure 4.36 and Table 4.15, respectively.
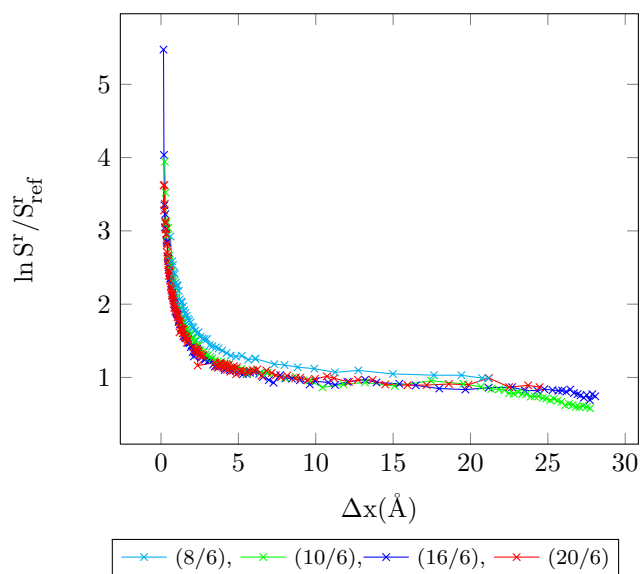
Figure 4.36: Entropy vs. MC shift parameter for linear Mie-potential argon trimers, T=200 K, acceptance ratio 50%.

Table 4.15: Begin of percolation for linear Mie-potential argon trimers, T=200 K.

Mie-potential	acceptance ratio	$V\,(\mathrm{cm}^3\mathrm{mol}^{-1})$
(8/6)	50%	630
(10/6)	50%	730
(16/6)	50%	1210
(20/6)	50%	1340

4.2.8   Non-linear Mie-potential argon trimers
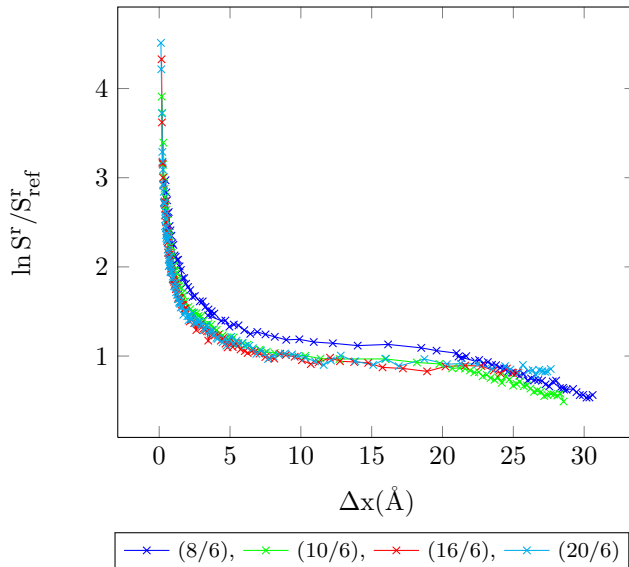
Figure 4.37: Entropy vs. MC shift parameter for non-linear Mie-potential argon trimers, T=200 K, acceptance ratio 50%

The simulation results for non-linear Mie-potential argon trimers are presented in Figure 4.37. The details of simulation are given in section 4.2.4. It can be seen that the change of residual entropy vs. Monte Carlo shift parameter in non-linear Mie-potential argon trimers (8/6) is slightly different from the results for (10/6),(16/6) and (20/6) at same temperature and number of particles.

The beginning of percolation in non-linear Mie-potential argon trimers argon is presented in Table 4.16. According to the results, with increasing of exponent in repulsive term of non-linear Mie-potential argon trimers, percolation sets in lower density (under the same temperature and acceptance average).

Table 4.16: Begin of percolation for non-linear Mie-potential argon trimers, T=200 K.

Mie-potential	acceptance average	$V\,(\text{cm}^3\text{mol}^{-1})$
(8/6)	50%	590
(10/6)	50%	690
(16/6)	50%	1110
(20/6)	50%	1240

By comparing the results of Table 4.15 (entropy against Monte Carlo shift parameter for linear Mie-potential argon trimers) and Table 4.16 (entropy against Monte Carlo

shift parameter for non-linear Mie-potential argon trimers) it can be seen that percolation starts for linear Mie-potential argon trimers at lower density than for non-linear Mie-potential argon trimers under the same conditions.

4.2.9 Dimer CH_3-CH_3

Simulation were performed for CH_3-CH_3, which was modeled as a 2-center Lennard-Jones molecule. The details of simulation are presented in Table 4.17. The simulation results are presented in Figure 4.38.

In Figure 4.38, small deviations can be seen after percolation in the change of the residual entropy vs. the Monte Carlo shift parameter at temperature 700 K, but before percolation, the results for all temperatures are in very good agreement with each other.

Table 4.17: Simulation details for CH_3-CH_3.

site	acceptance ratio	σ_{LJ} (Å)	σ_{hs}(Å)	ε/k_B(K)	number of atoms	atom coordinates (Å)
1	50%	3.825	3.06	100.6	500	$(0.00, 0.00, 0.00)$
1	50%	3.825	3.06	100.6	500	$(1.54, 0.00, 0.00)$
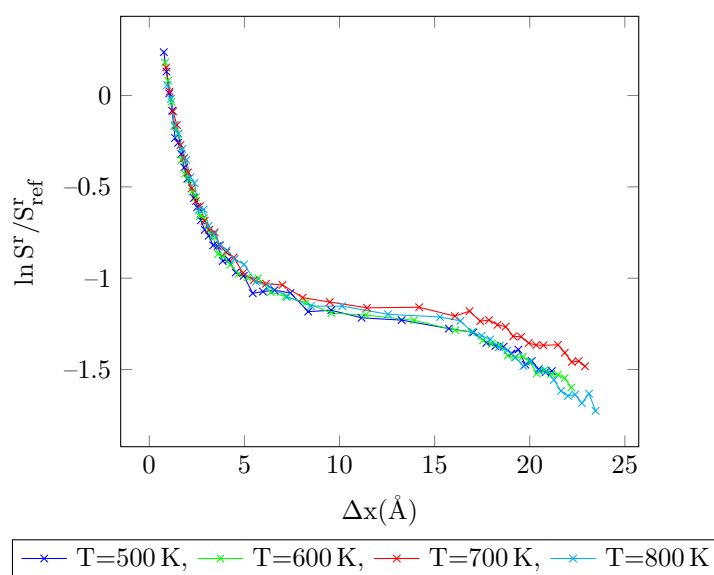
Figure 4.38: Entropy vs. MC shift parameter for CH_3-CH_3 at different temperatures, acceptance ratio 50%.

Table 4.18: Start of percolation for CH_3-CH_3 at different temperatures.

T (K)	V (cm^{3}mol^{-1})
500	390
600	350
700	330
800	320

4.3 Calculation of the residual entropy for hard-sphere fluids

The calculation of residual entropy for "hard-sphere argon" was performed at constant number of particles, volume and temperature (NVT ensemble). The details and results of simulation are presented in Table 4.19 and Figure 4.39, respectively.

Table 4.19: Simulation details for hard-sphere argon, acceptance ratio 50%.

simulation type	site	σ_{hs}(Å)	ε/k_B(K)	number of atoms	atom coordinates (Å)
1	1	2.724	119.8	500	$(0.00, 0.00, 0.00)$
2	1	2.724	119.8	100	$(0.00, 0.00, 0.00)$
3	1	2.724	119.8	100	$(0.00, 0.00, 0.00)$

simulation type	number of compression cycles	number of equilibration cycles	number of production cycles
1	30000	60000	150000
2	3000	10000	15000
3	30000	60000	100000

Figure 4.39 shows that in the percolation region, the change of Monte Carlo shift parameter in type(1) hard-sphere argon (with 500 particles) is more than types(2) and (3) (with 100 particles) under the same conditions (temperature, molar volume, etc).

At constant molar volume, the volume of simulation box increases with increasing number of particles. With increase the volume of simulation box, the particles have more place to move and the move is accepted with more probability. Because of this case, the change of Monte Carlo shift parameter in type(1) hard-sphere argon with higher number of particles is more than in types(2) and (3) (only true in the percolation region).
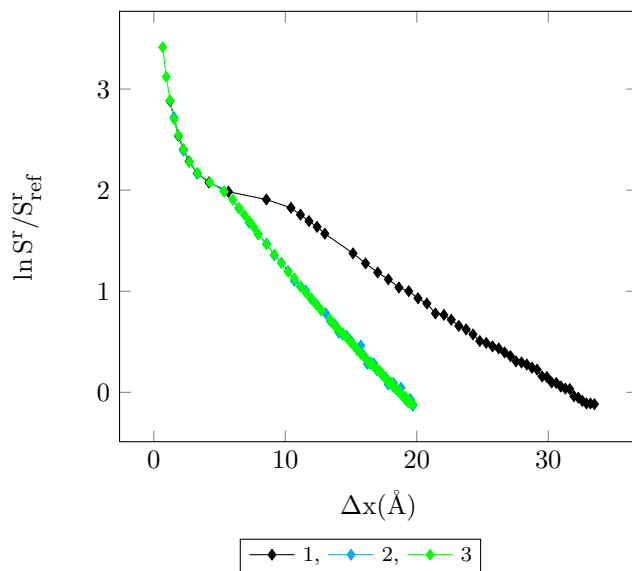
Figure 4.39: Entropy vs. MC shift parameter for hard-sphere argon, acceptance ratio 50%.
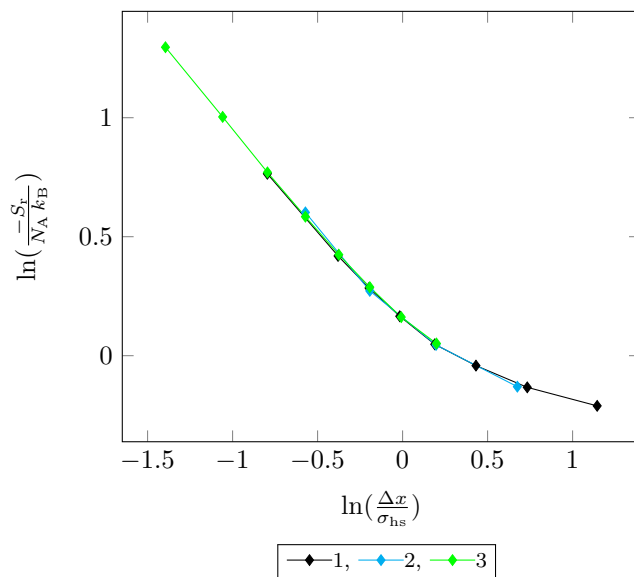
Figure 4.40: Entropy vs. MC shift parameter for a hard-sphere fluid, acceptance ratio 50%. (For simulation details, please See Table 4.19.)

Equation (4.1) expresses a master function for the hard-sphere system describing the connection between the residual entropy, S_r, and the Monte Carlo shift parameter, x (see Figure 4.40). This equation is valid for the region before beginning of percolation.

$$\boxed{y = 0.2263X^2 - 0.5795X + 0.1607}$$

(4.1)

where $y = \ln(\frac{-S_r}{N_A k_B})$, $X = \ln\left(\frac{\Delta x}{\sigma_{hs}}\right)$.

4.4 Calculation of the residual entropy for LJ fluids
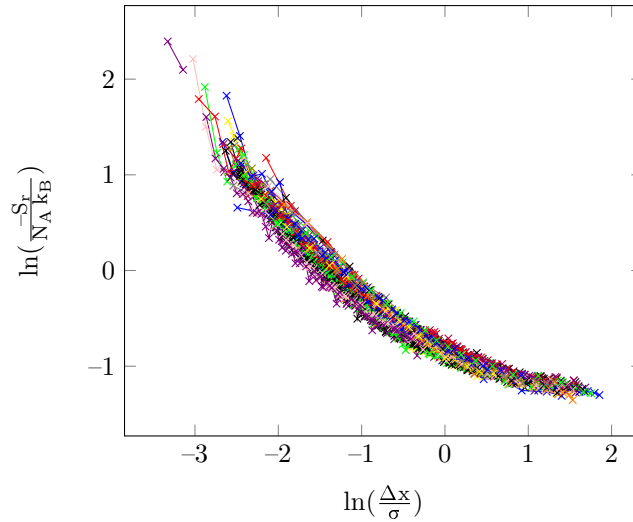
Figure 4.41: residual entropy vs. MC shift parameter in Lennard-Jones fluids at various temperatures.

The simulation results for Lennard-Jones fluids are presented in Figure 4.41. The details and results of simulations are presented in sections 4.2.1 to 4.2.9.

The results are obtained from more than 2100 simulations at temperatures above the critical point. According to Figure 4.41, in Lennard-Jones fluids, there is a master function that relates the residual entropy, S_r, to the Monte Carlo shift parameter, x, (Equation (4.2)).

This equation is only valid for Δx range with stable acceptance average (before beginning of percolation). The closer the volume gets to the percolation volume, the more accurate the Equation (4.2) becomes, according to calculation of residual entropy.

The calculated diagram in Figure 4.41 is described with Equation (4.2). Although this equation is a second degree polynomial equation, it matches the diagram, because only its descending range is taken into account.

$$\boxed{y = 0.1543X^2 - 0.419X - 0.8764} \tag{4.2}$$

where $y = \ln(\frac{-S_r}{N_A k_B})$, $X = \ln(\frac{\Delta x}{\sigma})$, x is the Monte Carlo shift parameter and S_r is residual entropy.

4.5 Estimating the errors

Some of the problems that are the causes of errors in calculations of the residual entropy with the simulation program, are:

• poor sampling of the configuration space (small trial-move distance, or in other words high density of the system).

• It should be noted that the number of equilibration cycles has to be high enough. The number of cycles required for equilibration is not known beforehand and it should ideally be determined by test runs (e.g, by plotting density vs. cycle number) [77].

• sufficient numbers of production cycles.

• The volume, pressure and temperature must be chosen in a single-phase state.

• The choice of cut-off distance has an important effect on the estimated error. Moreover, if the cut-off distance exceeds half of the box size, the error increases.

4.6 Calculation of the residual entropy and estimation of relative errors

In this section, the results of the residual entropy from Equations (4.1) and (4.2) are compared with the results of simulation program. The relative errors is also estimated. The achieved results of Equations (4.1) and (4.2) are already presented in Tables 4.20 and 4.21, and Figures 4.42 and 4.43.
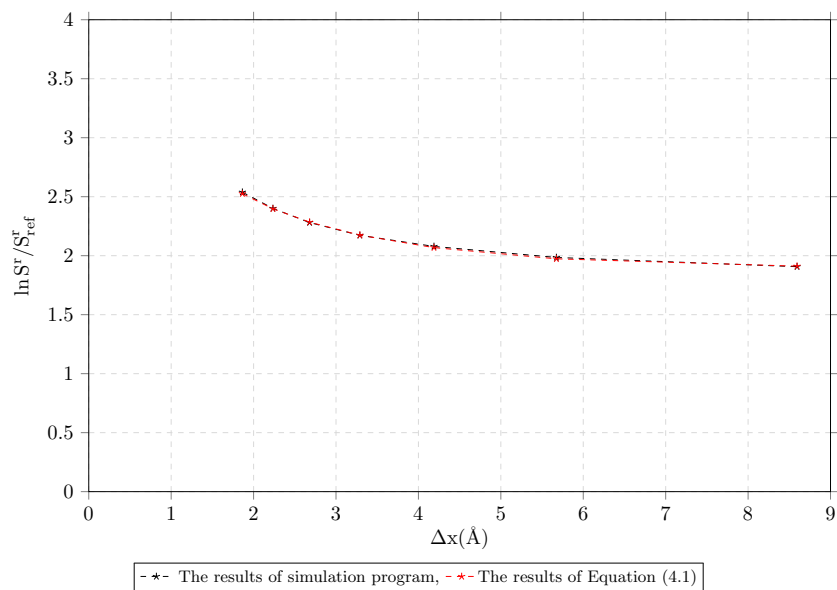
Figure 4.42: Entropy vs. MC shift parameter for hard sphere argon, T=400 K, acceptance ratio 50%.
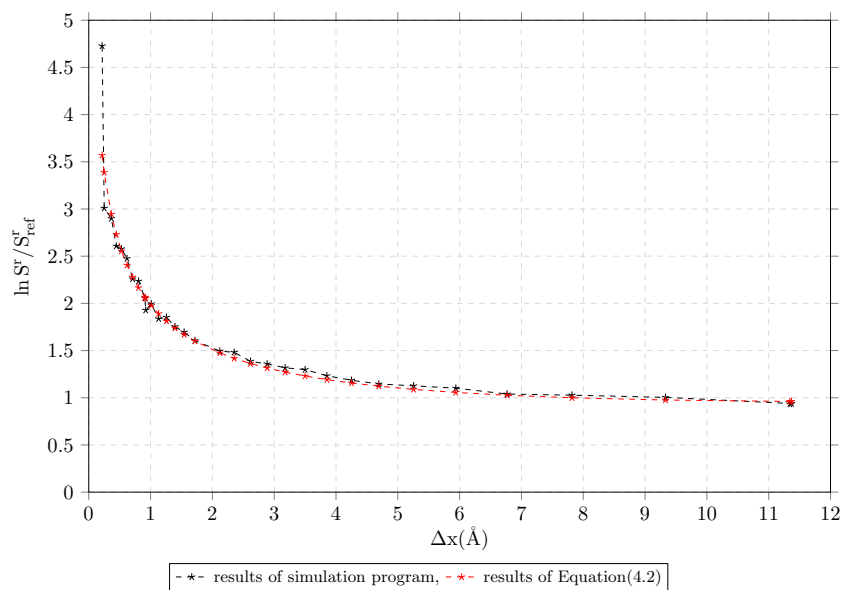
Figure 4.43: Entropy vs. MC shift parameter for Mie-potential argon dimers (10/6), T=200 K, acceptance ratio 50%.

Table 4.20: Estimates of the relative error for hard-sphere argon, T=400 K, 500 particles, acceptance ratio 50%.

$V_{\mathrm{m}}(\mathrm{cm}^3/\mathrm{mol})$	$\Delta x\,(\text{Å})$	$\ln(S^{\mathrm{r}}/S^{\mathrm{r}}_{\mathrm{ref}})$ (from simulation program)	$\ln(S^{\mathrm{r}}/S^{\mathrm{r}}_{\mathrm{ref}})$ (from Equation (4.1))	relative error in %
50	2.234700	2.400705	2.397578	0.001303
60	3.289410	2.172442	2.173946	0.000692
70	5.674070	1.984928	1.973536	0.005739
75	8.594130	1.906757	1.911153	0.002305

Table 4.21: Estimates of the relative error for Mie-potential argon dimers (10/6), T=200 K, 500 particles, acceptance ratio 50%.

$V_{\mathrm{m}}(\mathrm{cm}^3/\mathrm{mol})$	$\Delta x\,(\text{Å})$	$\ln(S^{\mathrm{r}}/S^{\mathrm{r}}_{\mathrm{ref}})$ (from simulation program)	$\ln(S^{\mathrm{r}}/S^{\mathrm{r}}_{\mathrm{ref}})$ (from Equation (4.1))	relative error in %
50	0.216313	4.727951	3.568644	0.686297
100	0.619039	2.474837	2.404331	0.068078
200	0.921472	1.927562	2.052780	0.133395
300	5.255410	1.126608	1.088754	0.037146

4.7 Calculation of the residual entropy with different methods

4.7.1 Lennard-Jones fluids

In sections 2.9.5 and 2.9.6 two alternative methods were presented for the calculation of the residual entropy of Lennard-Jones fluids. In the current and the next sections we try to compare the results of these methods (Scheraga theory (section 2.9.5) and calculation the residual entropy from the radial distribution function (section 2.9.6)) with results obtained with different equations of state and results of the simulation.

In order to calculate residual entropy according to the Scheraga theory, simulations were run with different acceptance ratios ranging from 2% to 95%. The results are presented in Figures 4.44 and 4.45. The calculation of residual entropy, according to Scheraga theory, is presented in section 2.9.5, page 57, in detail.

To estimate the entropy from radial distribution function (RDF), first of all, we need to calculate the RDF. For this, we used an algorithm that was presented by

Frenkel and Smidt to write a program [30]. The algorithm is presented in Chapter 6 on page 119. The results of the RDF program are presented on the page 124 and 125.

The details of simulations in this section were presented before in sections 4.1 to 4.2.9. The comparison between the results of ThermoC, simulation program, Scheraga theory, and Equation (4.2) for the residual entropy of Lennard-Jones argon in different temperatures and volumes are presented in Tables 4.23 and 4.25.
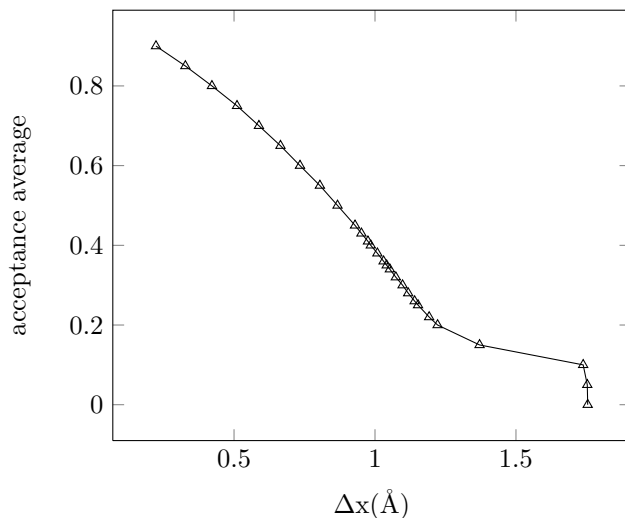
Figure 4.44: Acceptance ratio vs. MC shift parameter for argon, $T = 200$ K, $V = 50$ cm^{3}mol^{-1}, 500 molecules.

According to Tables 4.23 and 4.25, it can be seen that the results of the simulation program are in very good agreement with Equation (4.2), KN-LJ and mBW2-nLJ equation of states. However, the residual entropy values calculated with the Scheraga theory do not agree with the other methods.

The low accuracy of Scheraga theory for calculation of residual entropy, is due to the difficulties to obtain residual entropy for acceptance ratios between 0% to 5% and 95% to 100% .

On the other hand, it is not always possible to obtain the best equation to explain the connection between acceptance average and Monte Carlo shift parameter in Lennard-Jones fluids. These two points impress the accuracies of Scheraga theory results and cause high inaccuracies of results.

According to Tables 4.23 to 4.25, the results of Equation (4.2), which gives us the residual entropy of Lennard-Jones fluids, are in very good agreement with the results of various equations of state (KN-LJ, CSJS-LJ, mBW1-LJ and mBW2-nLJ). This fact confirms the high accuracy of this equation. According to the results, the accuracy of Equation (4.2) is more than 92% compared to ThermoC.

Table 4.22: Results of the simulation program for argon, $T=200$ K, $V=50$ cm^{3}mol^{-1}, 500 molecules.

Thermodynamic properties	simulation results
Z	0.72115
U_r	-3.09208×10^3 J/mol
μ	-1.37630×10^3 J/mol
Δx	8.67082e-01 Å

Table 4.23: Calculation of the residual entropy with different EOS for argon, $T=200$ K, $V=50$ cm^{3}mol^{-1}, 500 molecules.

Theory	S_r(J/molK)
KN-LJ	-10.010
CSJS-LJ	-9.9836
mBW1-LJ	-9.7793
mBW2-nLJ	-10.0085
Simulation program	-10.8973
Scheraga theory	-10.2381
Equation (4.2)	-8.22507
estimate from radial distribution function	-7.77701

Table 4.24: Results of the simulation program for argon, $T=300$ K, $V=100$ cm^{3}mol^{-1}, 500 molecules.

Thermodynamic properties	simulation results
Z	0.95587
U_r	-1.45578×10^3 J/mol
μ	-3.28170×10^3 J/mol
Δx	2.57859 Å
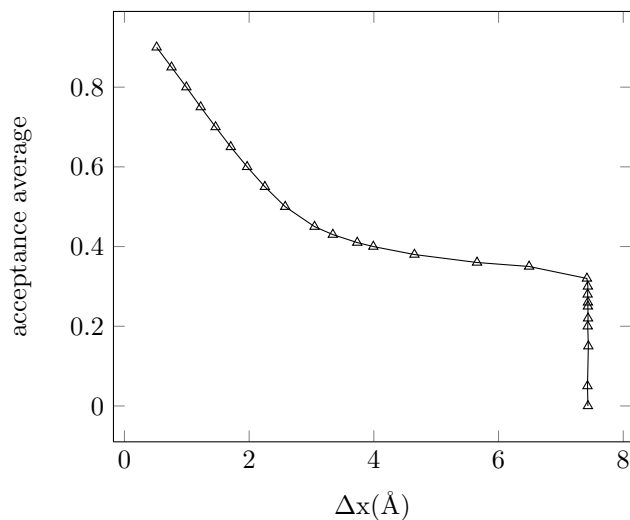
Figure 4.45: Acceptance ratio vs. MC shift parameter for argon, T=300 K, V=100 cm^{3}mol^{-1}, 500 molecules.

Table 4.25: Calculation of the residual entropy with different EOS for argon, T=300 K, V=100 cm^{3}mol^{-1}, 500 molecules.

Theory	S_r(J/mol K)
KN-LJ	-3.9847
CSJS-LJ	-3.9782
mBW1-LJ	-3.9574
mBW2-nLJ	-4.0499
Simulation program	-4.1256
Scheraga theory	-5.8611
Equation (4.2)	-3.9545
estimate from radial distribution function	-2.93523

4.7.2 Hard-sphere fluids

To assess the accuracy of Equation (4.1) for the hard-sphere fluid, the results for the this equation were compared with simulation results, calculation of entropy from radial distribution function and Scheraga theory.

The details of simulation are shown in section 4.3 page 102. The results for the residual entropy, calculated from radial distribution function, simulation and Equation (4.1) for different volumes of hard-sphere argon are presented in Tables 4.26 to 4.31.

The radial distribution functions (RDF) of hard-spheres are calculated from the Percus-Yevick method, which was presented before in section 2.8.2 on page 49. The results of these calculations are presented on pages 126 to 131.
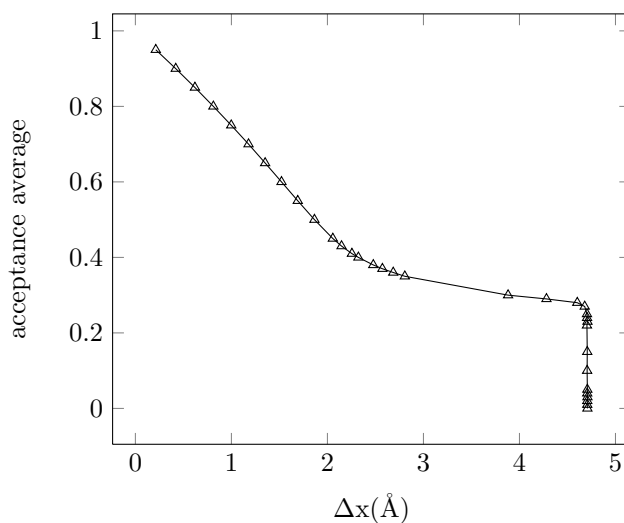
Figure 4.46: Acceptance ratio vs. MC shift parameter for hard-sphere argon, T=200 K, V=45 cm^{3}mol^{-1}, 500 molecules.

Table 4.26: Calculation of the residual entropy with different EOS for hard-sphere argon, T=200 K, V=45 cm^{3}mol^{-1}, 500 molecules.

Theory	S_r(J/mol K)
Simulation program	-12.6567
Equation (4.1)	-11.77089
Scheraga theory	-8.81749
estimate from radial distribution function	-9.74095
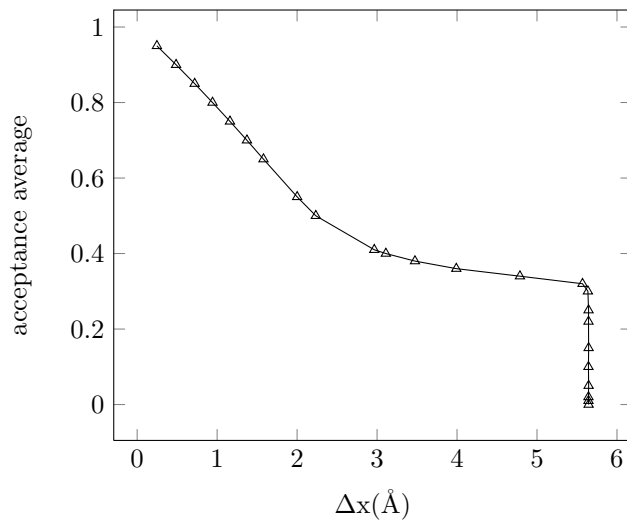
Figure 4.47: Acceptance ratio vs. MC shift parameter for hard-sphere argon, T=200 K, V=50 cm³mol⁻¹, 500 molecules.

Table 4.27: Calculation of the residual entropy with different EOS for hard-sphere argon, T=200 K, V=50 cm³mol⁻¹, 500 molecules.

Theory	S_r(J/molK)
Simulation program	-11.00425
Equation (4.1)	-10.8548
Scheraga theory	-12.7779
estimate from radial distribution function	-14.22126
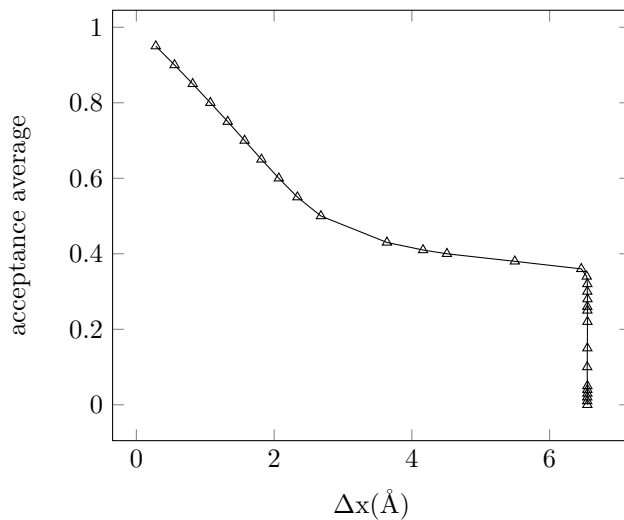
Figure 4.48: Acceptance ratio vs. MC shift parameter for hard-sphere argon, $T=200$ K, $V=55$ cm^{3}mol^{-1}, 500 molecules.

Table 4.28: Calculation of the residual entropy with different EOS for hard-sphere argon, $T=200$ K, $V=55$ cm^{3}mol^{-1}, 500 molecules.

Theory	S_r(J/mol K)
Simulation program	-9.7853
Equation (4.1)	-9.85524
Scheraga theory	-9.181425
estimate from radial distribution function	-10.67601
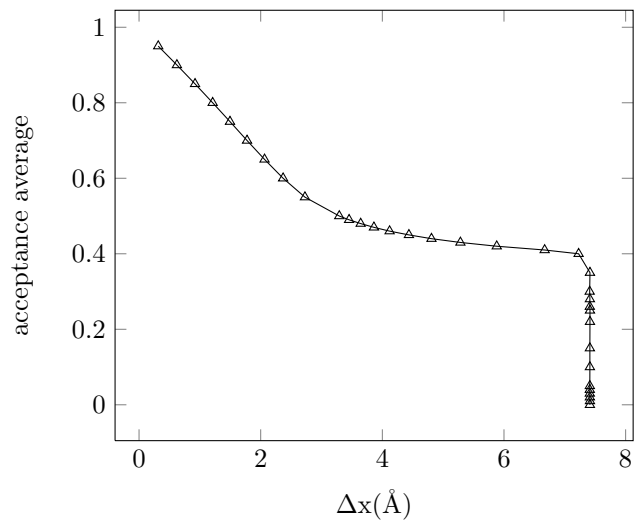
Figure 4.49: Acceptance ratio vs. MC shift parameter for hard-sphere argon, T=200 K, V=60 cm^{3}mol^{-1}, 500 molecules.

Table 4.29: Calculation of the residual entropy with different EOS for hard-sphere argon, T=200 K, V=60 cm^{3}mol^{-1}, 500 molecules.

Theory	S_r(J/mol K)
Simulation program	-8.7769
Equation (4.1)	-8.8198
Scheraga theory	-9.6343
estimate from radial distribution function	-8.2386
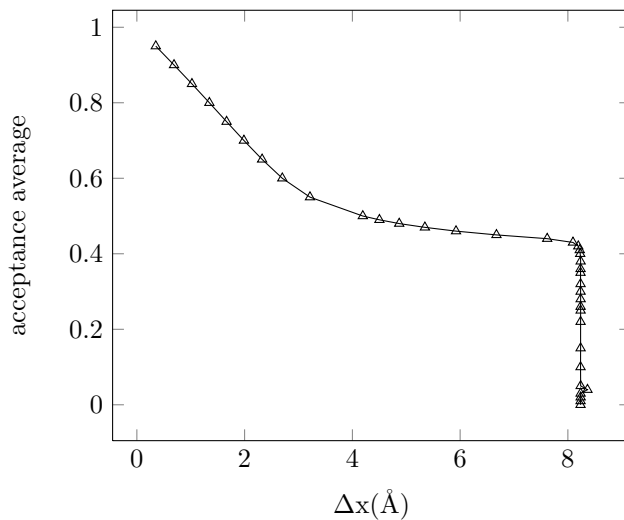
Figure 4.50: Acceptance ratio vs. MC shift parameter for hard-sphere argon, T=200 K, V=65cm^{3}mol^{-1}, 500 molecules.

Table 4.30: Calculation of the residual entropy with different EOS for hard-sphere argon, T=200 K, V=65 cm^{3}mol^{-1}, 500 molecules.

Theory	S_r(J/mol K)
Simulation program	-7.9659
Equation (4.1)	-7.9308
Scheraga theory	-8.838335
estimate from radial distribution function	-6.470996
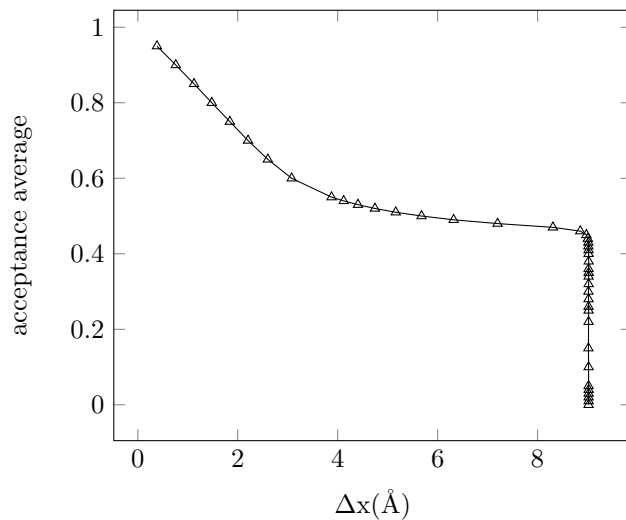
Figure 4.51: Acceptance ratio vs. MC shift parameter for hard-sphere argon, T=200 K, V=70 cm^{3}mol^{-1}, 500 molecules.

Table 4.31: Calculation of the residual entropy with different EOS for hard-sphere argon, T=200 K, V=70 cm^{3}mol^{-1}, 500 molecules.

Theory	S_r(J/mol K)
Simulation program	-7.2752
Equation (4.1)	-7.2075
Scheraga theory	-6.40174
estimate entropy from radial distribution function	-5.1855

Chapter 5

Conclusion

Conclusion

The relation between the residual entropy and the Monte Carlo shift parameter in Lennard-Jones fluids at high densities was studied. A new computer program was developed to perform canonical ensemble (N, V, T) and isothermal-isobaric ensemble (N, p, T) Monte Carlo simulations.

The Widom test particle insertion method was applied to calculate the chemical potentials, while the intermolecular interactions were modeled as two-body interactions to decrease the computing time. Moreover, periodic boundary conditions (PBC) were applied to avoid problems with boundary and finite-size effects.

The calculations were performed on 1-center, dimers, Mie-potential argon, linear and nonlinear Lennard-Jones trimers of argon, a dimer (CH_3CH_3) and hard-sphere argon at higher density.

Our research shows that percolation can occur during the simulation. Its starting point depends on the number of sites in Lennard-Jones fluids as well as the temperature.

According to the results, under the same conditions, the percolation occurs at low densities where the number of sites is increased. In other words, the percolation occurs in Lennard-Jones argon trimers at lower reduced densities than in 1-center Lennard-Jones argon and Lennard-Jones argon dimers at same temperature and number of particles. In addition, a comparison of the results for linear Lennard-Jones argon trimers and nonlinear Lennard-Jones argon trimers shows that the percolation occurs in nonlinear Lennard-Jones argon trimers at lower densities than for linear Lennard-Jones argon trimers.

The temperature is another factor that influences the starting point of percolation, i. e. by increasing the temperature, the percolation is shifted to higher densities.

Our simulations show that the connection between residual entropy and the Monte Carlo shift parameter in Lennard-Jones fluid can be described with a second degree equation at temperatures above the critical point. It was also shown that this equation is not valid for hard-sphere fluids.

We propose another second degree equation for hard-sphere fluids to calculate the residual entropy with the help of a Monte Carlo shift parameter.

At last, our results from the simulation program and our second degree equation are compared with the other methods (Scheraga theory and estimate entropy from radial distribution function) and the results of different equation of states. It is shown that the relative error to calculation of residual entropy from Monte Carlo shift parameter with this new second degree equation is about 5%, which shows the high accuracy of this method.

Chapter 6

Appendix

Algorithm 1: Algorithm to calculation of radial distribution function. Taken from
[30].

```
subroutine gr(switch)                          radial distribution function
                                                  switch=0 initialization,
                                                 =1 sample, and =2 results
  if(switch.eq.0) then                               initialization
     ngr=0
     delg=box/(2*nhis)                                 bin size
     do i=0, nhis                             nhis total number of bins
        g(i)=0
     enddo
  else if (switch.eq.1) then                            sample
     ngr=ngr+1
     do i=1,npart-1
        do j=i+1,npart                           loop over all pairs
           xr=x(i)-x(j)
           xr=xr-box*nint(xr/box)           periodic boundary conditions
           r=sqrt(xr**2)
           if (x.lt.box/2) then              only within half the box length
              ig=int(r/delg)
              g(ig)=g(ig)+2                 contribution for particle i and j
           endif
        enddo
     enddo
  else if (switch.eq.2) then                       determine g(r)
     do i=1, nhis
        r=delg*(i+0.5)                              distance r
        vb=((i+1)**3-i**3)*delg**3          volume between bin i+1 and i
        nid=(4/3)*pi*vb*rho               number of ideal gas part. in vb
        g(i)=g(i)/(ngr*npart*nid)                 normalize g(r)
     enddo
  endif
  return
  end
```

Table 6.1: Vapour-pressure curve of argon from mBWR2-nLJ equation of state.

T(K)	p(MPa)	V_{ml}(cm^3/mol)	V_{mg}(cm^3/mol)	d_{Hm}(J /mol)
55.00	1.04817e-03	2.86509e+01	4.35772e+05	1.88740e+03
60.00	1.83862e-03	2.78031e+01	2.70896e+05	4.15091e+03
65.00	3.90628e-03	2.73373e+01	1.37980e+05	5.51981e+03
70.00	8.59005e-03	2.72183e+01	6.74292e+04	6.29497e+03
75.00	1.81816e-02	2.73941e+01	3.40094e+04	6.65756e+03
80.00	3.59566e-02	2.77882e+01	1.82405e+04	6.75394e+03
85.00	6.60236e-02	2.83257e+01	1.04701e+04	6.70091e+03
90.00	1.13124e-01	2.89527e+01	6.40083e+03	6.57453e+03
95.00	1.82475e-01	2.96394e+01	4.13132e+03	6.41482e+03
100.00	2.79666e-01	3.03747e+01	2.78970e+03	6.23871e+03
105.00	4.10571e-01	3.11602e+01	1.95488e+03	6.05087e+03
110.00	5.81291e-01	3.20057e+01	1.41193e+03	5.85020e+03
115.00	7.98095e-01	3.29277e+01	1.04508e+03	5.63292e+03
120.00	1.06739e+00	3.39495e+01	7.88889e+02	5.39386e+03
125.00	1.39569e+00	3.51042e+01	6.04693e+02	5.12662e+03
130.00	1.78969e+00	3.64407e+01	4.68721e+02	4.82305e+03
135.00	2.25630e+00	3.80361e+01	3.65799e+02	4.47185e+03
140.00	2.80287e+00	4.00255e+01	2.85855e+02	4.05539e+03
145.00	3.43754e+00	4.26818e+01	2.21812e+02	3.54170e+03
150.00	4.17008e+00	4.67079e+01	1.67996e+02	2.85792e+03
155.00	5.01377e+00	5.52877e+01	1.16863e+02	1.72817e+03

Table 6.2: Acceptance ratio vs. residual entropy for argon, $T=200$ K, $V_m=50$ cm^{3}mol^{-1}, 500 molecules.

average acceptance	shift parameter (Å)
0.00	1.75441
0.05	1.75295
0.10	1.73839
0.15	1.37087
0.20	1.22201
0.22	1.19210
0.25	1.15265
0.26	1.14055
0.28	1.11780
0.30	1.09782
0.32	1.07386
0.34	1.05268
0.35	1.04138
0.36	1.03046
0.38	1.00848
0.40	0.98504
0.41	0.97500
0.43	0.95187
0.45	0.92917
0.50	0.86708
0.55	0.80457
0.60	0.73400
0.65	0.66470
0.70	0.58826
0.75	0.51058
0.80	0.42160
0.85	0.32739

Table 6.3: Acceptance ratio vs. residual entropy for argon, T=300 K, V_m=100 cm^{3}mol^{-1}, 500 molecules.

average acceptance	shift parameter (Å)
0.00	7.43342
0.05	7.42646
0.15	7.44014
0.20	7.43059
0.22	7.43527
0.25	7.43273
0.26	7.43314
0.28	7.42887
0.30	7.43286
0.32	7.41710
0.35	6.48966
0.36	5.65498
0.38	4.65097
0.40	3.99152
0.41	3.73372
0.43	3.34246
0.45	3.04891
0.50	2.57859
0.55	2.25255
0.60	1.96793
0.65	1.70541
0.70	1.46176
0.75	1.22313
0.80	0.99372
0.85	0.75540
0.90	0.51628

Table 6.4: Radial distribution function of argon, T=200 K, V_m=50 cm^{3}mol^{-1}, 500 molecules.

r (Å)	$g(r)$
0.17313	0.0
0.51939	0.0
0.86565	0.0
1.21191	0.0
1.55817	0.0
1.90443	0.0
2.25069	0.0
2.59695	0.0
2.94321	0.0132015
3.28947	0.7241257
3.63573	1.6963705
3.98199	1.6524852
4.32825	1.3723297
4.67451	1.2193380
5.02077	0.9344992
5.36703	0.9509565
5.71329	0.8906442
6.05955	0.8795952
6.40581	0.9228505
6.7507	0.9846405
7.09833	1.0522400
7.44459	1.0616450
7.79085	1.0523715
8.13711	1.0001695
8.48337	1.0188215

r (Å)	$g(r)$
8.82963	0.9977570
9.17589	0.9687530
9.52215	0.9683970
9.86841	0.9956817
10.21467	1.0013775
10.56093	1.0077912
10.90719	1.0043280
11.25345	1.0234830
11.59971	0.9986065
11.94597	0.9847462
12.2923	0.9832162
12.63849	0.9932750
12.98475	0.9913702
13.33101	0.9930452
13.67727	1.0049100
14.02353	0.9959717
14.36979	1.0007632
14.71605	1.0155492
15.06231	0.9975710
15.40857	0.9901307
15.75483	1.0073580
16.10109	1.0029187
16.44735	0.9933725
16.79361	0.9903150
17.13987	1.0067615

Table 6.5: Radial distribution function of argon, T=300 K, V_{m}=100 cm^{3}mol^{-1}, 500 molecules.

r (Å)	$g(r)$	r (Å)	$g(r)$
0.218125	0.0	11.124375	0.995554
0.654375	0.0	11.560625	1.007956
1.090625	0.0	11.996875	1.037207
1.526875	0.0	12.433125	0.992351
1.963125	0.0	12.869375	0.974130
2.399375	0.0	13.305625	0.992052
2.835625	0.060152	13.741875	1.002724
3.271875	0.856046	14.178125	1.005554
3.708125	1.236568	14.614375	0.995486
4.144375	1.305540	15.050625	0.982740
4.580625	1.197268	15.486875	1.000390
5.016875	1.098049	15.923125	1.009998
5.453125	1.019066	16.359375	1.007553
5.889375	0.922633	16.795625	0.994763
6.325625	0.978386	17.231875	0.980022
6.761875	0.951618	17.668125	1.005771
7.198125	1.013371	18.104375	1.012129
7.634375	0.994415	18.540625	0.995196
8.070625	1.016763	18.976875	1.000850
8.506875	1.024813	19.413125	0.991336
8.943125	0.995444	19.849375	0.995903
9.379375	1.004500	20.285625	0.993721
9.815625	0.987305	20.721875	0.999086
10.251875	0.969625	21.158125	1.007297
10.688125	0.983561	21.594375	0.995070

Table 6.6: Radial distribution function of a hard-sphere fluid in the Percus-Yevick approximation, T=200K, V_{m}=45 cm^{3}mol^{-1}, 500 molecules.

r (Å)	$g(r)$
1.0	1.0492
1.1	1.0403
1.2	1.0321
1.3	1.0247
1.4	1.0182
1.5	1.0125
1.6	1.0078
1.7	1.0041
1.8	1.0014
1.9	0.9999
2.0	0.9995
2.1	0.9997
2.2	0.9998
2.3	0.9999
2.4	0.9999
2.5	1.0000
2.6	1.0000
2.7	1.0000
2.8	1.0000
2.9	1.0000
3.0	1.0000

Table 6.7: Radial distribution function of a hard-sphere fluid in the Percus-Yevick approximation, T=200K, V_m=50 cm^{3}mol^{-1}, 500 molecules.

r (Å)	$g(r)$
1.0	1.0441
1.1	1.0362
1.2	1.0289
1.3	1.0223
1.4	1.0164
1.5	1.0113
1.6	1.0071
1.7	1.0037
1.8	1.0014
1.9	0.9999
2.0	0.9996
2.1	0.9997
2.2	0.9998
2.3	0.9990
2.4	1.0000
2.5	1.0000
2.6	1.0000
2.7	1.0000
2.8	1.0000
2.9	1.0000
3.0	1.0000

Table 6.8: Radial distribution function of a hard-sphere fluid in the Percus-Yevick approximation, T=200K, V_m=55 cm^{3}mol^{-1}, 500 molecules.

r (Å)	$g(r)$
1.0	1.0400
1.1	1.0329
1.2	1.0262
1.3	1.0202
1.4	1.0149
1.5	1.0103
1.6	1.0065
1.7	1.0035
1.8	1.0013
1.9	1.0000
2.0	0.9996
2.1	0.9998
2.2	0.9999
2.3	0.9999
2.4	1.0000
2.5	1.0000
2.6	1.0000
2.7	1.0000
2.8	1.0000
2.9	1.0000
3.0	1.0000

Table 6.9: Radial distribution function of a hard-sphere fluid in the Percus-Yevick approximation, T=200K, V_m=60 cm^{3}mol^{-1}, 500 molecules.

r (Å)	$g(r)$
1.0	1.0366
1.1	1.0301
1.2	1.0240
1.3	1.0186
1.4	1.0137
1.5	1.0095
1.6	1.0060
1.7	1.0032
1.8	1.0012
1.9	1.0000
2.0	0.9997
2.1	0.9998
2.2	0.9999
2.3	0.9999
2.4	1.0000
2.5	1.0000
2.6	1.0000
2.7	1.0000
2.8	1.0000
2.9	1.0000
3.0	1.0000

Table 6.10: Radial distribution function of a hard-sphere fluid in the Percus-Yevick approximation, T=200K, V_m=65 cm^{3}mol^{-1}, 500 molecules.

r (Å)	$g(r)$
1.0	1.0337
1.1	1.0227
1.2	1.0222
1.3	1.0171
1.4	1.0127
1.5	1.0088
1.6	1.0056
1.7	1.0030
1.8	1.0012
1.9	1.0001
2.0	0.9997
2.1	0.9998
2.2	0.9999
2.3	0.9999
2.4	1.0000
2.5	1.0000
2.6	1.0000
2.7	1.0000
2.8	1.0000
2.9	1.0000
3.0	1.0000

Table 6.11: Radial distribution function of a hard-sphere fluid in the Percus-Yevick approximation, T=200K, V_m=70 cm^{3}mol^{-1}, 500 molecules.

r (Å)	$g(r)$
1.0	1.0313
1.1	1.0257
1.2	1.0206
1.3	1.0159
1.4	1.0118
1.5	1.0082
1.6	1.0052
1.7	1.0028
1.8	1.0011
1.9	1.0001
2.0	0.9998
2.1	0.9999
2.2	0.9999
2.3	0.9999
2.4	1.0000
2.5	1.0000
2.6	1.0000
2.7	1.0000
2.8	1.0000
2.9	1.0000
3.0	1.0000

Table 6.12: The results of MC++ simulation program for argon, T=200 K, 500 particles, acceptance ration 50%.

V(cm3/mol)	μ_r(J/mol)	U_r(J/mol K)	Z	Δx(Å)	S_r(J/mol K)
5.00000e+01	-1.53824e+03	-3.09733e+03	0.72229	0.86640	-10.1043
6.00000e+01	-1.56630e+03	-2.60493e+03	0.63389	1.78060	-8.23698
7.00000e+01	-1.48082e+03	-2.25563e+03	0.62337	1.29217	-7.00535
8.00000e+01	-1.44544e+03	-1.99472e+03	0.62875	1.50365	-5.83297
9.00000e+01	-1.28668e+03	-1.78386e+03	0.64659	1.51210	-20.2560
1.00000e+02	-1.21035e+03	-1.61515e+03	0.66377	1.98964	-4.81941
1.10000e+02	-1.13893e+03	-1.47993e+03	0.68215	2.24506	-4.34760
1.20000e+02	-1.10517e+03	-1.36231e+03	0.70190	2.54542	-3.76410
1.30000e+02	-1.00561e+03	-1.26382e+03	0.71118	2.88513	-3.69229
1.40000e+02	-9.75017e+02	-1.17721e+03	0.73081	3.29612	-3.24900
1.50000e+02	-9.10018e+02	-1.10388e+03	0.74303	3.81927	-3.10570
1.60000e+02	-8.50972e+02	-1.03588e+03	0.75534	4.53683	-2.95864
1.70000e+02	-8.29578e+02	-9.78244e+02	0.76822	5.41672	-2.67034
1.80000e+02	-7.62059e+02	-9.26589e+02	0.77488	6.63814	-2.69429
1.90000e+02	-7.58404e+02	-8.77937e+02	0.78646	8.55248	-2.37303
2.00000e+02	-7.08778e+02	-8.35334e+02	0.79427	11.5604	-2.34325
2.10000e+02	-6.77741e+02	-7.97377e+02	0.80207	13.8122	-2.24377
2.20000e+02	-6.63403e+02	-7.61825e+02	0.81034	14.6729	-2.06894
2.30000e+02	-6.16041e+02	-7.29946e+02	0.81736	15.3075	-2.08799
2.40000e+02	-5.81970e+02	-7.00787e+02	0.82539	15.8575	-2.04579
2.50000e+02	-5.83617e+02	-6.74257e+02	0.83074	16.3943	-1.86042
2.70000e+02	-5.34646e+02	-6.23710e+02	0.84137	17.4404	-1.76416
2.80000e+02	-5.21362e+02	-6.02320e+02	0.84718	17.9128	-1.67558
2.90000e+02	-5.03224e+02	-5.82248e+02	0.85168	18.4030	-1.62850
3.10000e+02	-4.76715e+02	-5.45426e+02	0.85921	19.3385	-1.51408
3.20000e+02	-4.61726e+02	-5.28895e+02	0.86236	19.7739	-1.48183
3.30000e+02	-4.50303e+02	-5.12609e+02	0.86710	20.2193	-1.41641
3.40000e+02	-4.40167e+02	-4.97974e+02	0.87132	20.6555	-1.35888
3.50000e+02	-4.23879e+02	-4.84268e+02	0.87371	21.0732	-1.35196
3.60000e+02	-4.16374e+02	-4.70304e+02	0.87781	21.4916	-1.28553
3.70000e+02	-3.92966e+02	-4.57617e+02	0.88093	21.8922	-1.31320
3.80000e+02	-4.00053e+02	-4.46490e+02	0.88207	22.2873	-1.21027
3.90000e+02	-3.84384e+02	-4.34697e+02	0.88708	22.6771	-1.19038
4.00000e+02	-3.79409e+02	-4.24250e+02	0.88817	23.5090	-1.15395
4.10000e+02	-3.55600e+02	-4.14614e+02	0.89206	23.4298	-1.19248
4.20000e+02	-3.62337e+02	-4.04596e+02	0.89380	23.7957	-1.09420

V(cm3/mol)	μ(J/mol)	U_r(J/mol K)	Z	Δx(Å)	S_r(J/mol K)
4.30000e+02	-3.55991e+02	-3.95094e+02	0.89619	24.1523	-1.05859
4.40000e+02	-3.34571e+02	-3.85967e+02	0.89862	24.5262	-1.09985
4.50000e+02	-3.53554e+02	-3.77368e+02	0.90029	24.8745	-0.98058
4.60000e+02	-3.27121e+02	-3.69972e+02	0.90162	25.2013	-1.03218
4.70000e+02	-3.24097e+02	-3.61568e+02	0.90478	25.5532	-0.97901
4.80000e+02	-3.03718e+02	-3.54685e+02	0.90594	25.8829	-1.03684
4.90000e+02	-3.05721e+02	-3.46810e+02	0.90744	26.2192	-0.97498
5.00000e+02	-3.01264e+02	-3.40353e+02	0.90908	26.5329	-0.95135
5.10000e+02	-2.92577e+02	-3.33966e+02	0.91190	26.8504	-0.93940
5.20000e+02	-2.94875e+02	-3.27283e+02	0.91247	27.1571	-0.88974
5.30000e+02	-2.84895e+02	-3.21032e+02	0.91447	27.4935	-0.89178
5.40000e+02	-2.90760e+02	-3.16086e+02	0.91523	27.7738	-2.83140
5.50000e+02	-2.80301e+02	-3.09637e+02	0.91744	28.0900	-0.83308
5.60000e+02	-2.67002e+02	-3.04394e+02	0.91869	28.3735	-0.86130
5.70000e+02	-2.75386e+02	-2.99136e+02	0.92035	28.6658	-0.78096
5.80000e+02	-2.67475e+02	-2.93550e+02	0.92191	28.9659	-0.77961
5.90000e+02	-2.71924e+02	-2.88901e+02	0.92314	29.5531	-0.72389
6.00000e+02	-2.60219e+02	-2.83954e+02	0.92435	29.5389	-0.74762
6.10000e+02	-2.45421e+02	-2.79625e+02	0.92584	29.8040	-0.78750
6.20000e+02	-2.48140e+02	-2.75068e+02	0.92661	20.0820	-0.74480
6.30000e+02	-2.40448e+02	-2.70742e+02	0.92712	30.3521	-0.75738
6.40000e+02	-2.51260e+02	-2.66281e+02	0.92870	30.6223	-0.66789
6.50000e+02	-2.36666e+02	-2.62633e+02	0.92979	30.8861	-0.71356
6.60000e+02	-2.43516e+02	-2.58671e+02	0.93036	31.1450	-0.65476
6.70000e+02	-2.30836e+02	-2.54766e+02	0.93101	31.4107	-0.69326

Bibliography

[1] N. Metropolis, A. W. Rosenbluth, A. H. Teller, and E. Teller, J. Chem. Phys. 21 (1953) 1087.

[2] B. J. Alder and T. E. Wainwright, J. Chem. Phys. 27 (1957) 1208.

[3] B. Widom, J. Chem. Phys. 39 (1963) 2808.

[4] B. Widom, J. Stat. Phys. 19 (1978) 563.

[5] S. D. Hong, H. Shin, and K. Cho, Bull. Korean Chem. Soc. 26 (2005) 1673.

[6] D. J. Adams, Mol. Phys. 32 (1979) 647.

[7] D. J. Adams, Mol. Phys. 37 (1979) 211.

[8] D. Fincham, N. Quirke, and D. J. Tildesley, Mol. Phys. 84 (1986) 4535.

[9] A. Z. Panagiotopoulos, U. W. Suter, and R. C. Reid, Mol. Phys. 37 (1979) 211.

[10] A. Z. Panagiotopoulos, Mol. Phys. 61 (1987) 813.

[11] A. Z. Panagiotopoulos, J. Phys. Condens. Matter 12 (2000) R25.

[12] G. C. Boulougouris, I. G. Economou, and D. N. Theodorou, J. Chem. Phys. 115 (2001) 8231.

[13] D. A. Kofke, J. Chem. Phys. 98 (1993) 4149.

[14] D. A. Kofke, Adv. Chem. Phys. 105 (1999) 405.

[15] J. C. Berthet, Modelling of Relaxation Processes in Polymers in the Glassy State, Ph. D. thesis, The University of Leeds, 2005.

[16] C. Hoheisel and U. Deiters, Mol. Phys. 37 (1979) 95.

[17] R. J. Styer, Am. J. Phys. 68 (2000) 1090.

[18] R. J. Speedy, J. Chem. Soc. Faraday Trans. II 77 (1981) 329.

[19] J. L. Bretonnet, J. Chem. Phys. 120 (2004) 8231.

[20] N. Lu and D. A. Kofke, AIChE Symp. Ser. 97 (2001) 146.

[21] N. G. Parsonage, J. Chem. Soc. Faraday Trans. 92 (1996) 1129.

[22] N. G. Parsonage, Mol. Phys. 89 (1996) 1133.

[23] O. Coskuner and U. K. Deiters, Z. Phys. Chem. 220 (2006) 349.

[24] O. Coskuner and U. K. Deiters, Z. Phys. Chem. 221 (2007) 785.

[25] H. H. Barrett and K. J. Myers, Foundations of Image Science, John Wiley & Sons, New York, 2003.

[26] D. A. McQuarrie, Statistical Mechanics, Harper & Row, New York, 1976.

[27] O. Coskuner, Investigation of hydrophobic interactions by Monte Carlo simulation, Ph. D. thesis, University of Cologne (2003).

[28] N. Metropolis, J. Chem. Phys. 21 (1953) 1087.

[29] F. Vesely, Computerexperimente an Flüssigkeiten, Physik-Verlag, Weinheim, 1978.

[30] D. Frenkel and B. Smit, Understanding Molecular Simulation, Academic Press, London, 1996.

[31] D. P. Landau and K. Binder, A Guide to Monte Carlo Simulations in Statistical Physics, Cambridge University Press, 2000.

[32] J. B. Ott and J. Boerio-Goates, Chemical Thermodynamics, Academic Press, San Diego, 2000.

[33] https://www.tug.org/texshowcase/EulerGibbsDuhem.pdf

[34] R. Eppenga and D. Frenkel, Mol. Phys. 52 (1984) 1303.

[35] A. J. Schultz and D. A. Kofke, Phys. Rev. E84 (2011) 046712.

[36] J. P. Hansen and I. R. McDonald, Theory of simple liquids, Academic Press, London, 1986.

[37] L. L Lee, Molecular Thermodynamics of Electrolyte Solution, World Scientific, 2008.

[38] H. Goldstein, Classical Mechanics, Addison-Wesley, 1980.

[39] J. A. Barker and D. Henderson, Rev. Mod. Phys. 48 (1976) 587.

[40] J. K. Johnson, J. A. Zollweg, and K. E. Gubbins, Mol. Phys. 78 (1993) 591.

[41] B. Tadmor and E. Miller, Modeling Materials, Cambridge University Press, 2011.

[42] M. P. Allen and D. J. Tildesley, Computer Simulation of Liquids, Oxford University Press, 1991.

[43] J. O. Hirschfelder, C. F. Curtiss, and R. B. Bird, Molecular Theory of Gases and Liquids, John Wiley & Sons, New York, 1954.

[44] D. Henderson, Condens. Matter Phys. 12 (2009) 127.

[45] T. Boublík, J. Chem. Phys. 63 (1975) 4084.

[46] A. Z. Panagiotopoulos, U. W. Suter, and R. C. Reid, Ind. Eng. Chem. Fundam. 25 (1986) 525.

[47] K. Binder, Rep. Prog. Phys. 60 (1997) 487.

[48] R. P. A. Dullens, D. G. A. L. Aarts, W. K. Kegel, and H. N. W. Lekkerkerker, Mol. Phys. 103 (2005) 3195.

[49] D.C. Wallace, Phys. Rev. A 39 (1989) 4843.

[50] K. Lucas, Applied Statistical Thermodynamics, Springer-Verlag, Berlin, 1991.

[51] http://www.ncnr.nist.gov/staff/hammouda/the_SANS_toolbox.pdf

[52] B. J. Yoon and H. A. Scheraga, J. Mol. Struct. 199 (1989) 33.

[53] B. J. Yoon, S. D. Hong, M. Sh. Jhon, and H. A. Scheraga, Chem. Phys. Lett. 181 (1991) 73.

[54] R. C. Reid, J. M. Prausnitz, and B. E. Poling, The properties of gases and liquids, McGraw-Hill, New York, 1987.

[55] K. Lucas, Berechnungsmethoden für Stoffeigenschaften, VDI-Verlag, Düsseldorf, 1984.

[56] H. Ravenché, J. Chem. Phys. 55 (1971) 2242.

[57] S. Han, Phys. Rev. E84 (2011) 051204.

[58] J. R. Errington, T. M. Truskett, and J. Mittal, J. Chem. Phys. 125 (2006) 244502.

[59] W. P. krekelberg, J. Mittal, V. Ganesan, and T. M. Truskett, J. Chem. Phys. 127 (2007) 044502.

[60] H. S. Green, The Molecular Theory of fluids, North-Holland Pub. Co., Amsterdam, 1958.

[61] R. E. Nettleton and M. S. Green, J. Chem. Phys. 29 (1959) 1365.

[62] J. Mittal, W. P. Krekelberg, and J. R. Errington, Rev. Comput. Chem. 25 (2007) 125.

[63] A. Baranyai and D. J. Events, Phys. Rev. 40 (1989) 3817.

[64] Z. Yan, S. V. Buldyrev, and H. E. Stanley, Phys. Rev. E78 (2008) 051201.

[65] D. B. Amotz, Understanding Physical Chemistry, John Wiley & Sons, New York, 2014.

[66] D. Stauffer and A. Aharony, Introduction to Percolation Theory, Taylor & Francis, London, 1992.

[67] M. Sahimi, Application of Percolation Theory, Taylor & Francis, London, 1994.

[68] U. K. Deiters and T. Kraska, High-Pressure Fluid Phase Equilibria, Elsevier, Amsterdam, 2012.

[69] H. A. Lorentz, Ann. Phys., 248 (1881) 127 .

[70] J. W. Perram, Mol. Phys. 30 (1975) 1505.

[71] B. B. Laird and A. D. J. Haymet, J. Chem. Phys. 97 (1992) 2153.

[72] A. Bunde and W. Dietrich, J. Electroceram. 5(2) (2000) 81.

[73] G. R. Grimmett, Percolation, 2nd edition , Springer-Verlag, New York, 1999.

[74] J. M. Hammersley, Monte Carlo Methods, John Wiley & Sons, New York, 1964.

[75] http://www.mit.edu/~ levitov/8.334/notes/percol_notes.pdf

[76] M. Shikhabbasi and F. Feyzi, IJChE 9 (2012) 33.

[77] R. J. Sadus, Molecular Simulation of Fluids Theory, Algorithms and Object-Orientation. Bd. 2. Elsevier, Amsterdam, 2002.

[78] W. H. Press, B. P. Flannery, S. A. Teukolsky, and W. T. Vetterling, Numerical Recipes, Cambridge University Press, Cambridge, 1986.

[79] M. Scott Shell, Thermodynamics and statistical Mechanics, Cambridge University Press, 2015.

[80] A. R. Leach, Molecular Modeling: principles and application, Prentice Hall, 2001.

[81] J. J. Nicolas, K. E. Gubbins, W. B. Streett, and D. J. Tildesley, Mol. Phys. 37 (1979) 1429.

[82] J. K. Johnson, J. A. Zollweg, and K. E. Gubbins, Mol. Phys. 78 (1993) 591.

[83] J. K. Johnson, E. A. Müller, and K. E. Gubbins, J. Phys. Chem. 98 (1994) 6413.

[84] http://thermoc.uni-koeln.de/thermoc.

[85] http://thermoc.uni-koeln.de/thermoc/eos/mBWR1-LJ.html.

[86] J. Kolafa, I. Nezbeda, Fluid Phase Equilib. 100 (1996) 1.

[87] M. Mecke, A. Müller, J. Winkelmann, J. Vrabec, J. Fischer, R. Span, and W. Wagner, Int. J. Thermophys. 17 (1996) 391.

[88] M. Mecke, A. Müller, J. Winkelmann, J. Vrabec, J. Fischer, R. Span, and W. Wagner, Int. J. Thermophys. 19 (1998) 1493.

[89] C. D. Wick, M. G. Martin, and J. I. Siepmann, J. Phys. Chem. 104 (2000) 8008.

[90] J. M. Stubbs, J. J. Potoff, and J. I. Siepmann, J. Phys. Chem. 108 (2004) 17597.

[91] M. Hloucha and U. K. Deiters, Fluid Phase Equilib. 149 (1998) 41.

Erklärung

Ich versichere, dass ich die von mir vorgelegte Dissertation selbständig angefertigt, die benutzten Quellen und Hilfsmittel vollständig angegeben und die Stellen der Arbeit – einschließlich Tabellen, Karten und Abbildungen –, die anderen Werken im Wortlaut oder dem Sinn nach entnommen sind, in jedem Einzelfall als Entlehnung kenntlich gemacht habe; dass diese Dissertation noch keiner anderen Fakultät oder Universität zur Prüfung vorgelegen hat; dass sie – abgesehen von unten angegebenen Teilpublikationen – noch nicht veröffentlicht worden ist sowie, dass sich eine solche Veröffentlichung vor Abschluss des Promotionsverfahrens nicht vornehmen werde. Die Bestimmungen dieser Promotionsordnung sind mir bekannt.

Die von mir vorgelegte Dissertation ist von (Prof. Dr. Ulrich K. Deiters) betreut worden.

Name: Simin Yazdi Nezhad

Datum............................ Unterschrift..

Curriculum Vitae

Personal details:

Name:	Yazdi Nezhad
Vorname:	Simin
Geschlecht:	Weiblich
Geburstsdatum:	1 Sep. 1981
Geburstort:	Mashhad (Iran)
Familienstand:	Ledig

Addresse:

Universität zu Köln
Physikalische Chemie Institut
A. K. Prof. U. K. Deiters
Luxemburger Str. 116
50939 Köln
Deutschland

E-mail: simin_yazdinezhad@yahoo.de

Education:

• 11.11.2010-20.01.2016: Ph. D., Physical chemistry, University of Cologne, Germany.
Ph. D. Thesis: Calculation of entropy-dependent thermodynamic properties of fluids at high pressure with computer simulation.
Supervisor: Prof. Dr. Ulrich Deiters.

• 20.09.2005-30.02.2009: Master of Science, Physical chemistry, University of Birjand, Iran.
M. Sc. Thesis: Thermodynamic modelling of free energies of DNA -Dendronized polymer nanocluster.
Supervisor: Dr. A. Nikakhtar.

• 01.07.2001-21.07.2005: Bachelor of Science, Applied chemistry, University of payamnoor, Mashhad, Iran.

• 10.09.1998-10.06.1999: Pre-university Eslambolchy, Mathematics and physics, Mashhad, Iran.

Selected conferences, summer schools and workshops

- 05.01.2015-16.01.2015: Molsim2015, Amsterdam, Niederland.

- 15.09.2014-19.09.2014: workshop, Atomistic Monte Carlo simulations of bio-molecular Systems, Forschunszentrum Jülich, Germany.

- 07.10.2013-09.10.2013: VDI-Gesellschaft Technologies of Life Sciences, Thermodynamik-Kolloquium, S. Yazdi Nezhad, U. Deiters, Berechnung entropieabhängiger thermodynamischer Größen von Fluiden durch Computersimulationen, TU Hamburg-Harburg, Germany.

- 25.09.2013-29.09.2013: Graduiertenakademie, Berlin, Germany.

- 13.09.2012-25.09.2012: Sommerakademie Rot an der Rot, Memmingen, Germany.

- 04.12.2009: Write Scientific Texts for International Journals, Mehre KhavaranInstitute, Mashhad, Iran.

- 27.04.2009-28.04.2009: National Kongress about Nanomaterialen and Nanotechnologie, Islamic Azad university of Najafabad, Iran.

- 14.07.2009-16.07.2009:Nanosensoren and Nanomaterial im Medizin Wissenschaft, Medizin department Of Mashhad University, Iran.

- 20.05.2008-22.05.2008: Nano thermodynamic workshop, Isfahan TU university, Iran.

- 11.03.2008-13.03.2008: Yazdinezhad, S., Nikakhtar, A, Modification of Charge distribution on electrostatic modelling of DNA-dendronized polymer nanocluster , Presented as a poster at the 8th Iranian Biophysikal Chemistry, Zahedan, Iran.

- 13.10.2008-15.10.2008: Yazdinezhad, S., Nikakhtar, A, Thermodynamic Investigation of DNA-dendronized polymer Nanocluster with Modification of Charg Distribution, presented as a poster, 1. Regional Symposium im Bioelectrochemie Conference, Tehran university, Teheran, Iran.

- 06.11.2008-07.11.2008: A Preface to Nanotechnology, Sharif TU university Tehran, Iran.

Prices & Awards:

- 01.10.2011-01.10.2015: Research grant from The German Academic Exchange Service (DAAD), Germany.

• 01.04.2011-30.09.2011: Study grant for German language in Carl Duisberg Centren (CDC) from The German Academic Exchange Service, Germany.

• 23.03.2008: Best nominee of the first chemical competition in Birjand University as a poster presenter, Birjand,Iran.

• 23.03.2008: The first ranking in technical department of Birjand University as poster presenter.

Experiences and skills:

Computer skills
Operating system:
• Linux (Suse)
• MS Windows
Programming languages:
• C/C++
• Fortran
Scientific Codes:
• Matlab, Mathematica
Computer applications:
• Microsoft and open Office Package
• LATEX

Language knowledge

• Persian Native (mother tongue)
• English (fluent in speaking and writing)
• German (fluent in speaking and writing)